The Design and Mechanical Assessment of a Prosthetic Foot for Transtibial Amputees

by

Carlos Zerpa (Jr)

A thesis presented to Lakehead University

in fulfillment of the

thesis requirement for the degree of

Master of Applied Science

In

Mechanical and Mechatronics Engineering

Thunder Bay, Ontario, Canada, 2026

I hereby declare that I am the sole author of this thesis.

I authorize Lakehead University to lend this thesis to other institutions or individuals for the purpose of scholarly research.

I further authorize Lakehead University to reproduce this thesis by photocopying or by other means, in total or in part, at the request of other institutions or individuals for the purpose of scholarly research.

Lakehead University requires the signatures of all persons using or photocopying this thesis. Please sign below and give address and date.

Abstract

This thesis focuses on the development of an affordable prosthetic foot using 3D modeling. The aim is to provide a more accessible option for the average person. The study includes a detailed examination of the commercial prosthetics currently available on the market. By analyzing existing designs, the research compares their effectiveness with the new design being developed. The project utilizes SolidWorks to design each component and assemble the entire prosthetic foot. Simulations are conducted to assess how an average load affects the heel and forefoot of the design, as well as to determine whether the chosen material effectively reduces impact during walking. In addition to simulations, lab experiments were performed using the Chatillon force tester to analyze various prosthetic designs, including the 3D-printed model. These tests apply the required load to compute data on measures of absorbed energy and stiffness. The study also incorporated a 3D-printed insole designed to diminish impact during walking. These findings could lead to the creation of more affordable prosthetics, offering greater flexibility and comfort for transtibial amputees.

Acknowledgements

I would like to express my heartfelt gratitude to my supervisor, Dr. Meilan Liu, for her invaluable guidance, advice, and support throughout the thesis writing process. Her dedication and commitment to my research were instrumental in helping me complete my thesis and successfully finish my master's degree.

I want to express my gratitude to my parents for their emotional support throughout my thesis process, which provided me with confidence and strength during my master's journey.

Contents

List of Figures

List of Tables

Chapter 1: Introduction

1.1 Overview

There are presently 5.6 million people in the U.S. living with limb loss (White & Harold, 2024), while it is estimated that at least 227000 Canadians are living with the same condition. The most common causes of lower limb amputations, including transtibial (below-knee) amputations, are vascular diseases such as diabetes and peripheral artery disease (Dillingham et al., 2002). In Canada, nearly 8000 lower limb amputations are performed each year, with the majority being transtibial amputations (Imam et al., 2017). These amputations have not only caused people to lose the functionality of their legs to perform activities of daily living, but also emotional trauma due to this life-changing event.

Prosthetics have provided the option to replicate the missing limb, allowing for improvement in walking symmetry by mimicking the mechanisms of the foot, ankle, and shank, while applying the gait cycle (Gailey et al., 2008). Traditional passive prosthetic devices, however, trigger problems in other body limbs and increase the risk of developing degenerative joint conditions, resulting in pain in the knees, hips, lumbar spine, and other musculoskeletal problems (Gailey et al., 2008). These issues occur due to limitations of the prosthetic device to properly absorb the impact forces needed to mimic a symmetrical walking pattern for a transtibial amputee (Collins & Whittle, 1989; Gailey et al., 2008). Although more technologically advanced prosthetics can overcome these problems, the cost is very high. Patients opt to use passive prosthetic devices because they are cheaper despite the health problems they can cause due to prolonged use of these devices (Pitkin, 2009).

Unfortunately, existing research on prosthetic foot design has predominantly focused on comparing the effects of various prosthetic foot designs on comfort and gait functionality (Adamczyk et al., 2017). More attention must be paid to the shock-absorbing capabilities of prosthetic feet and their impact on the biomechanics of symmetrical gait patterns (Adamczyk et al., 2017). Exploring mechanical properties, such as foot stiffness, could offer a means to modify impact forces at different parts of the prosthetic foot to align it with the sound leg to improve gait symmetry (Berge et al., 2005). This approach, in turn, could have a positive impact on the activities of daily living of a transtibial amputee, such as standing, walking, jogging, running, and overall quality of life (Adamczyk et al., 2017; Berge et al., 2005). As stated by Major et al. (2011), designing a prosthetic with different rotational stiffness levels that can produce greater dorsiflexion compliance may provide an avenue for greater knee flexion and lower vertical forces on the prosthetic leg during early stance, minimizing the impact forces at heel strike to improve the symmetry of walking. Based on these concerns, this research work aims to design a prosthetic foot with adjustable stiffness levels at the heel, midfoot, and toe. The goal is to mimic the gait pattern of a sound leg as an avenue to improve the symmetry of the gait cycle for a transtibial amputee. This led the researcher to identify specific gaps in the current knowledge and formulate objectives to guide the study.

1.2 Research Gaps and Objectives

While there have been many commercial models, many of these designs are not able to fully address the issue of each transtibial amputee. This includes users' comfort when using their prosthetic to walk during their daily lives. Additionally, it has also been proven difficult for the models to adapt to an average user's weight to absorb the impact during the gait cycle. Based on this issue, this research aimed to develop a prosthetic foot with adjustable stiffness at the heel,

midfoot, and toe regions as an avenue to replicate the gait pattern of a healthy leg and enhance gait symmetry in amputees. The design focuses on flexibility, cost-effectiveness, and enhanced shock absorption to reduce lower extremity injuries and improve user comfort. In addition, the study focuses on utilizing affordable materials - such as thermoplastic polyurethane (TPU) and nylon - in the prosthetic design. Using 3D modeling software, various designs were simulated to assess their performance. Subsequently, static analysis was performed by applying an average human body load of 850 N to evaluate changes in stiffness across different material combinations.

The aim of this study led to the following goals when assessing the created prosthetic model and comparing it to commercial models, such as the Sierra, Otto Bock Trias, and the Wooden Foot:

1) Evaluating the created prosthetic design through simulations, by applying several material combinations, and analyzing the resulting force distribution.
2) Applying both the design and commercial models through a force tester in different foot positions, to create an effective comparison based on stiffness and absorbed energy.

1.3 Thesis Outline

The content of this thesis is divided into chapters for the foot design simulations and physical experimental measurements. Chapter 3 outlines the fundamentals of finite element analysis, while also detailing the determination of energy absorption ratios for the prosthetic designs.

Chapter 4 presents the experimental results and discussions for various commercial designs, including the Otto Bock Trias, Sierra, and Wooden foot. This chapter presents the findings from each testing protocol for the commercial prosthetic models with and without insoles on the

surface of the force tester and on the 15-degree wedge. The results include the average stiffness demonstrated by each model as well as the average computed ratio of energy absorption.

Chapter 5 employs a similar approach; however, this section primarily focuses on the design created using SolidWorks. It covers the results obtained from the simulations, including node force and node displacement, which are analyzed to identify the optimal version of the design and material combination. As in Chapter 4, this chapter lists the average stiffness and the computed ratio of energy absorption for each material combination presented, allowing for the determination of the best version for the presented design.

Chapter 6 contains the final section of this thesis. This section serves to conclude the thesis and summarize the key findings from Chapters 4 and 5. It also presents some recommended future work.

Additionally, Appendices A and B contain a list of the data obtained from the individual experimental tests reported in Chapters 4 and 5. Finally, Appendix C lists the equipment, instruments and software used in this thesis research.

1.4 Terminology

Transtibial Amputees: Individuals who have lost a limb below the knee.

Prosthetic: Artificial replacement for a missing limb.

Dorsiflexion: Walking stance, heel strike.

Plantarflexion: Walking stance, toes push from the ground.

Kinematics: Study of motion.

Kinetics: Study of the forces that cause motion.

Gait cycle: The complete cycle of a person's walking motion.

Gait pattern: The way a person walks.

Node: A point that represents a location on a finite element model.

Element: A small part of a finite element model that is connected to other parts via a node.

Mesh: The entire network of elements and nodes on a model.

SACH Foot: A prosthetic foot that does not have a moving ankle joint.

ESAR Foot: A prosthetic foot that is made to store energy during walking and release it to push off from the floor.

Loading phase: When force is applied to the foot.

Unloading phase: When force is removed from the foot.

Chapter 2: Literature Review

2.1 Prosthetic Development

This literature review examines the development, challenges, and potential improvements in the design of prosthetic devices specifically tailored to the needs of transtibial amputees. It also provides an analysis of the phases and kinetics of the gait cycle, offering a comprehensive understanding of how these factors influence prosthetic design.

2.1.1 Design challenges

Designing a prosthetic is a long and complex process that may come with several complications. To address these challenges, it is important to identify the issues that arise to improve future designs. Firstly, replicating human movement requires a thorough understanding of the gait cycle, encompassing both the stance and swing phases. Additionally, understanding the foot's anatomy, which is divided into three regions—the hindfoot (heel), midfoot, and forefoot (toe)—is crucial for replicating the foot's adaptive nature (Weerakkody et al., 2017). Choosing the right material is vital; it must be lightweight, durable, and sufficiently stiff while ensuring it does not irritate the user's skin. Lastly, every patient has different needs, making adaptability an essential consideration (Manz et al., 2022). While designing a prosthetic presents various challenges, overcoming these obstacles can lead to more effective solutions, ultimately making a difference for many people.

2.1.2 Design considerations

Foot Anatomy

The primary purpose of a prosthetic foot is to replicate the natural motion of a real foot, enabling the gait cycle and providing the necessary mobility and stability for daily living activities. This goal can be achieved by examining the static and kinetic properties of the prosthetic material in absorbing ground reaction forces to mimic a human foot to maintain proper posture during ambulation (Weerakkody et al., 2017; Zelik et al., 2011). The human foot is highly flexible and elastic, allowing for a range of actions such as walking, running, climbing, jumping, and even standing on tiptoe. To replicate these capabilities, it is essential to understand the muscles and joints of the foot's three regions: the hindfoot, midfoot, and forefoot. The hind foot consists of the calcaneus and talus. The midfoot consists of the navicular, cuboid, and the three cuneiforms. The forefoot consists of the metatarsals and phalanges. These regions contain five major joints: the ankle joint, the subtalar joint, the tarsometatarsal joint, the metatarsophalangeal (MTP) joint, and the interphalangeal joint, as shown in Figure 2.1 (Weerakkody et al., 2017).

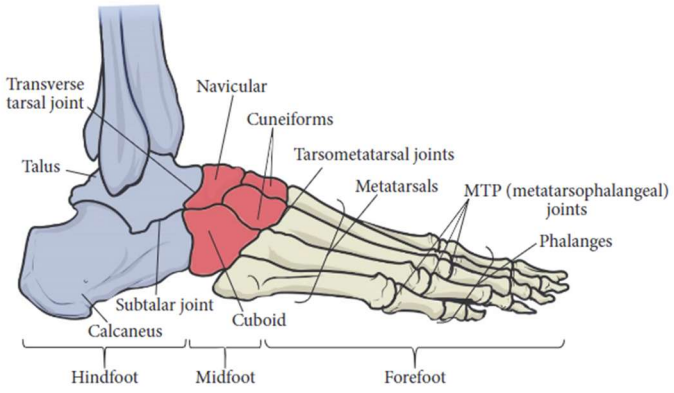

Figure 2.1: Foot Anatomy Diagram. Adapted from Figure 3, Weerakkody et al. (2017).

Joint Function

Each joint contributes to the foot's overall function. The ankle joint enables dorsiflexion and plantarflexion, while the subtalar joint allows for inversion and eversion. The tarsometatarsal joint connects the midfoot to the forefoot, facilitating stability. The metatarsophalangeal and interphalangeal joints are crucial in adjusting the foot's arch to different ground surfaces. Understanding each joint's specific motions and roles allows for more effective replication of the foot's stability and mobility through prosthetic design (Weerakkody et al., 2017).

2.1.3 The human gait cycle

Understanding the human gait cycle is essential for replicating a human foot and representing a person’s natural motion when walking on a ground surface (Kharb et al., 2011). In a gait cycle, each foot goes through the stance and swing phases as shown in Figure 2.2. Each phase can then be split into several subphases representing the foot as it leaves the ground and swings forward (Kharb et al., 2011). During the cycle, there is a period known as single support, during which one foot is off the ground, with the person's weight supported by the other foot. This happens for each leg. However, when both feet are on the ground, this is called the double support phase, which accounts for 10% of the human gait cycle, while the remainder is divided between the swing and stance phases (Kharb et al., 2011; Pirker et al., 2017).

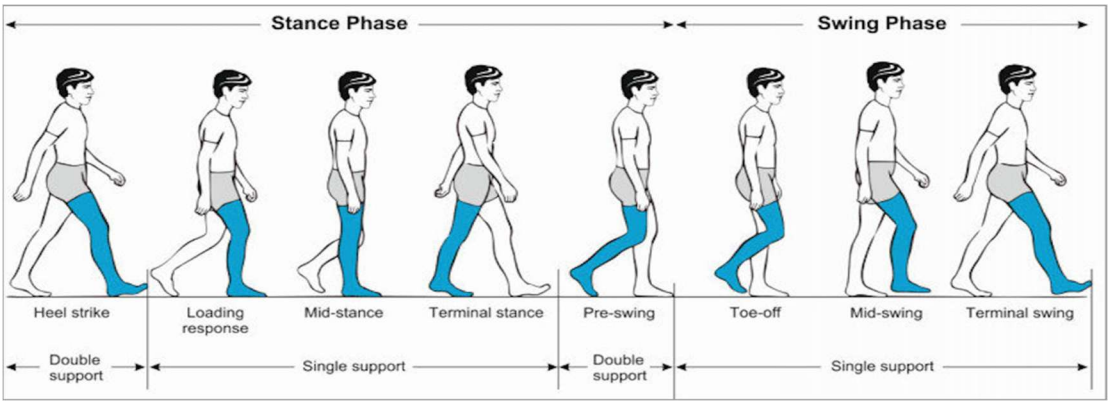

Figure 2.2: Phases of the Gait Cycle. Adapted from Figure 1, Pirker et al. (2017).

Stance Phase

This phase of the human gait cycle represents the foot before it leaves the ground. It consists of four segments, beginning after the initial contact of the heel. First is the loading phase, where the body weight is transferred onto the stance limb. Next, the heel acts as a rocker, and the knee flexes to absorb shock. Then comes the mid-stance, where the body is supported on the stance foot while the opposite foot swings past it. This is followed by the terminal stance, during which the heel of the stance foot begins to elevate and ends when the opposite foot touches the ground, completing single support (Kharb et al., 2011). Subsequently, the opposite foot touches the ground, marking the beginning of double support due to both feet being on the ground. From this point, the weight of the stance foot is transferred to the opposite foot, allowing the stance foot to swing forward, thus ending the pre-swing phase and initiating the swing phase (Kharb et al., 2011; Pirker et al., 2017).

Swing Phase

During the swing phase of the human gait cycle, the foot is in the air. This phase consists of three segments: the initial swing, mid-swing, and terminal swing (Kharb et al., 2011; Pirker et

al., 2017). In the initial swing, the foot lifts off the ground and continues until the opposite foot is placed in its mid-stance. The mid-swing involves the limb advancing with an extended knee and the ankle dorsiflexing, and the foot swinging forward to exchange places with the opposite foot, ending in front of the body. Lastly, in the terminal swing, the limb finishes advancing while the opposite limb is in its terminal stance. The swing phase completes when the foot of the advancing limb lands on the ground (Kharb et al., 2011; Pirker et al., 2017). To effectively replicate the foot's walking patterns and symmetry, it is crucial to measure the ground reactions at the foot.

2.1.4 Ground reaction forces and walking symmetry

Ground reaction forces (GRFs) are the forces exerted by the ground on the human body during movement. In human gait, these forces are crucial for understanding the dynamics of walking (Winter, 1991). These forces are commonly measured using a force plate, as shown in Figure 2.3, which provides data on three vector components that make up the GRFs. These vectors include a vertical force component and two shear components referred to as anterior-posterior and medial-lateral forces when performing a gait analysis (Marasovic et al., 2009).

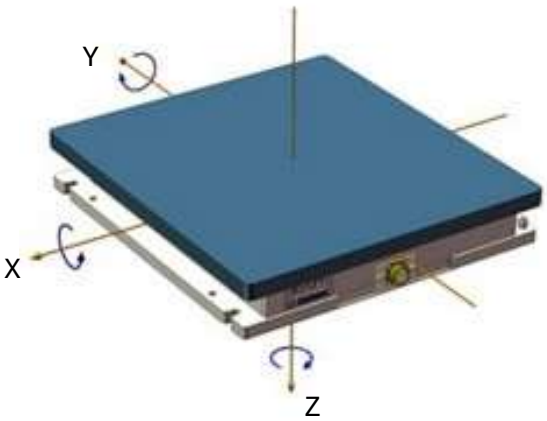

Figure 2.3: Ground Reaction Force Platform. Adapted from Applicazioni pratiche e benefici dell'utilizzo delle pedane di forza in riabilitazione - News Ability Group fisioterapia e riabilitazione - Ability Group

Vertical GRF

The vertical GRF has the highest magnitude during the gait cycle, reflecting the upward and downward acceleration of the body's center of mass (Marasović et al., 2009). As shown in Figure 2.4, the force starts at heel strike, when the foot first touches the ground, and initially registers zero force (Marasović et al., 2009). As the body's weight transfers onto the foot, the force rapidly increases, peaking at about 107% of body weight due to gravitational and inertial forces acting together (Marasović et al., 2009). During the mid-stance phase, the curve dips as the center of mass lowers, reducing the force to around 85% of body weight (Marasović et al., 2009). A second peak occurs as the body prepares for forward motion in the terminal stance phase, with the force reaching approximately 105% of body weight. The GRF then sharply declines to zero as the body weight shifts to the opposite leg during pre-swing (Marasović et al., 2009). Analyzing vertical GRF, especially at heel strike, is vital for assessing the symmetrical walking patterns of a transtibial amputee (Marasović et al., 2009).

The following text describes three graphs, Figures 2.4, 2.5, and 2.6, which illustrate the results of ground reaction forces: vertical (Fz), anteroposterior (Fy), and mediolateral (Fx). Each figure features both a vertical and a horizontal axis (Vaverka et al., 2015). The vertical axis indicates the magnitude of ground reaction forces (GRF) in Newtons. The results vary according to the movement and stance phase of the gait cycle. Meanwhile, the horizontal axis represents time (t), highlighting how GRF changes during the stance phase, which encompasses the braking and propulsion phases, double support, and the total duration of the stance phase (Vaverka et al., 2015).

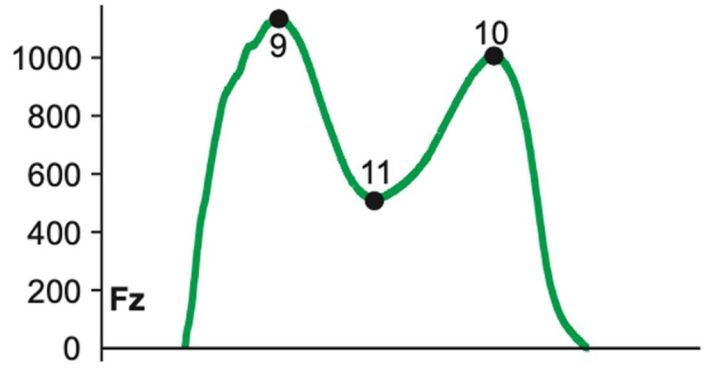

Figure 2.4: Vertical GRF. Adapted from Figure 1, Vaverka et al. (2015).

The Anterior-Posterior GRF

The anterior-posterior GRF is the horizontal component of the ground reaction force, aligned with the direction of walking (Vaverka et al., 2015). Unlike the vertical GRF, which primarily counteracts the body's weight, this horizontal force is smaller, generally peaking at about 20% of body weight (Vaverka et al., 2015). As shown in Figure 2.5, at the start of the gait cycle, a negative anterior-posterior force appears as the foot makes initial ground contact and begins to decelerate the body's center of mass. As the stance phase progresses, this force shifts to a positive value, indicating the forward propulsion that moves the body ahead. The force then gradually drops to zero as the foot lifts off the ground during the toe-off phase (Vaverka et al., 2015). An equal magnitude of the braking and propulsive forces is an indication of a symmetrical walking pattern.

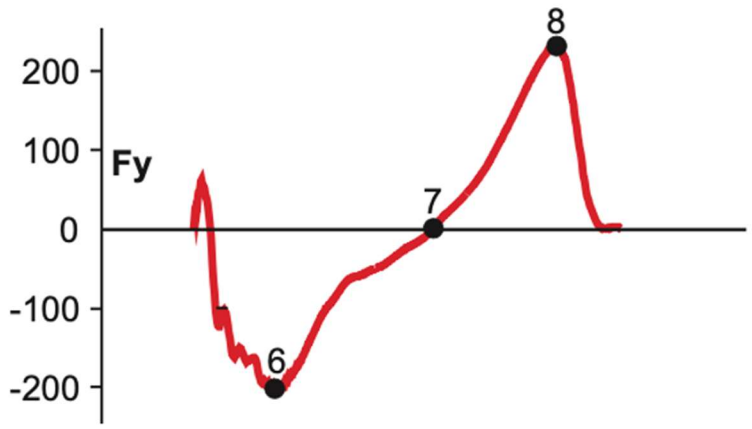

Figure 2.5: Anteroposterior GRF. Adapted from Figure 1, Vaverka et al. (2015).

Medial-Lateral GRF

The medial-lateral GRF is influenced by the position of the center of mass relative to the stance foot. This force initially spikes as the center of mass shifts laterally during a heel strike (Marasović et al., 2009). As shown in Figure 2.6, the force then transitions into a medial direction and gradually decreases throughout the stance phase until it reaches zero (Vaverka et al., 2015). This force is essential for analyzing lateral stability, center of mass acceleration, and limb positioning during walking (John et al., 2012). Abnormalities in this force component may indicate an asymmetrical gait pattern (Yazji et al., 2015).

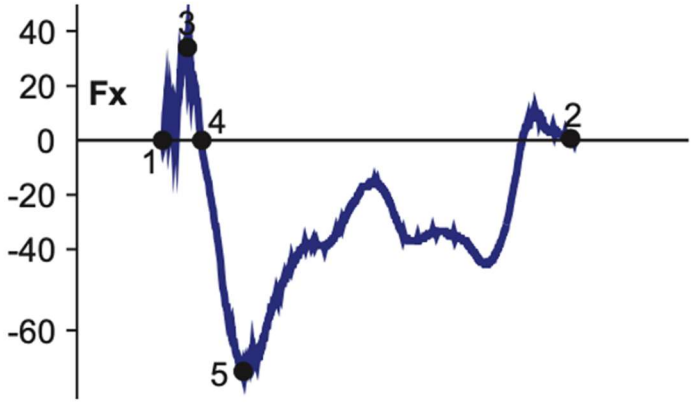

Figure 2.6: Mediolateral Ground Reaction Forces for Right or Left Foot. Adapted from Figure 1, Vaverka et al. (2015).

2.1.5 Human comfortability

When designing a prosthetic foot, it is important to ensure that it meets the user's personal needs during motion. It has been observed that an amputated leg can significantly impact a person's social life and lead to emotional depression (Burger et al., 1997). This outcome highlights the importance of addressing individual needs when creating a prosthetic for the leg, allowing users to achieve goals such as independent walking and self-sufficiency (Fosse et al., 2009). These needs can vary depending on functional, emotional, ergonomic, and other specific requirements.

Functional requirements

In terms of functionality, it is shown that people with amputation to the lower limb desire prosthetics that allow them more adaptability when performing activities of daily living, such as getting in and out of a vehicle (Legro et al., 1999; Van Schaik et al., 2022). Adding knee joints that lock and unlock may be a possible solution to allow amputees to bend or kneel to meet some of these needs in daily living. Additionally, people have expressed the desire to use prosthetics for walking long distances without getting tired and spending too much energy. A potential solution that has been proposed to meet this demand is a powered knee ankle (Chin et al., 2006; Kaufman et al., 2008; Gardinier et al., 2018; Seymour et al., 2007). Another approach, however, is the design of a prosthetic foot that minimizes impact forces and uses the absorbed force to propel the body forward during the walking cycle. This approach allows the amputee to expend less energy when walking and multi-tasking during daily life activities (Edhe et al., 2000).

Emotional Requirement

When applying a prosthetic to a person, it is important to consider how they feel emotionally about their new experience. It is revealed that when using their new prosthetic limb,

walking can be challenging due to a loss of confidence and the fear of falling, causing amputees to be self-conscious about every step on any terrain (Burnfield et al., 2012). Microprocessor-controlled knee joints have been suggested to improve stability (Burnfield et al., 2012; Kaufman et al., 2007). However, users may need a prosthetic, which is simpler and more effective in improving walking symmetry. In addition, with this type of prosthetic, they may feel more confident in public, as body image has been shown to affect their social life due to potential judgment based on their appearance when using prosthetics (Legro et al., 1999; Thompson et al., 1984; Van Schaik et al., 2022). In essence, it is important that they feel accepted when dealing with people during their social life.

Ergonomic Requirements

When designing a prosthetic, it is crucial to ensure that the wearer feels comfortable and can easily put it on. The design of the socket is essential with a proper distribution of forces as it affects the user's performance to maintain balance and control during daily activities such as driving, walking, and standing (Wong et al., 2020).

One specific design amputees use is the Total Surface Bearing sockets, which have proven to provide comfort by spreading the load over the entire limb instead of focusing on a single area (Highsmith et al., 2007). Hence, the socket design must provide a comfortable feeling for the amputee when wearing it. This outcome can be accomplished by using a smoother texture for the device to reduce pain and skin irritation in the amputated area (Paternò et al., 2018).

It is also essential for the amputee to easily put on and remove the prosthetic device, which contributes to his/her comfort. Various designs, such as magnetic suspension systems or pin-locks, have been proposed and proven to provide overall satisfaction for putting a prosthetic on an

amputated limb (Gholizadeh et al., 2016). Additionally, the weight of the prosthetic when attached to the amputated leg is a concern in terms of comfort, as some people may find it too heavy. One possible solution to address this issue is to provide sensory feedback controllers, which can help the patient adjust their mechanical limb more easily during their daily activities to minimize muscle effort (Preatoni et al., 2021). Despite several advanced prosthetic options, many patients do not opt for these new technologies due to their high cost. Moreover, patients are required to replace their prosthetic devices every four to six years, leading to higher long-term costs with new prosthetic technologies (Pitkin, 2009). Consequently, many patients continue to use older passive prosthetic devices despite the discomfort that arises from prolonged use (Pitkin, 2009). This issue highlights the need to select materials that are effective to create simpler, lighter, and more affordable prosthetic foot designs.

2.1.6 Types of materials

When it comes to designing and creating prosthetic sockets and feet for lower limb injuries, material selection plays an important role in achieving the necessary clinical and functional requirements. For the materials to be effective, they need to be flexible, rigid, durable, and safe, allowing them to meet every patient's needs. For example, relieving pain, controlling deformities, and protecting tissues require materials that can adapt to the body’s movement and limited joint motion (Hsu et al., 2008). Prosthetics must be sufficiently strong to withstand the stresses of weight-bearing and gait, such as the tensile, compressive, and tangential forces of a regular limb (Hsu et al., 2008).

Rigid Materials

Thermostable or thermoplastic polymers are the preferred materials for creating prosthetic rigid sockets. Thermostable polymers, such as polyester resins, epoxy, and vinyl ester, are known for their ability to maintain stability and rigidity under extreme temperatures, preventing them from melting (Arun et al., 2015; Van der Spoel et al., 2015; Wise et al., 1996). However, these materials require a complex manufacturing process. On the other hand, thermoplastic polymers, like polyethylene (PE) and polypropylene (PP), have high molecular weight and can be easily molded. These materials are very useful for designing prosthetics as they can be adapted to the specific needs of each patient. For example, the PE is very flexible, lightweight, and can be molded easily, which allows it to be used in prosthetics that require flexibility (Hsu et al., 2008; van der Spoel., 2015). When it comes to the PP, they are mostly applied to the sockets that require more rigidity since they provide high tensile strength, stiffness, and hardness. However, PP can easily be deformed, and its surface is affected by heat (Hsu et al., 2008; Van der Spoel., 2015).

Fiber Materials

Fiber materials are another consideration when designing prosthetic sockets. These materials act as reinforcing agents to strengthen the design and improve the performance of the mechanical properties of the materials, such as strength, stiffness, and even hardness of the prosthetic structure (Hsu et al., 2008). Fiber materials include, for example, fiberglass and carbon fiber reinforcements. Fiberglass is usually in prosthetics that utilize PE and high-density PP material, which significantly improves the device's mechanical properties (Scholz et al., 2011). The carbon fiber is usually applied within prosthetics that utilize thermoplastic composites, which grant additional stiffness and resistance while reducing the weight of the device (Van der Spoel E., 2015). This feature reveals the effectiveness of these reinforcing agents when applied to the sockets of the prosthetic devices.

Soft Interfaces

Soft interfaces are used to provide the cushioning and filling within a prosthetic device. A special type of foam made from polyurethane is used to absorb shock, which has several densities and may be applied in several areas based on the required flexibility and compressive strength (Wise et al., 1996). When dealing specifically with lower limbs, it is common to use silicone gel and thermoplastic elastomers by applying them within soft cushioning layers known as liners (Laferrier et al., 2010). Silicone gel liners, known to be smooth and adaptable when under load, can accommodate the area with the missing limb. The silicone thermoplastic elastomers are considered to be crosslinked, allowing this material to be more rigid and durable and have more compressive strength, shear, and tensile stiffness than silicone gel in prosthetic foot designs (Sanders et al., 2004).

2.1.7 Prosthetic foot designs

Prosthetic foot designs, whether for amputees or robots, aim to replicate the function and movement of a natural foot. For amputees, prosthetic feet range from simple models that offer basic support to more advanced and costly designs with sensors and microprocessors that adapt to the user's movements, helping create a smoother and more natural walking experience.

Soft Foot

The soft foot design proposed by Piazza et al., (2016), for example, was meant to enhance the stability of humanoid robots when they encounter uneven terrain and obstacles. This concept can be applied to individuals who require a prosthetic lower limb. Initially, traditional rigid flat feet were suggested, which were effective on flat surfaces but struggled with obstacles due to reduced contact area and the need for additional stability from the ankle (Bicchi et al., 2011). A

potential solution is the compliant flat feet, which incorporate soft layers beneath the foot to absorb obstacles while maintaining contact area. However, achieving sufficient stiffness for using ankles and passive stability is challenging (Li et al.,2008; Najmuddin et al., 2012; Tsagarakis et al., 2011). Some studies advocate for adaptive foot mechanisms, which combine the stability of rigid feet with the flexibility to adapt to rough terrain. Nonetheless, this approach introduces a trade-off between stability and shock absorption (Davis & Caldwell., 2010; Kang et al., 2010; Kuehn et al., 2012). By considering the balance of stiffness, stability, and adaptability in foot design based on the evolution of natural feet, it is possible to enhance the performance of prosthetics across various terrains.

To tackle this issue, a soft foot design was proposed by Piazza et al., (2016), which was modeled after key features of the human foot. The design mimics the foot's adaptability, energy storage, and stabilization by replicating its structural and functional anatomy. The soft foot essentially uses a mechanical structure that takes inspiration from the distribution of the bones in the arches of the human foot, such as the longitudinal and transverse arches, specifically the windlass mechanism (Hicks, 1954).

Additionally, the design as shown in Figures 2.7 and 2.8 consists of modular and elastic components that provide flexibility and compliance under low loads, and rigidity under increased weight, proving that it can support the user's weight (Seo et al., 2009). The design features five parallel sagittal mechanisms that provide stability on uneven terrain and springs that recreate the elasticity of the plantar fascia to absorb shock when walking (Piazza et al., 2016).

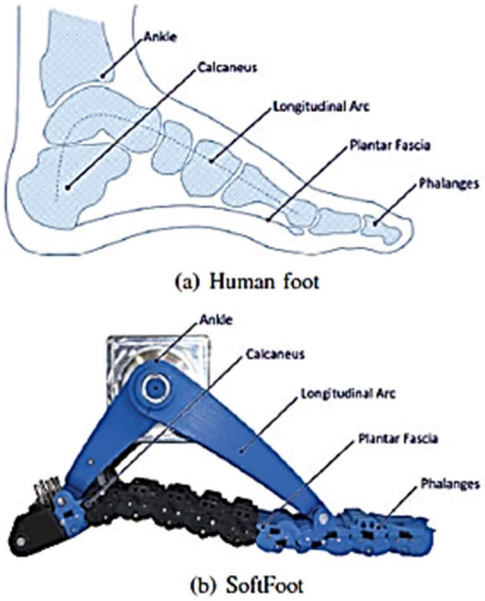

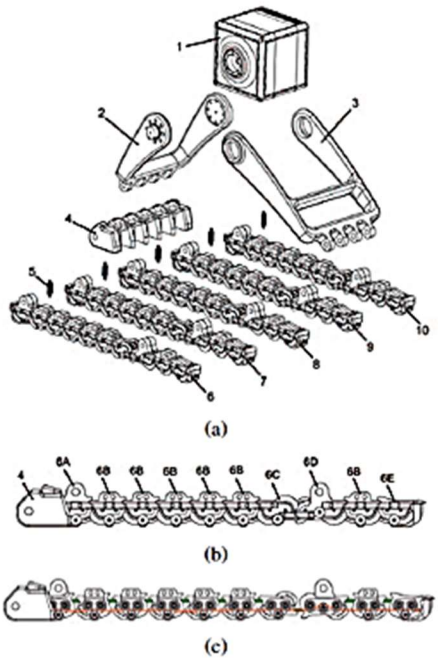

Figures 2.7 (left) and 2.8 (right): Soft Foot Design (Left: Human foot and Softfoot; Right: 3D CAD Model of Softfoot). Adapted from Figures 4 and 7, Piazza et al. (2016).

The design of the prosthetic may be effective initially, but certain challenges need to be considered over time. Firstly, while the modular and elastic components of the design proposed by Piazza et al., (2016) offer flexibility, prolonged and repeated use may lead to loss of flexibility. Balancing both elasticity and rigidity is crucial, as an excessive amount of elasticity may lead to the limb's inability to support sufficient weight, while too much rigidity may hinder its ability to adapt to different terrains (Piazza et al., 2016). Another issue is that the current design may not fully replicate a human foot, affecting its ability to adapt to uneven terrain and provide comfort. The design utilizes parallel sagittal mechanisms, allowing it to adapt to different surfaces and obstacles, but more research is required for full replication of the human foot adaptability by designing prosthetics with proper hindfoot and forefoot stiffness. Addressing these challenges can lead to improved designs that offer better stability while walking.

Hindfoot and forefoot stiff foot prostheses

For this prosthetic design proposed by Adamczyk et al., (2017), the goal was to understand the connection between the device's mechanical properties and the gait biomechanics. The researchers stated that this approach leads to the understanding of different foot stiffnesses since many patients have certain preferences regarding the forefoot and hindfoot when walking. Varying stiffness may improve comfort and the gait function of the limb; however, the researchers advocated that this sector still has its limits in knowledge when it comes to mechanical properties, which leads to difficulties when creating prosthetics for different patients (Adamczyk et al., 2017). The researchers also added that based on previous research, most patients prefer prosthetics with a compliant hindfoot (Lehmann et al., 1993; Raschke., 2015) and moderate forefoot stiffness (Klodd et al., 2010; Raschke., 2015), which allow for sufficient impact absorption and flexibility for the springs. Finally, Adamczyk et al., (2017) stated that the effects of different types of stiffness, such as angular, forefoot, and whole-foot stiffness, with varying dorsiflexion and plantarflexion values have been tested by various researchers. However, there is still insufficient information when testing the mechanical properties of prostheses with human biomechanics, making it difficult to understand the relationship fully. This is one reason that research should focus on the gait outcomes with the changes in prosthetic foot stiffness, which could allow for better-designed prosthetics that meet different individuals' needs.

Due to these concerns, Adamczyk et al. (2017) proposed a design for a new prosthetic foot, as shown in Figure 9, that utilizes a stiff metal structure made of aluminum 7075-T6. The design includes interchangeable hindfoot and forefoot components with the required flexibility. The stiffness for the hindfoot and forefoot can vary, ranging from 22 to 69 N/mm for the hindfoot and 29 to 90 N/mm for the forefoot (Adamczyk et al., 2017). During the experiment, users walked on

a treadmill at five different speeds using five combinations of stiffness for both the hindfoot and forefoot. This approach allowed for measurements of body motion, foot keel motion, and required ground reaction forces under each leg. The user's height and weight are considered in adjusting the prosthetic, which leads to adjustments in the forefoot keel location of the pyramid adapter and the side keel mounting blocks (Adamczyk et al., 2017). This adjustment allows the length of the foot to be 13%, while the pyramid adapter is 31 to 34% of the foot length to the hindfoot. This model allowed for testing several variations of the hindfoot and forefoot stiffness and to view the relationship of the mechanical parameters with the behavior parameter of walking speed (Adamczyk et al., 2017). This information provides a better understanding of the relationship between mechanical properties and human biomechanics.

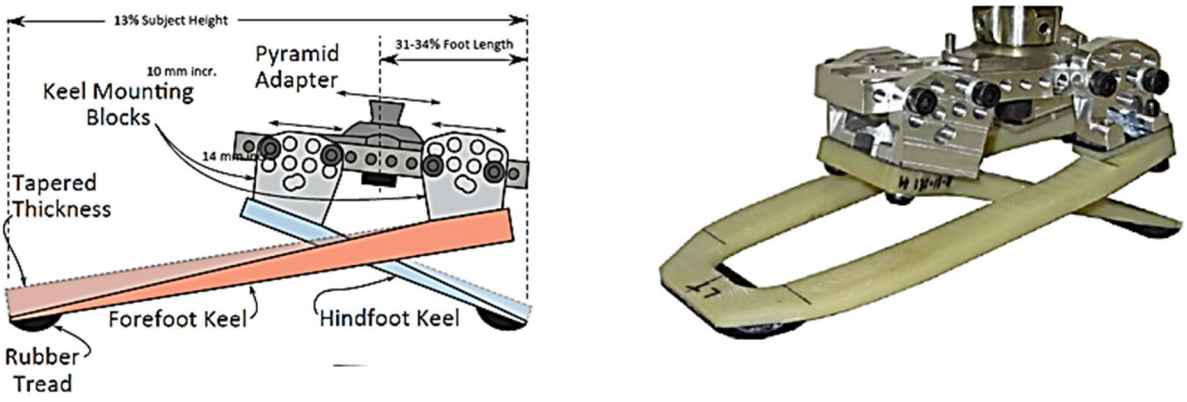

Figure 2.9: Hindfoot and Forefoot Design. Adapted from Figure 1, Adamczyk et al. (2017).

While this design may be effective, especially when dealing with the stiffness of the hindfoot and forefoot. The design may not account for most, if not all, interactions between mechanical properties and human biomechanics for different users (Adamczyk et al., 2017). This is because every patient has different conditions, such as different gait patterns, muscle strength, and adaptation to certain prosthetic limbs, which may affect how a patient reacts to several

variations of stiffness (Adamczyk et al., 2017). It may also not be able to fully replicate the capabilities of a human foot, as it may struggle to adjust to various terrains, including uneven terrain with obstacles that could affect the patient's walking dynamics (Adamczyk et al., 2017). This concern highlights the need to use other techniques, such as finite element analysis, to better understand the behaviors of the material used in the prosthetic design (Adamczyk et al., 2017).

2.2 Finite element analysis

Application of FEM

While the finite elements method (FEM) allows the possibility of understanding the mechanical behaviors of materials and structures within the engineering sector, it has also been applied to many complex structures within biomechanics (Prendergast, 1997; Schuller-Gotzburg et al., 1999; Zhang, et al., 1998). FEM has permitted the analysis of human body structures, including the bones, tissues, and organs, due to modern-day technology (Prendergast, 1997; Schuller-Gotzburg et al., 1999; Zhang et al., 1998). This approach has opened up a range of possibilities, such as designing prosthetics. The FEM enables the analysis of stress distribution, deformation, and material behavior for simulating real-life situations where loads are applied to structures (Prendergast, 1997; Schuller-Gotzburg et al., 1999; Zhang et al., 1998). In the case of prosthetics, several designs have used FEM, allowing the model to be adaptable to satisfy the required needs of the average user; however, improvements are always possible.

FEM application in prosthetics

The FEM allows designers to replicate the essential movement needs of patients by utilizing the elastic properties of flexible materials. (Bonnet et al., 2012). When designing a prosthetic, the FEM has allowed the analysis of asymmetrical stress to better understand the

behavior of the prosthetic device during the gait cycle, and provide the stress, strain, and displacement distribution within each stance (Figueroa et al., 2009). These FEM measures allow the structure of the device to be modified using the results obtained from each distribution. For example, stress distribution could involve reducing the maximum stress by adding material in weak areas or removing material in less needed areas to reduce weight, add flexibility to the prosthesis (Figueroa et al., 2009), and energy-storing (Bonnet et al., 2012).

FEM applied with different types of prosthetics

Bonnet et al. (2012) conducted a study in which the researchers attempted to combine the boundary conditions of the gait analysis with a finite element model of a prosthetic foot to calculate stress, strain, and strain energy from the prosthetic model shown in Figure 2.10 within the stance phase. The process consisted of several stages. The first stage involved constructing the finite element model by defining the appropriate geometry, material properties, and boundary conditions. This resulted in a J-shape design that was connected to a split sol. The next step was to apply the boundary conditions corresponding to various walking speeds and fast walking speeds. This information led to the final stage, which entailed calculating the prosthetic foot's stress, strain, and strain energy (Bonnet et al., 2012). The J-shape (Figure 2.10) was designed using SolidWorks and later imported into Ansys for meshing with brick-shaped elements (Bonnet et al., 2012). The material used exhibited linear and isotropic properties. For the foot portion of the design, carbon and glass fibers were utilized, which had a Young’s modulus of 35,000 MPa and a Poisson's ratio of 0.3. The model contained approximately 9,006 nodes and 4,574 elements (Bonnet et al., 2012).

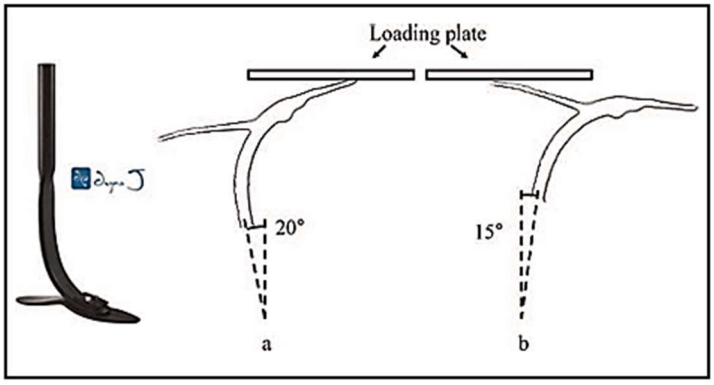

Figure 2.10: J-shaped Prosthetic Foot. Adapted from Figure 1, Bonnet et al. (2012).

In this study by Bonnet et al. (2012), mechanical testing was conducted on a standard prosthetic foot using a testing machine called the Instron. This machine simulated a 20-degree plantar flexion push-off and a 15-degree dorsal flexion orientation for heel loading, applying a constant load rate of 250 N/s. The test was then repeated for the finite element model (Bonnet et al., 2012). The obtained results from both the regular prosthetic and finite element models (Figure 2.11) were compared using the load-displacement curves to validate the finite element model.

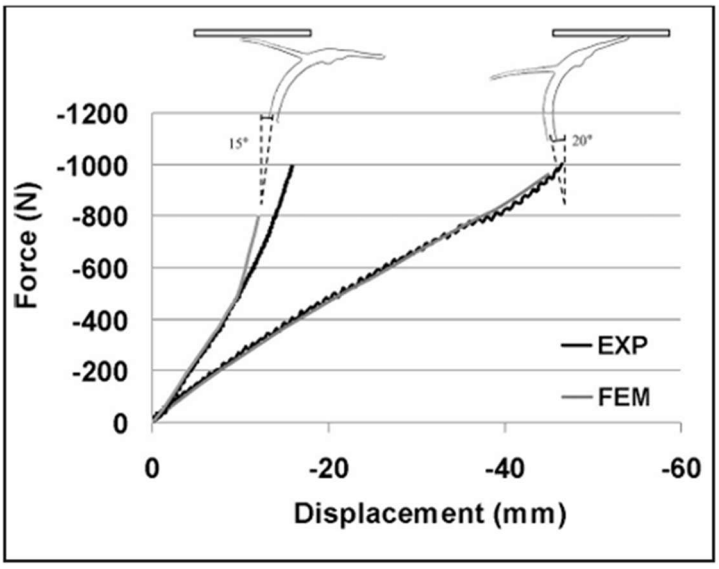

Figure 2.11: Load-Displacement Curves. Adapted from Figure 4. Bonnet et al. (2012).

Bonnet et al. (2012) obtained the necessary boundary conditions of the gait analysis from a patient who had undergone an amputation several years prior. Gait analysis was conducted over several trials to capture the required data, including the ground reaction forces applied during the experiments. (Bonnet et al., 2012). This information made it possible to simulate the stance phase of the gait cycle, where the stress, strain, and strain energy of the prosthetic foot were calculated. This approach provides an avenue to create lightweight prosthetics for different populations.

Dynamic Energy Return Analysis of Prosthetic Feet

In countries like Venezuela, there are at least 900.000 people who have a disability, which makes it difficult when many of them require prosthetics since they can only rely on imported devices to meet their needs (Figueroa et al., 2009). However, the selection of prosthetics has evolved over the years, leading to lightweight prosthetics created with materials such as polymers and carbon fiber composites (Figueroa et al., 2009). A design stated by Figueroa et al. (2009), as shown in Figure 2.12, aims to provide a dynamic response without the use of joints, effectively meeting the needs of patients classified under level 2 functionality as defined by the U.S. Health Care Financing Agency (HCFA) (Figueroa et al., 2009). Dynamic response return feet are designed to store and release energy during the gait cycle. (Hafner B.J, 2005). This specific type of prosthetic is desired in the market, as most users have expressed a preference for energy-return prosthetics (Hsu M, 2006). This user preference led to the acquisition of essential information such as kinematics, kinetics, and energy expenditure of a prosthetic, as it directly impacts the user's performance. However, in the absence of a prototype, it becomes necessary to employ an experimental method stated in Figueroa et al. (2009). This method requires a numerically modeled foot that can measure the non-linear and time-dependent properties of the components. This

information allows the design to align with the mechanical properties required to meet the needs of a user for a standard prosthetic (Hafner B.J, 2005).

In the foot design proposed by Figueroa et al. (2009), the design process involved utilizing a 3D parametric model of a prosthetic foot where the gait cycle was simulated to perform a stress analysis while applying FEM to determine the stress, strain, and displacement distribution. These measures allow the geometry of the foot design to be modified to address problems such as maximum stress reduction, reduced weight, and increased flexibility. After conducting several stress analyses, material was either added in specific areas or removed from regions with no stress (Figueroa et al., 2009). Each analysis utilized the corresponding load and boundary conditions for heel and forefoot contact during the gait cycle. This process led Figueroa et al. (2009) to the next phase, where the model's weight was optimized. For this, the finite element method alongside a technique known as design of experiments (DoE) was implemented to assess all factors, including geometric variables and their interactions that impact the design. Subsequent experiments were conducted based on these analyses, resulting in a weight reduction of 9.5%. The final weight for the design in the toe area was 592 grams (Figueroa et al., 2009).

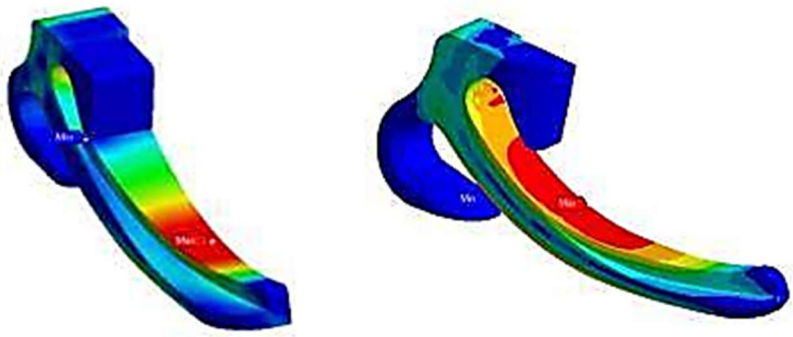

Figure 2.12: Stress Analysis of the Prosthetic. Adapted from Figure 1, Figueroa et al. (2009)

Design Requirements for Ankle-Foot Prosthetics with Finite Element Analysis

Any design of a prosthetic foot requires the examination of the normal human foot, as illustrated in Figure 2.13. This examination is crucial for understanding its biomechanical behaviours and the internal stresses and strains experienced during movement (Hamzah et al., 2018). This process is often challenging and typically requires computer models and finite element analysis. These tools enable researchers to model structures with complex geometry and material properties, along with the necessary boundary conditions to simulate the necessary load distribution, stress, strain, and absorbed energy (Hamzah et al., 2018). Overall, this process has enabled numerous researchers to achieve success using finite element analysis for creating the necessary geometric models that fulfill the design requirements, facilitating proper foot analysis.

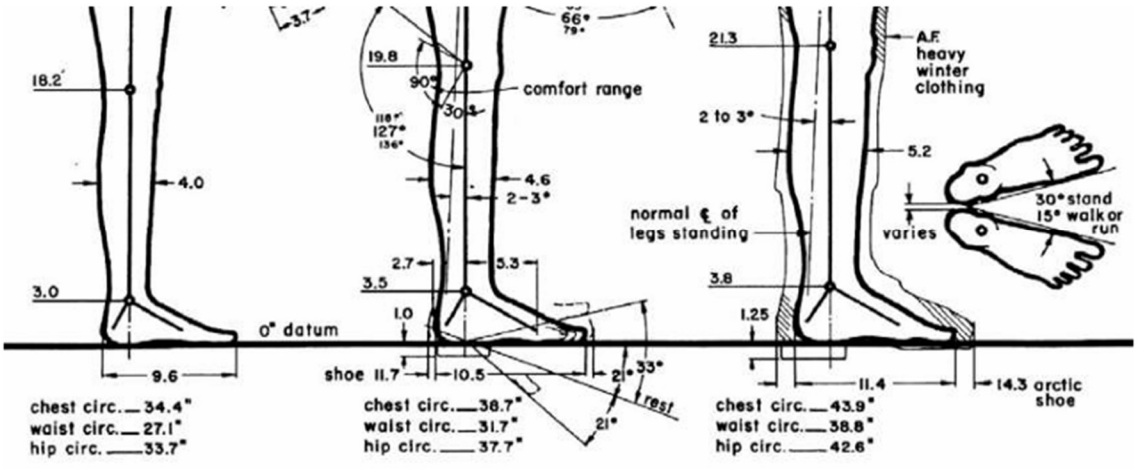

Figure 2.13: Analysis of Human Lower Limb. Adapted from Figure 1, Hamzah et al. (2018).

When designing a prosthetic foot, Hamzah et al. (2018) considered several factors to ensure the device functioned properly. Some factors included the ISO Standard, which essentially defines the procedures used for testing the prosthetic leg and foot systems, leading to accurate and usable results. Next, the researchers used the anthropometry, which essentially involves human

measurements to obtain the necessary body sizes and shapes to design the prosthetic. The researchers used the method named roll-over shape, which analyzes the function of the ankle-foot mechanisms. This method essentially helps study the position of the foot when walking forward (Hansen et al. 2004). Hamzah et al. (2018) also looked at the biomechanics of the ankle joint when influenced by a dynamic load while performing a gait cycle, which provided an understanding of how to replicate the human movement for a prosthetic foot. This biomechanics information was possible by examining the stages of the gait cycle such as controlled plantarflexion, controlled dorsiflexion, and powered plantarflexion. By utilizing all these methods, it was possible for the researchers to design a prosthetic foot with CAD software.

Once the prosthetic model was designed, Hamzah et al. (2018) applied finite elements and considered this process essential to pre-evaluate either the entire design or a separate part, allowing them to save time and money during the development process. The researchers performed this analysis before proceeding to the experimental stages using Ansys simulation software to determine the most suitable material to meet the required needs of the design. In this situation, the researchers selected epoxy carbon fiber woven wet material for their design.

To evaluate the material's performance when used in a prosthetic foot, Hamzah et al. (2018) conducted three Finite Element analysis tests, which included the heel test, the keel test, and the vertical loading test under a load of 300 N. The heel test evaluated the heel strike during the gait cycle. It was found that the stress and strain observed from the model remained within the limits of the material properties and demonstrated good safety factors. The keel test evaluated the toe stage during the gait stance phase, contributing to the forward motion of the human body. The results indicated that both stress and strain remained stable, while also demonstrating favorable deformation that reflected the dynamic response. Finally, the vertical load test, which essentially

replicated the stance phase of the gait cycle, revealed that the design did not deflect sufficiently to meet the requirements of the test. However, the stress remained within the safe range.

2.3 Analysis of Patients' Requested Features

Group Interviews

To achieve an effective design, it is important to observe the most important needs of patients, which allows researchers to have a better understanding of the physical and psychological challenges that patients may face throughout their daily lives. This information can be obtained by conducting interviews with patients. On that note, Schaffalitzky et al. (2011) conducted a study with 24 participants, each of whom suffered an above-the-knee amputation and were placed within six groups. A series of questions was posed to each group, revealing their top priorities. The topics covered included achieving independence, avoiding the use of a wheelchair, maintaining balance and safety, enhancing quality of life, and reaching personal potential. According to Schaffalitzky et al. (2011), this approach provides each patient with an achievable goal. However, individual priorities may differ, particularly regarding physical outcomes, where maintaining balance and safety, as well as avoiding wheelchair use, are critical.

Schaffalitzky et al. (2011) also stated that for others, psychological well-being is crucial, which includes independence and self-reliance in their own home instead of being in a care facility. The definition of independence is viewed differently by service providers and users. Service providers view it as functional independence, while users perceive it as a psychological outcome—the feeling of relying on themselves daily (Schaffalitzky et al., 2011). This difference highlights the importance of discussing the situation with the user to determine the necessary course of action in the prosthetic design. This strategy allows for the relevant goals to be applied to the patient,

while also making sure that the patient completely understands the procedure to obtain the required prosthetic (Siegert et al., 2004).

Priorities for Prosthetic Users

The impact of limb loss on an individual's lifestyle is substantial, underscoring the necessity of understanding the specific needs of patients. A survey was conducted for several prosthetic users, which revealed that the most desired aspect was better skin care when wearing the prosthetic leg since users experience many conditions, such as redness, swelling, blisters, and bad smell, fungal infections, open sores, and tumor cysts. To allow the user to live a normal life, several questions must be asked such as general information on the prosthetic use, its functionality, and the patient's comfort level. Many prosthetic users expend significant energy while walking daily, making certain movements, such as kneeling, difficult to perform (Dede et al., 2012).

The survey enables researchers to focus on key aspects, such as better solutions for skin conditions and addressing user fatigue during walking. Proposed solutions involve designing prosthetic joints to mimic natural ones by allowing movement in two axes: pronation, which involves turning the foot outward, and supination, which involves turning the foot inward. The solution for the skin condition involves combining an antibacterial coating with a material designed to resist debonding. Debonding is a process that alters the physical and chemical structure of the liner, leading to the issues mentioned earlier (Dede et al., 2012). Among the two proposed solutions, the treatment for skin conditions is most crucial for the patient, according to the survey results, as it allows them to live a more normal life.

Chapter 3: Methodology

3.1 Finite Element Method

Based on Cook et al. (2002), when implementing finite element method, the goal is to determine the total potential energy, denoted as π_P, which is the sum of the strain energy stored in an elastic body and the potential energy of the external loads. For an elastic body to acquire equilibrium, it is necessary to make π_P stationary with respect to the nodal degrees of freedom (DOFs). The nodal DOFs represent a series of independent values that can be calculated at a specific location known as the node in the elastic body.

Let U represents the strain energy and Ω the potential of the applied loads, the total potential energy π_P is, based on Cook et al. (2002),

$$\pi_P = U + \Omega \tag{1}$$

The many DOFs are collected in the global displacement vector $\{D\} = [D_1\ D_2\ \dots\ D_n]^T$, where n represents the number of DOFs. Since π_P is a function of D_i, symbolically, $\pi_P = \pi_P (D_1, D_2, \dots, D_n)$, the requirement of making π_P stationary with respect to the DOFs leads to the following equation:

$$d\pi_p = 0 \tag{2}$$

or

$$d\pi_P = \frac{\partial \pi_P}{\partial D_1} dD_1 + \frac{\partial \pi_P}{\partial D_2} dD_2 + \cdots + \frac{\partial \pi_P}{\partial D_n} dD_n = 0 \tag{3}$$

which requires:

$$\frac{\partial \pi_P}{\partial D_i} = 0 \quad \text{or} \quad \left\{\frac{\partial \pi_P}{\partial D}\right\} = \{0\} \tag{4}$$

For a linear elastic body with initial stresses $\{\sigma_0\}$ or strains $\{\varepsilon_0\}$, the equation for U becomes:

$$U = \frac{1}{2}\int [\{\sigma\}^T \{\varepsilon\} - \{\varepsilon\}^T [E]\{\varepsilon_0\} + \{\varepsilon\}^T \{\sigma_0\}] dV$$
$$= \int \left(\frac{1}{2}\{\varepsilon\}^T [E]\{\varepsilon\} - \{\varepsilon\}^T [E]\{\varepsilon_0\} + \{\varepsilon\}^T \{\sigma_0\}\right) dV \quad (5)$$

Here, {σ} represents the stress vector, and {ε} the strain vector; [E] represents the material property matrix. The integrals are volume integrals preformed over the volume of the elastic body. Equation 5 becomes, if the applied loads are conservative loads:

$$\pi_P = \int \left(\frac{1}{2}\{\varepsilon\}^T [E]\{\varepsilon\} - \{\varepsilon\}^T [E]\{\varepsilon_0\} + \{\varepsilon\}^T \{\sigma_0\}\right) dV$$
$$- \int \{u\}^T \{F\}\, dV - \int \{u\}^T \{\Phi\}\, dS - \{D\}^T \{P\} \quad (6)$$

where {F} represents the body forces, while $\{\Phi\}$ represents the surface tractions. The first and second integrals are again volume integrals preformed over the volume of the body. The remaining integral is a surface integral that covers only the surfaces where $\{\Phi\}$ is applied. {u} is evaluated over the volume of the body (in $\int \{u\}^T \{F\}\, dV$) or over the surface on which $\{\Phi\}$ is applied (in $\int \{u\}^T \{\Phi\}\, dS$). Finally, {P} represents the applied load vector.

Now the elastic body is represented by an assembly of Nels elements. Each element consists of a number of nodes. The {u} within element i is determined by

$$\{u\} = [N]\{d\}_i \quad (7)$$

where [N] is the shape function matrix and $\{d\}_i$ represents the nodal DOFs of the element. The size and specific form of the [N] matrix depends on several factors: the shape of the element, the number of nodes, and finally, the dimensionality (1D, 2D or 3D) of the situation. For brevity, the details of [N] will not be presented in this thesis. Readers are to refer to Cook et al. (2002).

From here, the strains are determined through differentiation:

$$\{\varepsilon\} = [\partial]\{u\} = [B]\{d\} \tag{8}$$

where:

$$[B] = [\partial][N] \tag{9}$$

Matrix [B] is known as the strain-displacement matrix, while $[\partial]$ is a symbolic matrix containing the required differentiations. Equation (8) is then substituted into Equation (6), resulting in the following:

$$\pi_P = \frac{1}{2}\sum_{i=1}^{N_{els}} \{d\}_i^T [k]_i \{d\}_i - \sum_{i=1}^{N_{els}} \{d\}_i^T \{r_e\}_i - \{D\}^T \{P\} \tag{10}$$

The $[k]_i$ matrix and $\{r_e\}_i$ vector are the stiffness matrix and load vector, respectively, for element i. They are evaluated as follows:

$$[k]_i = \int [B]^T [E][B] dV \tag{11}$$

and

$$\{r_e\}_i = \int [B]^T [E][\varepsilon_0] dV - \int [B]^T [\sigma_0] dV + \int [N]^T \{F\} dV + \int [N]^T \{\Phi\} dS \tag{12}$$

Here the volume integrals are performed over the volume of element i. For the surface integral, it is evaluated over a certain face of element i where Φ is applied. In equation (10), the element's DOFs, $\{d\}_i$, is connected to $\{D\}$, the global DOFs, via the following equation:

$$\{d\}_i = [L]_i \{D\} \tag{13}$$

$[L]_i$ is a matrix, with the size of m_i by m, where m_i is the number of DOFs in element i, while m is the number of global DOFs. Now, substituting equation (13) into equation (10) leads to the following:

$$\pi_P = \frac{1}{2}\{D\}^T \left(\sum_{i=1}^{N_{els}} [L]_i^T [k]_i [L]_i \right) \{D\} - \{D\}^T \sum_{i=1}^{N_{els}} [L]_i^T \{r_e\}_i - \{D\}^T \{P\} \quad (14)$$

Based on Cook et al. (2002), requiring π_P be stationary with respect to {D} yields:

$$\left(\sum_{i=1}^{N_{els}} [L]_i^T [k]_i [L]_i \right) \{D\} = \{P\} + \sum_{i=1}^{N_{els}} [L]_i^T \{r_e\}_i \quad (15)$$

It is stated by Cook et al. (2002), $[L]_i^T [k]_i [L]_i$ has a size of m by m, while $[L]_i^T \{r_e\}_i$ has a size of m by 1. Often, the term $\sum_{i=1}^{N_{els}} [L]_i^T [k]_i [L]_i$ is designated as the global stiffness matrix. That is,

$$[K] = \sum_{i=1}^{N_{els}} [L]_i^T [k]_i [L]_i \quad (15)$$

According to Cook et al. (2002), the above theoretical development arises from two essential components: a functional (which is the total potential π_P) that describes the physical problem, and a nodal interpolation represented by the shape function matrix [N], which characterizes the element. To obtain the necessary equations for the element matrices, it becomes necessary to decide on the shape of the element and the functions inside the shape-function matrix [N], while also considering the number of DOFs and the distribution of the DOFs in an element. This will allow for accurate and efficient calculation results. For brevity, the details of matrix [N] will not be presented in this thesis. The elements used for this thesis research included the 8-node brick element and 6-node wedge element, both being 3-dimensional.

3.2 Static Testing Equations

Every material used in the prosthetic design underwent a static compression test on the force tester, providing a better understanding of its energy-absorption capabilities. Additionally,

by incorporating a 15-degree wedge, the test can simulate both plantarflexion and dorsiflexion stances, resulting in the application of compressive (normal) and shear forces. The samples consist of various TPU materials used in the heel and forefoot areas. When the material is placed between the foot and the floor, it must effectively absorb energy to compensate for the loss of the leg's natural energy storage and release mechanisms. These mechanisms are typically provided by the muscles in the shank and the heel pad.

Measurements such as vertical force and displacement are computed from the force tester, obtaining data from the loading and unloading conditions within the X, Y, and Z directions for several materials. This included the total, shear, and compression displacements, while also including the forces such as the shear, compression, vertical, and horizontal (Berry, 2022). These forces and displacements are shown in Figure 3.1.

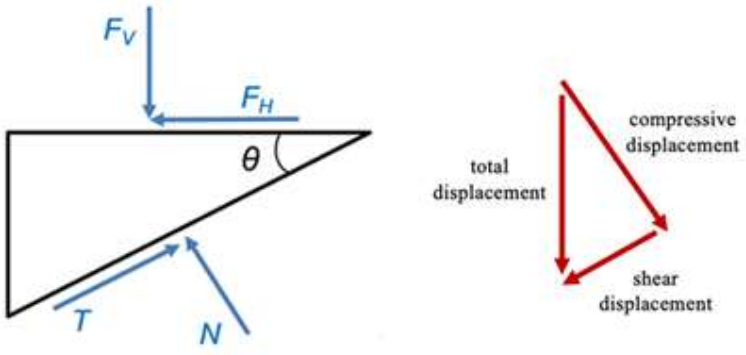

Figure 3.1: (Left: Free Body Diagram for Forces; Right: Displacement Diagram.) Adapted from Figure 14, Berry (2022).

From the X and Y directions, the respective forces are obtained using the force tester, which allows the determination of the horizontal force, leading to equation (16) (Berry, 2022).

$$F_H = \sqrt{Fx^2 + Fy^2} \tag{16}$$

With the utilization of the resultant horizontal force, the compressive force (N) and the shear force (T) can then be obtained with the following two equations.

$$N = F_V cos\theta - F_H sin\theta \tag{17}$$

$$T = F_H cos\theta + F_V sin\theta \tag{18}$$

where F_X is the force in the X direction. F_Y is the force in the Y direction. F_H represents force on the X-Y plane. $F_V = F_Z$, force in the Z direction; and $\theta = 15°$.

These forces are next used to the determination of energy absorption ratios for shear, compression, and total energy using equations (19) through (21) (Berry, 2022). The ratios obtained from these equations are presented in Appendices A and B alongside the respective figures; however, the ratios shown in Chapters 4 and 5 are averages of the energy absorption ratios across three trials. The energy absorption ratios are:

$$Shear\ Energy\ Absorption = \frac{enclosed\ area\ within\ shear\ force - displacement\ curve}{area\ under\ loading\ curve\ of\ shear\ force - displacement} \tag{19}$$

$$Compression\ Energy\ Absorption = \frac{enclosed\ area\ within\ normal\ force - compression\ curve}{area\ under\ loading\ curve\ of\ normal\ force - compression} \tag{20}$$

$$Total\ Energy\ Absorption = \frac{enclosed\ area\ of\ vertical\ force - total\ displacement\ curve}{area\ under\ loading\ curve\ of\ vertical\ force - total\ displacement} \tag{21}$$

The enclosed areas (in the numerators) and the areas (in the denominators) are computed by MATLAB, employing numerical integration.

Chapter 4: Experimental Results and Discussions on the Commercial Prosthetic Designs

Four prosthetics were utilized in this research. Three were commercially available prosthetic designs: a wooden foot or a SACH, an Otto Bock Trias Foot, and a Sierra Foot. The fourth prosthesis was a passive prosthetic, designed using SolidWorks, featuring the material combination of nylon and TPU. This fourth prosthesis is presented in Chapter 5.

The wooden foot (https://ouhsc.edu/bserdac/dthompso/web/gait/pobmk/prosfeet.htm) is a SACH, solid ankle cushioned heel. It has a compressible heel wedge that provides "pseudo-plantar flexion" after heel strike. The rigid wooden keel is for midstance stability but provides little lateral movement. The SACH is frequently prescribed because it is inexpensive, light, durable, and available in various heel heights to accommodate different shoes.

The Otto Bock Trias (https://shop.ottobock.ca/en/Prosthetics/Lower-Limb-Prosthetics/Feet---Mechanical/Trias/p/1C30-1) is a commercial prosthetic foot constructed from carbon fiber, designed for users with an activity rating between levels 2 and 3. A level 2 prosthetic foot enables the user to walk freely indoors and outside with some limitations, while providing energy return. In contrast, a level 3 prosthetic foot allows for unrestricted movement both indoors and outdoors, making it suitable for individuals who engage in daily activities that require significant physical exertion. This indicates that the Otto Bock Trias is primarily intended for use in controlled environments such as walking indoors.

The Sierra foot (Steeper Group - Steeper Group - Sierra Foot) is designed for active users. It has a unique split keel and angled top design, maximizing energy return and flexibility, allowing

amputees to walk comfortably on uneven terrain. Figure 4.1 shows the three commercial prostheses.

(a) SACH

(b) Otto Bock Trias

(c) Sierra

Figure 4.1: Commercially Available Prosthetic Feet. (a) SACH. Photo credit: ps34121756-fresh_14cm_220lbs_polyurethane_sach_prosthetics_foot.jpg (929×929); (b) Otto Bock Trias. Photo credit: 1C30- Otto Bock | Produkty - Mark Protetik; (c) Sierra. Photo credit: SIERRA1.jpg (279×349)

A note is in order regarding the number of significant digits in presenting experimental results. The experimental results to be seen from herein are not the raw data recorded by the force

tester or the force plate. Instead, this thesis presents the processed (or computed by MATLAB) results. The number of significant digits is higher than the precision of the raw data.

4.1 Testing Prosthetic Designs without an Insole

The idea behind this protocol was to evaluate the three different commercial prosthetic foot designs (the wooden foot or SACH foot, the Otto Bock Trias foot, and the Sierra foot) to assess the effectiveness of each design when applying forces. The implementation of this protocol resulted in the use of a force tester, as shown in Figure 4.2. The test protocol is similar to the keel test set forth by AOPA, the American Orthotic and Prosthetic Association (AOPA, 2010). Based on research from the AOPA (AOPA, 2010), it was determined that 1230 N was the load applied by an average person during the gait cycle, as reported by Warder et al. (2018). This information facilitated the testing of the three prosthetic commercial designs, including the wooden foot, the Otto Bock Trias foot, and the Sierra foot. These designs were assessed in terms of loaded and unloaded energies, absorbed energy, and stiffness. For brevity, only the averages of the trials are presented below (Tables 4.1 to 4.3). Details such as the test setups are shown in Figures A.1, A.4, and A.7, respectively; the plots of force against compression are given in Figures A.2 and A.3 for the wooden foot, Figures A.5 and A.6 for the Otto Bock Trias foot, and Figures A.8 and A.9 for the Sierra foot. The tabulated results of loaded and unloaded energies, absorbed energy, and stiffnesses for the individual trails are presented in Tables A.1 to A.3. It is noted that all plots of force against compression are inclusive of second and subsequent load cycles. The reasons are discussed in Sec. 4.2.2.

Figure 4.2: Wooden Foot on Force Tester

4.1.1 Energy absorption

Each prosthetic foot was tested on the force tester, applying two different compression tests, CC and M5. The CC test provides a representation of the load applied to a foot when standing. The M5 test provides a representation of the load applied during the gait cycle of a human. When conducting the CC test, a compressive load of 1230 N was applied on the prosthetic foot for a series of 16 cycles at the speed of 22.25 mm/minute to determine energy and stiffness during both loading and unloading. The M5 test was to emulate the M-curve (Figure 4.3) with the compression load increasing from zero to 925 N (the first peak), decreasing from 925 N to 738 N (the trough), which was then increased to 915 N (the second peak), and finally the load was decreased from 915 N to zero. This compressive load was applied on the prosthetic foot for a series of 5 cycles at the speed of 22.25 mm/minute, which provided a pseudo-static representation of the load applied to the foot while in a gait cycle. Note that, given an average adult body weight of W = 890 N, 925 N represents 104% W; 915 N represents 103% of W; and 738 N is 83% of W. The percentages are based on Vaverka et. al. (2015). However, it should be noted that different peak and trough values have been reported in the literature. For example, Marasović et al. (2009)

reported outcomes of 107% (first peak), 85% (trough), and 105% (second peak) of body weight, respectively. These values were based on force plate measures of 40 human participants with differing age, sex, height, and weight (Marasović et al., 2009).

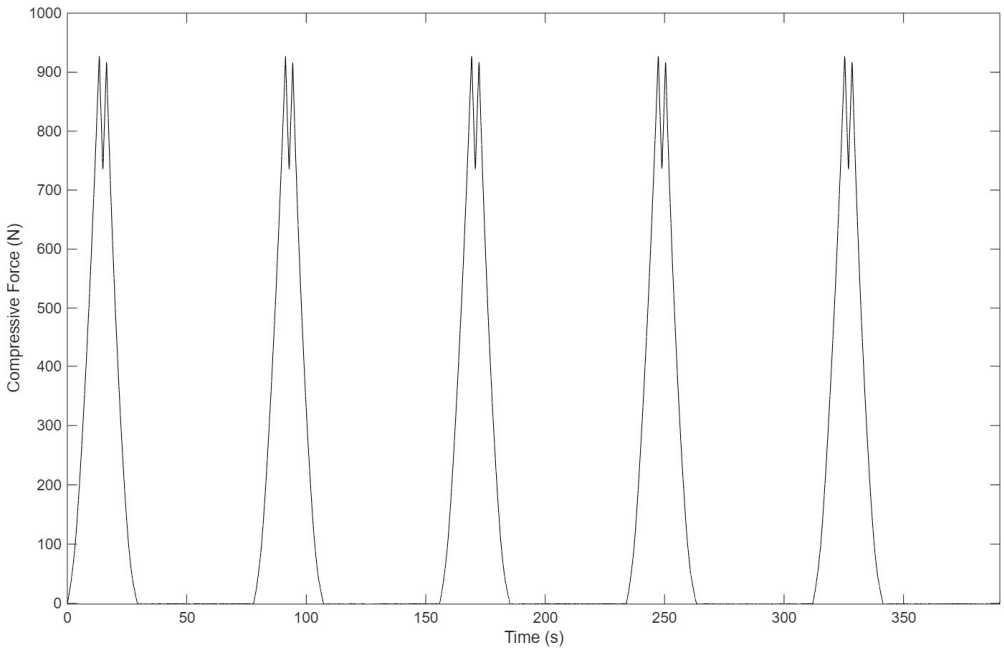

Figure 4.3: Force versus Time Plot for the M5 Test

Based on the results shown in Table 4.1, the wooden foot (SACH foot) absorbed the most energy with an absorption ratio of 0.158 for the CC test and an absorption ratio of 0.180 for the M5 test. When comparing the two ESAR feet, the Otto Bock Trias foot has the second-highest energy absorption ratio of 0.103 in the CC test and an energy absorption ratio of 0.130 in the M5 test. In comparison, the Sierra foot has a CC energy test ratio of 0.074 and an M5 energy test ratio of 0.101. These results suggest that the Otto Bock Trias performs slightly better in energy absorption than the Sierra foot.

The above outcome is not surprising, considering that the other two prosthetic feet are of the ESAR-type. That is, they would store and return energy for the next phase of the gait. Other

research studies revealed that SACH feet, such as the wooden foot, return less energy during the gait cycle (Prince et al., 1994). In the research work conducted by Prince et al. (1994), a SACH foot with a wooden keel was compared to other energy-storing prosthetics. The researchers fitted one participant with two ESAR prosthetic feet, plus a Golden-ankle fitted on a SACH foot. It was found that at initial contact of the heel, a lot of energy was absorbed by the SACH foot; however, most of this energy was dissipated within the cushion material, and only a small amount of energy was recovered. In addition, it was found that some energy was dissipated during push-off within the compliant forefoot of the SACH. From the human kinesiology perspective, there is a metabolic cost for walking. Metabolic cost of transport refers to the energy expenditure associated with movement. Kelly et al. (2018) recruited 14 individuals and examined the absorption ratio of the human foot across running speeds of 2.2, 3.3, and 4.4 m/s, respectively. The energy absorption ratios were found to be 29±20%, 48±20% and 63±22%, respectively. This absorption comes as a result of the human foot's energy dissipative process, where the foot's soft tissues, mainly the heel pad, absorb the energy from the impact forces during walking (and running) and convert it to heat. Therefore, the prosthetic feet would need to emulate not only the skeletal system of the human foot but also the soft tissues. As a result, the impact forces during heel strike (or walking in general) will not be transmitted upwards to the knee and hip joints, and the upper torso, causing discomfort and pain.

As to the absorptions during heel strike and push-off (or toe-off), respectively, Baines et al. (2018) recruited 12 human participants (10 trials per participant) to walk across force plates, and the GRFs versus time were recorded. The average walking speed was 1.3 m/s (Baines et al., 2018). Using numerical integration, the work done by the GRF during heel strike was determined. The researchers found that the energy expenditure during heel strike was 3.8±1.7 J (Baines et al., 2018).

They also reported an energy absorption of 1.4±0.1 J (Baines et al., 2018), which gave an average energy absorption ratio of 36.84% for heel strike. Meanwhile, Postema et al. (1997) examined the gait data of 10 individuals wearing six different prosthetic feet, and found that during push-off, the dissipated energy was 1.9 J (estimated value based off data from Table 5 in Postema et al., 1997), giving an absorption ratio of 41%, also estimated based off data from Table 5 (Postema et al. 1997).

The absorption ratios presented in Table 4.1 are lower than those quoted above. This is expected since the tests conducted were static (almost static, to be precise) with prosthetic feet *only*. The lower values of the ratio, as given in Table 4.1, however, suggest that improvements are desired. One of such improvements would be to employ insoles. As it will be demonstrated in Sec. 4.2, the absorption ratios can be increased to 30%, more or less, by adding an insole.

Table 4.1: Average Energy Absorption Ratios and Stiffnesses of Three Designs

Type of Prosthetic	Wooden		Otto Bock Trias		Sierra	
Type of test	CC	M5	CC	M5	CC	M5
Ratio of absorption	0.158	0.180	0.103	0.130	0.074	0.101
k for high load in loading, N/mm	307.585	-	343.351	-	193.953	-
k for high load in unloading, N/mm	444.719	-	440.897	-	231.199	-
k for low load in loading, N/mm	193.285	-	134.014	-	86.549	-
k for low load in unloading, N/mm	179.887	-	141.170	-	93.575	-

4.1.2 Stiffness at high loads

Figures A.2, A.5, and A.8 (with A.2 being repeated below as Figure 4.4) demonstrate nonlinear behaviors. Therefore, the stiffness is not constant. Following the approach by Turner et al. (2022), high-load stiffness and low-load stiffness are examined. Here, high load is defined as

loads greater than 90% of 1230 N (between the orange lines in Figure 4.4), while low load is defined as loads between 50 N and 50 N + 10% of 1230 N (between the purple lines in Figure 4.4). Two stiffness values were computed using linear regression, one for loading and another for unloading. Note that AOPA (AOPA, 2010) defined 50 N as the pre-load for prosthetic foot tests.

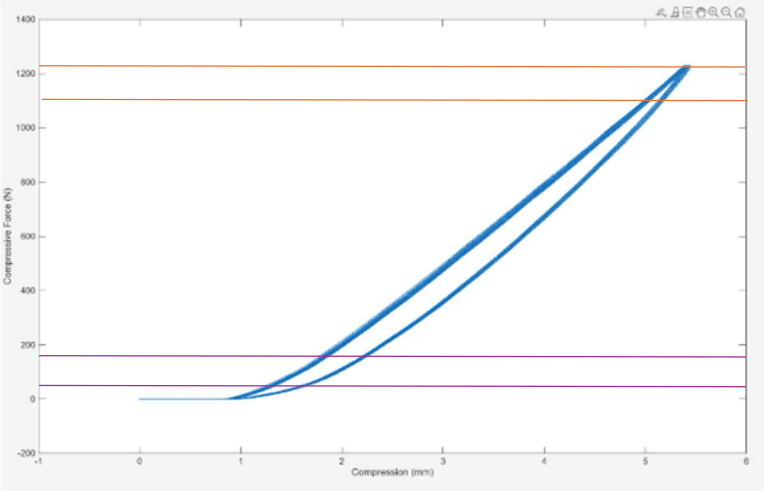

Figure 4.4: CC Test, Trial 2, Wooden Foot

As shown in Table 4.3, the stiffness values of the commercial prosthetics, such as the wooden foot, Otto Bock Trias foot, and Sierra foot, under the loading condition are shown to be lower than the unloading conditions. This outcome is quite common for commercial models since, based on Halsne et al. (2022), the nonlinearity of the feet affects the loading and unloading behavior, leading to lower stiffness within the loading condition and higher stiffness during the unloading condition.

When comparing the loading and unloading conditions under high loads, the Otto Bock model demonstrates the highest stiffness among the tested models. The Otto Bock Trias prosthetic has a stiffness value of 343.351 N/mm under high-load loading conditions, with an unloading stiffness of 440.897 N/mm. In comparison, the wooden foot has a high load loading stiffness of 307.585 N/mm and an unloading stiffness of 444.719 N/mm. This outcome indicates that during

the loading stage, the Otto Bock Trias design is more resistant to applied loads. However, during the unloading stage, the wooden foot's stiffness exceeds that of the Trias by 11.63%, suggesting that the wooden foot has a slightly reduced ability to return to its original shape. The Sierra foot, however, presents a different case, as its high-load stiffness, at 193.953 N/mm, during the loading stage, is lower than both the Otto Bock Trias and SACH, and its unloading stiffness is also lower than the Otto Bock Trias and SACH at 231.199 N/mm. This suggests that the Sierra model may be less resistant to loads when compared to the other designs.

4.1.3 Stiffness at low loads

The three commercial designs, the Sierra, the Otto Bock Trias, and wooden feet, were also compared in terms of stiffness measures at low loads as given in Table 4.1. The wooden foot has a low-load stiffness of 193.285 N/mm in the loading condition, while the unloading stiffness is 179.887 N/mm. Both values of the stiffness are larger than those of the Trias and Sierra models. In addition, the wooden foot has higher low-load stiffness in loading than in unloading, but the Otto Bock Trias and Sierra feet demonstrate the opposite (i.e., the unloading stiffness is slightly larger than the loading stiffness). Figures 4.5 and 4.6 (a repeat of Figures A.5 and A.8, respectively) show the force-compression plots of the Otto Bock Trias and Sierra feet under the CC test. It can be seen that, by comparing Figures 4.5 and 4.6 with Figure 4.4, the Otto Bock Trias and Sierra feet exhibit smaller gaps between the loading and unloading curves, with the curves seemingly parallel to each other at low loads, leading to the close values of low-load loading and low-load unloading stiffness for the Otto Bock Trias and Sierra feet. It is interesting to observe that, although the three prosthetic feet have similar overall behavior under the CC test, the Otto Bock Trias and Sierra feet, both being of the ESAR-type, have a smaller enclosed area between the loading and unloading curves, giving smaller energy absorption ratios.

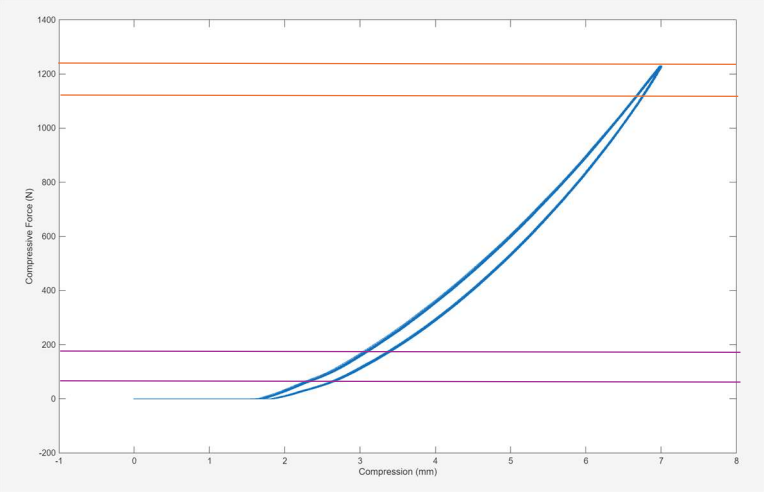

Figure 4.5: CC Test, Trial 2, Otto Bock Trias Foot

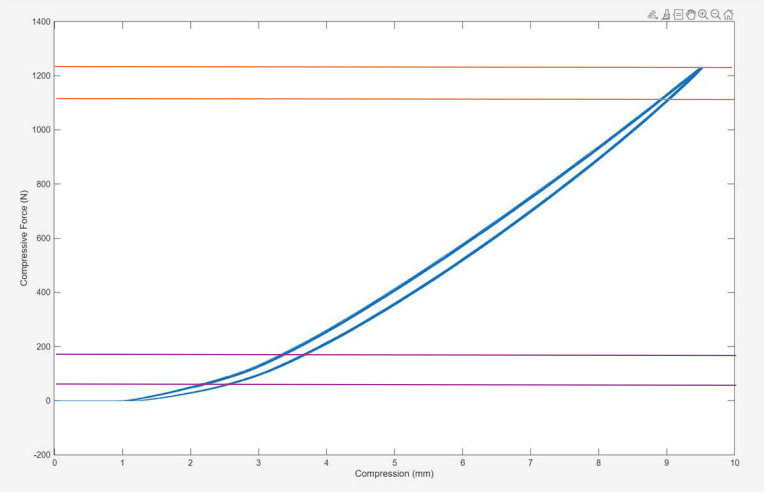

Figure 4.6: CC Test, Trial 2, Sierra Foot

In the literature, linear stiffness was used by some, as illustrated in Figure 4.7, adapted from Turner et al. (2022). Linear stiffness was also employed by Lestari and Adyono (2022) and Taboga and Grabowski (2017). EI-Mohandes and Ibrahem (2014) adopted a piecewise linear stiffness approach, as shown in Figure 4.8. On the other hand, Warder et al. (2018) employed the linear displacement offset method, where the stiffness was the average slope of the linear portion of the corresponding loading curves. A similar approach was employed by Webber and Kaufman

(2017). The stiffnesses reported in Warder et al. (2018) and Webber and Kaufman (2017) are therefore equivalent to the loading stiffnesses in high load used in this thesis.

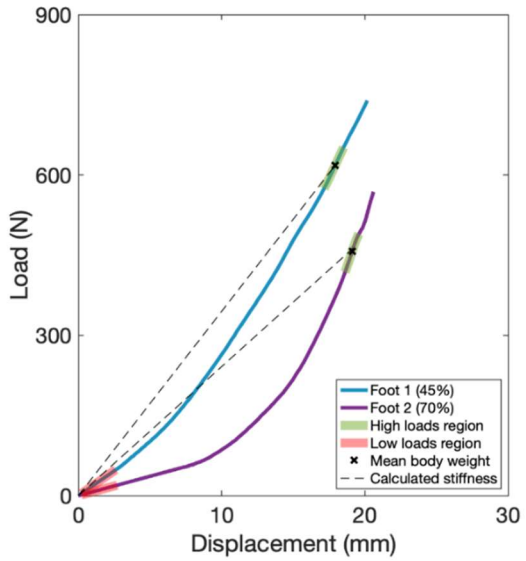

Figure 4.7: High and Low Load Regions and Calculated Stiffness. Adapted from Fig A. Example force-displacement data demonstrating methods used in determining stiffness and relative stiffness, Turner et al., 2022.

In terms of the values of stiffness, Lestari and Adyono (2022) created two ESAR-type prosthetic feet and conducted FEA static analysis using SolidWorks. The linear stiffness ($k = F/d$) was determined to be 20.736 and 28.088 N/mm, respectively. Taboga and Grabowski (2017) examined four pediatric prosthetic feet and reported a linear axial stiffness ranging from 57.3 to 361.4 kN/m (note: 1 kN/m = 1 N/mm), with the average (over the four feet) linear axial stiffness being 121.8 kN/m (= 121.8 N/mm). Based on FEA analyses of the four models created by the authors, EI-Mohandes and Ibrahem (2014) presented K1 values of 17.2 to 31.2 N/mm for the toe and 39.5 to 48.6 N/mm for the heel. The K2 values were 84.9 to 90.3 N/mm for the toe and 165.0 to 181.9 N/mm for the heel. Webber and Kaufman (2017) reported instantaneous stiffness at 120% body weight, which ranged between 38.0 and 195.2 N/mm. Finally, Warder et al. (2018) found that the average slope of the linear portion in loading was from 23.1 to 64.1 N/mm. Overall, the stiffness

values listed in Table 4.1 and those from the literature as mentioned above, are in reasonably good agreement.

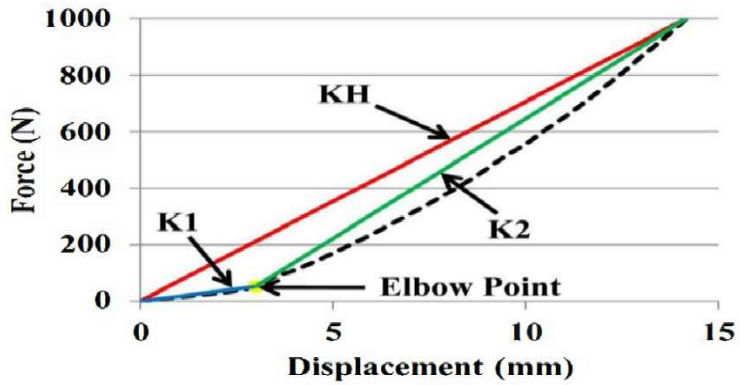

Fig. 2. Force displacement curve with K1, K2 and KH.

Figure 4.8: Piecewise Linear Stiffness. Adapted from Fig. 2, EI-Mohandes and Ibrahem, 2014; the dashed line indicates the loading curve.

4.2 Testing Wooden Foot with Insoles

The protocol here was performed only with the wooden foot, where a different insole was added to the bottom of the foot, see Figure 4.9. The goal was to examine the enhancement in prostheses' energy absorption by using insoles. It has been suggested that the need to reduce impact forces at the prosthetic foot by increasing energy absorption can lead to compensatory asymmetry in gait patterns, and it may aid in improving symmetry in amputee gait (Edhe et al., 2000).

For this protocol, thermoplastic polyurethane (TPU) was used to 3D-print the insoles. Each insole utilized a different brand of TPU filaments. The four insoles were made of Tronxy, Sain Smart, Pxmallion, and Polyflex, respectively, with an infill density of 10% for the heel and 15% for the forefoot (Figure 4.10). By comparing the energy absorption ratios, it is possible to determine the best material to maximize energy absorption.

Figure 4.9: Wooden Foot on Tronxy Insole

Figure 4.10: TPUs Used for Insoles

Each insole was designed using 3D design software, tailored to the shape of the human foot. The heel and forefoot have rounded edges to match the natural contours of the foot. Figures 4.11 and 4.12 illustrate the insole, with the toe and heel clearly marked.

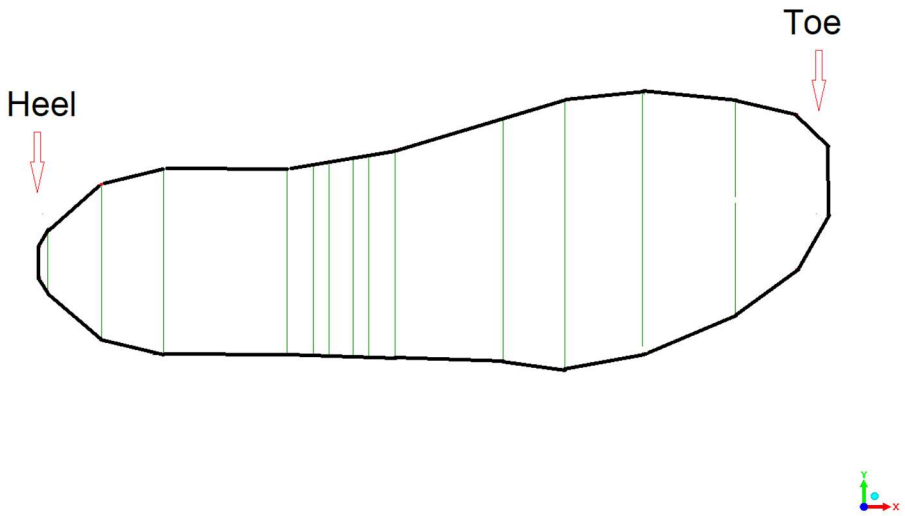

Figure 4.11: Top View of Insole

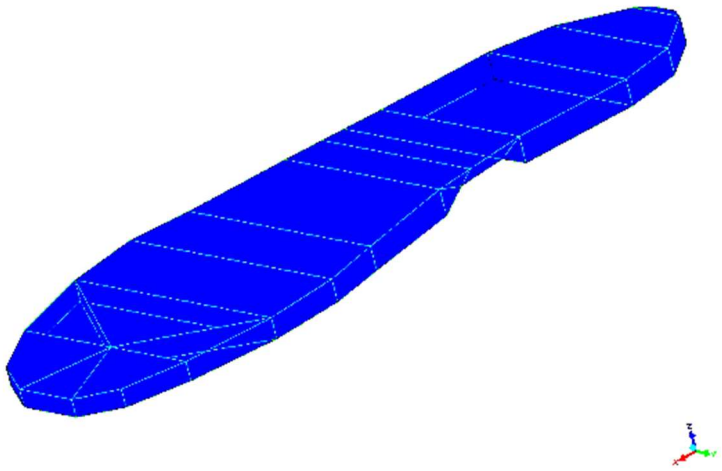

Figure 4.12: Isometric View of Insole

Again, for brevity, only the averages of the trials are presented below (Tables 4.2 and 4.3 for absorption ratios, and Table 4.4 for stiffnesses). The test setups are shown in Figures A.10, A.13, A.16 and A.19, respectively; the plots of force against compression are given in Figures A.11 and A.12 for the Tronxy insole; Figures A.14 and A.15 for the Polyflex insole; Figures A.17 and A.18 for the Sain Smart insole; and Figures A.20 and A.21 for the Pxmallion insole. The tabulated

results of loaded and unloaded energies, absorbed energy, and stiffnesses for the individual trails are presented in Tables A.4 to A.7.

4.2.1 Energy absorption

The analysis of the four insoles revealed distinct variations among the materials (here, materials mean the brands of TPU filament) when evaluated in terms of energy absorption for the CC and M5 tests. The results presented in Table 4.2 indicate that the Tronxy absorbed the highest amount of energy compared to all other TPU samples under both test conditions. In the CC test, the Tronxy demonstrated an average absorption ratio of 0.276, while the M5 test produced a higher average absorption ratio of 0.314, which are the highest values in Table 4.2 for the two tests. When examining the remaining materials, Polyflex seemed to be the least effective in terms of energy absorption, having a CC test ratio of 0.215 and an M5 ratio of 0.250, respectively. In contrast, Sain Smart and Pxmallion are observed to have similar absorption ratios.

As the aim was to examine the enhancement by insoles in the prostheses' energy absorption, the percent increases in absorption ratios, insoles over no insole, are presented in Table 4.3, which shows that the Tronxy insole was approximately twice as effective as the Polyflex insole in enhancing energy absorption. Based on the energy absorption ratio, the Tronxy absorbs the most. On the other hand, the Sain Smart and Pxmallion are approximately equal, showing them as a good second choice.

These increased energy absorptions may facilitate the wooden foot in reducing impact felt by the body during the gait cycle, thereby enhancing comfort and usability of the wooden foot for transtibial amputees. As stated in the literature, the natural impact-dampening mechanisms in non-amputees involving the heel pad, soft tissues and ligaments, which normally assist with energy

absorption during gait, are lost in transtibial amputees; therefore, energy dissipation only relies on the components of the prosthetic device and footwear materials (Collins & Whittle, 1989; Ros et al., 2015; Whittle, 1999).

Table 4.2: Average Energy Absorption Ratios of TPU Insoles on Wooden Foot

TPUs for insoles	Tronxy		Polyflex		Sain Smart		Pxmallion	
Type of test	CC	M5	CC	M5	CC	M5	CC	M5
Ratio of absorption	0.276	0.314	0.215	0.250	0.265	0.311	0.267	0.309

Table 4.3: Percentage Increases in Energy Absorption Ratio when Using Insoles

TPU for Insoles	Tronxy		Polyflex		Sain Smart		Pxmallion	
Type of test	CC	M5	CC	M5	CC	M5	CC	M5
Increase in absorption ratio, %	74.684	74.444	36.076	38.889	67.772	72.778	68.987	71.667

4.2.2 Stiffnesses at high and low loads

Table 4.4 compares the average stiffness values, under the CC test, of five conditions: no insole, and insoles made from Tronxy, Polyflex, Sain Smart, and Pxmallion. In the high-load situations and amongst insoles, it is shown that when the load was applied, the Tronxy and Pxmallion insoles had the highest stiffness values during the loading phase, demonstrating the ability of the materials to resist deformation. Specifically, the Tronxy insole had a stiffness of 291.725 N/mm, while the Pxmallion insole exhibited a stiffness of 297.012 N/mm. During the unloading stage, the stiffness of the Tronxy (at 523.198 N/mm) was higher than the Pxmallion (at 516.437 N/mm).

The remaining TPU insole materials, Polyflex and Sain Smart, exhibited a similar trend; however, they were less stiff than the Tronxy and Pxmallion insoles during the loading phase. Specifically, the stiffness value for the Polyflex was 253.991 N/mm, making it the least stiff of the

four insoles tested. The Sain Smart insole had a stiffness value of 288.002 N/mm, indicating that it can resist deformation better than the Polyflex insole. During the unloading phase, however, the stiffness of the Sain Smart insole was at 473.073 N/mm, which was greater than the Polyflex's stiffness of 295.388 N/mm.

When examining stiffness at a low load, as shown in Table 4.4, the Tronxy and Sain Smart insoles exhibited the highest stiffness values compared to other insole materials. During the loading stage, the Tronxy insole had a stiffness value of 114.504 N/mm, while the Sain Smart insole had a stiffness value of 111.959 N/mm. The behaviors, however, reversed during the unloading stage when the applied load was removed. The Saint Smart exhibited the highest stiffness at 117.307 N/mm, whereas the Tronxy had a stiffness value of 113.679 N/mm.

On the contrary, the Polyflex and Pxmallion insoles had the lowest stiffness values. For example, during the loading stage, the Polyflex had a stiffness value of 76.060 N/mm, while the Pxmallion insole had a stiffness value of 75.529 N/mm, making it less resistant to deformation than the Polyflex insole when the load was applied. Similarly to the material property behaviors of the Tronxy and Saint Smart insoles, the situation reversed during the unloading stage, with the Pxmallion insole having a higher stiffness value of 103.934 N/mm than the Polyflex stiffness value of 101.528 N/mm.

The outcome observed above suggests that the TPU insoles experienced stress softening. Pelayo et al. (2021) conducted experiments on flexible TPUs and observed that the “softening stress” phenomenon was affecting the material from the first and subsequent cycles (Figure 4.13). They inferred that the shift between the first and subsequent cycles reflected the initial damage in the materials induced by the Mullins effect. The Mullins effect refers to the phenomenon that, after the initial stretch, the material undergoes a microstructural rearrangement, causing stress softening

and resulting in the material offering less resistance to additional loading (Miao et al., Figure 4.14). Compared with the experiments conducted by Pelayo et al. (2021), where the maximum strain was set at fixed values (Figure 4.13), the experimental setup in this thesis research had the compressive force set at fixed values. But the difference between the first and subsequent cycles was nevertheless observed, see Figure 4.15. Additionally, the present experimental setup did not increase the loads in subsequent cycles. Therefore, the Mullins effect, as displayed in Figure 4.14, was not observed in this thesis research.

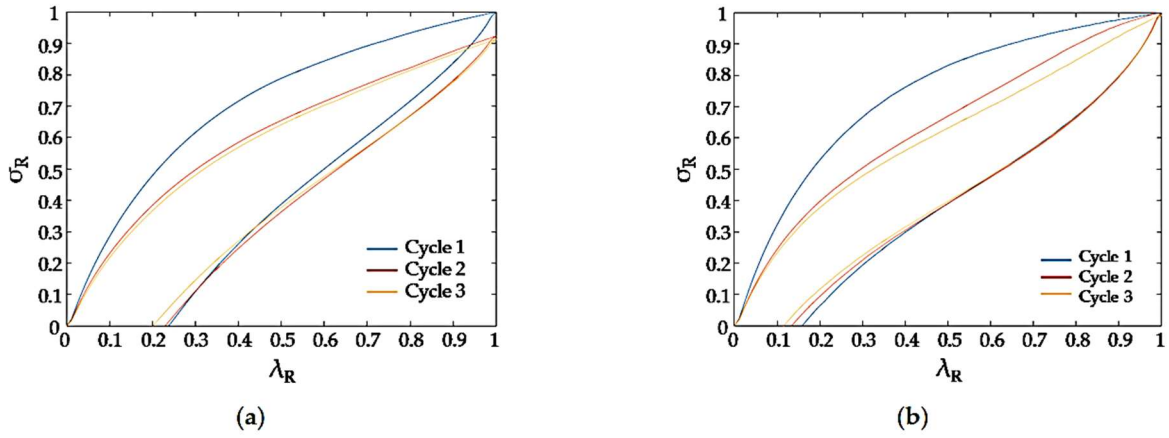

Figure 5. Stress–strain cycles. **(a)** For the feedstock filament; **(b)** for the extruded filament.

Figure 4.13: Stress-Strain Plots. Adapted from Figure 5, Pelayo et al, 2021.

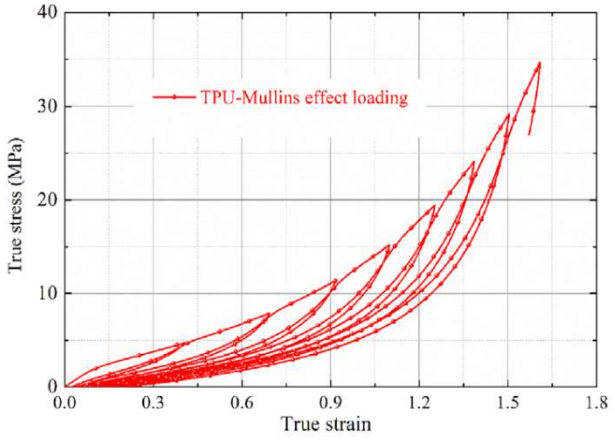

Figure 4.14: Mullins Effect. Adapted from Figure 5, Miao et al., 2019.

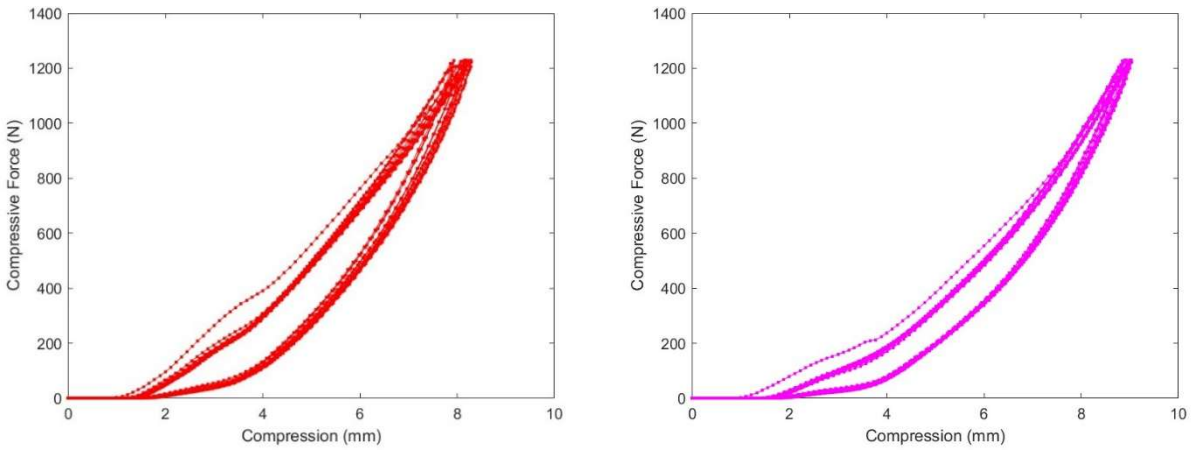

(a) (b)

Figure 4.15: Plots of Compressive Force versus Compression Including the First Cycle, Trial 1, CC Test. (a) Tronxy Insole; (b) Polyflex Insole.

Compared with the no-insole case, the four TPU insoles lowered the stiffness as expected. The exception was that in the high-load unloading condition, the Polyflex had lower stiffness. Anecdotally speaking, the Polyflex insole felt soft when it was walked on under a bare foot. A higher unloading stiffness would suggest a "steeper" removal or release of the compressive load.

Table 4.4: Average Stiffnesses (in N/mm), under CC Test, of TPU Insoles on Wooden Foot

Insoles	No insole	Tronxy	Polyflex	Sain Smart	Pxmallion
k for high load in loading	307.585	291.725	253.991	288.002	297.012
k for high load in unloading	444.719	523.198	295.388	473.073	516.437
k for low load in loading	193.285	114.504	76.060	111.959	75.529
k for low load in unloading	179.887	113.679	101.528	117.307	103.934

4.3 Prosthetic Foot with Insoles on 15-degree Wedge

The following protocol required the use of a 15-degree wedge, as shown in Figure 4.16. The selection of the 15-degree angle is based on the concept that during normal human walking at heel strike, the ankle is slightly dorsiflexed, allowing the heel to contact the ground in a controlled

manner. As the body advances over the stance limb, dorsiflexion increases and typically peaks around 10–15° in mid-stance. Toward the end of the stance, just before toe-off, the ankle transitions into plantarflexion, reaching approximately 15–20° to generate propulsion (Bari et al., 2023). It should be noted that the "Toe Up" and "Toe Down" setups are not ideal replicates of heel strike and toe-off. Arguably, the "Toe Up" setup is probably closer to heel strike than the "Toe Down" setup is to toe-off (or push-off) due to the manner of load application and support for the foot. Figure 4.17 displays a setup seen in the literature (Webber and Kaufman, 2017). However, the "Toe Up" and "Toe Down" setups simulate walking up and down a slope of 15°.

The testing protocol includes positions such as toe up, toe down, and standing on a flat surface (the mid-stance) for various prosthetic feet, including the wooden foot, SACH, Otto Bock Trias foot, and Sierra foot. During the mid-stance position, the wedge was removed. This protocol employed a test known as AA1, which involved applying a 1230 N load on the prosthetic at a 15-degree angle, as shown in Figure 4.16. Each AA1 test consisted of one cycle at a speed of 22.25 mm/min. While similar to the CC test, the AA1 test recorded force components (Fx, Fy, and Fz), whereas the CC test recorded only force component Fz. Three trials were conducted on each prosthetic foot, either on the 15-degree wedge or on a flat surface, to gather the necessary data. Subsequently, compressive, shear, and total energy absorbed were computed under loaded and unloaded conditions. The protocol also included testing the wooden foot with all four insoles: Tronxy, Sain Smart, Pxmallion, and Polyflex to determine the preferred TPU material. Tables 4.5 through 7 present the average energies and energy absorption ratios for the toe-up, mid-stance, and toe-down setups, respectively, for the SACH, Trias, and Sierra feet. Tables 4.8 through 4.11 show the average energies and ratios for the same positions with the SACH foot outfitted with insoles

made from Tronxy, Polyflex, Sain Smart, and Pxmallion. The energies and energy absorption ratios for individual trials are included in Appendix A, specifically Tables A.8 through A.14.

Figure 4.16: Wooden Foot on 15-degree Wedge with “Toe Up” and “Toe Down”

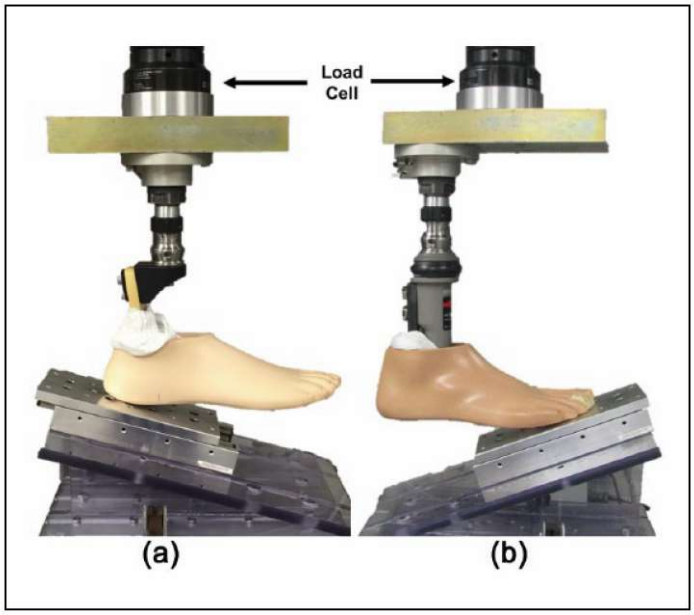

Figure 4.17: Vertically Loaded Tests on the Heel and Toe Regions. Adapted from Figure 2, Webber and Kaufman, 2017.

4.3.1 Average energy for walking stances

For this protocol, a 15-degree wedge was used to simulate the foot's position in three walking stances: Dorsiflexion when the heel lands on the ground (heel strike), midstance when the foot is standing flat on the ground, and Plantarflexion when the foot pushes off the ground (push-off or toe-off). Firstly, the commercial prosthetics were tested on the force tester, including the wooden foot, the Otto Bock Trias foot, and the Sierra foot. Tables 4.5 through 4.7 represent the average energy stored within each prosthetic foot at the three stances.

Based on Tables 4.5 through 4.7, more energy was loaded during the Dorsiflexion (heel strike) when reviewing the results from each foot model. For example, when examining the Sierra model, which loaded the most energy, the following total loading energy values were observed: 5.073 J during Dorsiflexion, 3.896 J when the foot was in a flat position, and 3.730 J during Plantarflexion. According to Womac et al. (2019), more energy is typically loaded in the walking stance, where the orientation of the force is applied to the heel and forefoot. But in this thesis research, the loaded energy during Dorsiflexion was higher than the loaded energy in the mid-stance. The loaded energy during Plantarflexion was, however, lower than the mid-stance loaded energy. Womac et al. (2019) also stated that "the energy results may also be affected by how the force is applied during the test scheme on the force tester". The experimental results of this thesis seem to suggest that more energy loading at the heel of the prosthetic does not imply more energy being stored during Dorsiflexion, as this energy seems to be lost due to the materials of the prosthetic. Hafner et al. (2002) stated that prosthetics are still limited in their energy dissipation capabilities, and their effects on measures of energy have varied across studies."

4.3.2 Energy absorption of the commercial prosthetics

When examining the energy absorption results of the prosthetic feet in more detail, it can be seen from the results presented in Tables 4.5 through 4.7 that the wooden foot showed higher energy absorption in the foot positions, even though it did not have higher energy loading than the Sierra. The energy absorption ratios for the wooden foot were 0.196 for the "Toe Up" (Dorsiflexion) position, 0.213 for the foot flat position, and 0.186 for the "Toe Down" (Plantarflexion) position. Based on these results from Table 4.5, the Wooden Foot was shown to absorb more energy than the other models; however, Postema et al. (1997) mentioned that most of the energy in conventional prosthetics (like the wooden foot) is dissipated in the material, and therefore, the foot prosthetic will return less energy during the gait cycle. However, when it comes to energy-storing prosthetic feet, such as the Otto Bock Trias and Sierra, Postema et al. (1997) stated that "most of the energy isn't dissipated in the material but in the spring mechanism, which is released after push-off." This finding suggests that although the wooden foot had greater energy absorption in all three positions, this outcome does not necessarily make it the best option to use for the walking motion. Postema et al. (1997) also stated that "when a foot releases more energy, this energy affects the ground reaction force known as the anteroposterior component in the forefoot, which allows a more push forward to help the amputee acquire more symmetry during the gait cycle."

Based on the results presented in Tables 4.6 and 4.7, during the "Toe Up" (Dorsiflexion) stance, the Sierra foot had an energy absorption ratio of 0.117, which was higher than the Otto Bock Trias' energy absorption ratio of 0.113. During the "Toe Down" (Plantarflexion) stance, however, the Sierra had an energy absorption ratio of 0.090, and the Trias had an energy absorption ratio of 0.170, almost twice that of the Sierra's. In analyzing the dorsiflexion stance, the Sierra exhibited superior energy absorption at the heel. Conversely, in the Plantarflexion position, the

Sierra demonstrated less energy absorption than the Otto Bock. This outcome suggests that the Sierra may help maintain momentum during the push-off phase of the walking cycle, as most of the energy required to propel the foot forward is derived from energy absorbed at the heel. By absorbing less energy during toe-off, the Sierra prosthetic could facilitate a more efficient and natural walking experience for the transtibial amputee, based on Zelik et al. (2011).

4.3.3 Average energy measures of the wooden foot with TPU insoles

For this protocol, the wooden foot was tested with four insoles on the 15-degree wedge to simulate a gait cycle using similar tests as those conducted in Section 4.3.2 with the commercial feet. When conducting these tests, a load was applied to the wooden foot to deform the material. This information was subsequently used to compute the loaded and unloaded energy as well as the ratio of energy absorption for all foot positions: Toe Up (Dorsiflexion), mid-stance, and Toe Down (Plantarflexion). The results revealed that the TPU insoles had more energy stored in the Dorsiflexion and mid-stance, but less stored energy during the Plantarflexion stance for all four TPU insoles.

The results displayed in Tables 4.8 to 4.11 contain the total energy absorption ratios based on different combinations of the wooden foot and TPU insoles. These results revealed that the Tronxy and Polyflex insoles, when combined with the wooden foot, had a higher energy absorption ratio during Plantarflexion (“Toe Down”) and flat stance, which may not help to use the stored energy to propel the foot forward during a walking cycle (Postema et al.,1997). The Sain Smart and Pxmallion TPU insoles, on the other hand, exhibited higher energy absorption during the Plantarflexion (“Toe Down”) and Dorsiflexion (“Toe Up”) stances, but had the lowest energy absorption ratio during the standing stance. The variability of these outcomes can be supported by the research work of Scetta et al. (2021). Those researchers compared rubber and TPU, noting that

while both materials exhibited the Mullins effect, different types of TPU undergo various forms of rearrangement of their microstructure when subjected to cyclic strain, which influences energy loss and stress softening. As a result, each type of TPU can yield different outcomes, such as varying levels of energy absorption.

Further discussions are as follows.

1. For mid-stance, the shear energies, loaded and unloaded, should ideally be zero. The total energy loaded and unloaded, and the compressive energy loaded and unloaded, should be equal. As a result, the absorption ratio for shear energy is undefined. In Tables 4.5 through 4.11, unfortunately, shear energies were not zero, and shear energy absorption ratios were of finite values. This was mainly because the tests were not ideally set up and performed.
2. Comparing the three prosthetic feet without an insole (Tables 4.5 to 4.7), in “Toe Up” and “Toe Down” setups, the wooden foot had the highest absorptions for total energy, compressive energy, and shear energy, followed by the Trias and Sierra. For mid-stance, the wooden foot also had the highest total (and compressive) energy absorptions, followed by Trias and Sierra. This finding is consistent with that reported in Section 4.1.1 and Table 4.1.
3. When different insoles were tested with the wooden foot (Tables 4.8 to 4.11), Tronxy and Polyflex insoles experienced the most absorption in the “Toe Down” setup, followed by mid-stance and “Toe Up”. Sain Smart and Pxmallion also saw the most absorptions in the “Toe Down”, followed by “Toe Up” and mid-stance.

Table 4.5: Average Absorption Ratios of Wooden Foot on 15-degree Wedge

	Toe Up	Mid-Stance	Toe Down
Total Loaded Energy, J	4.833	3.307	2.193
Loaded Compressive Energy, J	3.360	3.297	1.993
Loaded Shear Energy, J	0.877	0.060	0.173
Total Unloaded Energy, J	3.873	2.613	1.790
Unloaded Compressive Energy, J	3.220	2.603	1.630
Unloaded Shear Energy, J	0.720	0.050	0.140
Total Energy Absorption Ratio	0.197	0.213	0.187
Compressive Energy Absorption Ratio	0.203	0.213	0.183
Shear Energy Absorption Ratio	0.173	0.230	0.193

Table 4.6: Average Absorption Ratios of Otto Bock Trias Foot on 15-degree Wedge

	Toe Up	Mid-Stance	Toe Down
Total Loaded Energy, J	3.497	2.730	2.970
Loaded Compressive Energy, J	2.993	2.723	2.767
Loaded Shear Energy, J	0.533	0.020	0.200
Total Unloaded Energy, J	3.100	2.417	2.470
Unloaded Compressive Energy, J	2.647	2.417	2.283
Unloaded Shear Energy, J	0.480	0.013	0.180
Total Energy Absorption Ratio	0.113	0.113	0.170
Compressive Energy Absorption Ratio	0.113	0.113	0.173
Shear Energy Absorption Ratio	0.100	0.170	0.090

Table 4.7: Average Absorption Ratios of Sierra Foot on 15-degree Wedge

	Toe Up	Mid-Stance	Toe Down
Total Loaded Energy, J	5.073	3.897	3.730
Loaded Compressive Energy, J	4.213	3.897	3.540
Loaded Shear Energy, J	0.970	0.010	0.173
Total Unloaded Energy, J	4.473	3.503	3.403
Unloaded Compressive Energy, J	3.703	3.503	3.230
Unloaded Shear Energy, J	0.870	0.010	0.160
Total Energy Absorption Ratio	0.117	0.103	0.090
Compressive Energy Absorption Ratio	0.120	0.103	0.087
Shear Energy Absorption Ratio	0.100	0.027	0.097

4. Across the insoles, Sain Smart absorbed the most in all three setups. Pxmallion came next, followed closely by Tronxy. Polyflex stood last, as already seen in previous sections.

5. Focusing on mid-stance, a setup that mimics the real-life mid-stance, Tronxy and Sain Smart absorbed an equal amount of total (and compressive) energy. The increase in absorption ratio over that without an insole was 46.9% (= 0.313/0.213 - 1 = 0.469). Although Section 4.2.1 and Table 4.3 reported higher percent increases, the 46.9% here is nevertheless substantial.

In summary, Section 4.1 found, surprisingly, that the wooden foot as a SACH absorbed more energy than the Trias and Sierra. Adding TPU insoles underneath the wooden foot, Section 4.2 showed that the Tronxy was the most appropriate TPU material to be used as the insole. Putting the prosthetic feet, with or without the insoles, under the tester, the results were mixed. The mixed results can be attributed to the non-ideal setups used in this thesis research. In particular, the setups for the Plantarflexion ("Toe Down") and Dorsiflexion ("Toe Up") stances desire future improvements. Examining the total energy absorption during the mid-stance, Tronxy and Sain Smart insoles with the wooden foot exhibited the highest amount at 0.313.

Overall, the Tronxy seems to be an appropriate TPU material to be used as an insole. This will provide a strong starting point for designing the passive prosthetic foot created during this thesis research, the details of which will be presented in the next chapter.

Table 4.8: Average Absorption Ratios Wooden Foot on 15-degree Wedge with Tronxy Insole

	Toe Up	Mid-Stance	Toe Down
Total Loaded Energy, J	6.413	4.050	3.137
Loaded Compressive Energy, J	5.250	4.040	2.810
Loaded Shear Energy, J	1.293	0.070	0.290
Total Unloaded Energy, J	4.603	2.767	2.053
Unloaded Compressive Energy, J	3.737	2.763	1.843
Unloaded Shear Energy, J	0.967	0.050	0.190
Total Energy Absorption Ratio	0.283	0.313	0.343
Compressive Energy Absorption Ratio	0.287	0.313	0.343
Shear Energy Absorption Ratio	0.250	0.290	0.347

Table 4.9: Average Absorption Ratios of Wooden Foot on 15-degree Wedge with Polyflex Insole

	Toe Up	Mid-Stance	Toe Down
Total Loaded Energy, J	5.887	4.677	3.600
Loaded Compressive Energy, J	4.940	4.673	3.217
Loaded Shear Energy, J	1.040	0.083	0.343
Total Unloaded Energy, J	4.340	3.340	2.453
Unloaded Compressive Energy, J	3.650	3.333	2.200
Unloaded Shear Energy, J	0.753	0.060	0.227
Total Energy Absorption Ratio	0.263	0.287	0.320
Compressive Energy Absorption Ratio	0.260	0.287	0.313
Shear Energy Absorption Ratio	0.277	0.303	0.340

Table 4.10: Average Absorption Ratios of Wooden Foot on 15-degree Wedge with Sain Smart Insole

	Toe Up	Mid-Stance	Toe Down
Total Loaded Energy, J	7.377	3.970	3.113
Loaded Compressive Energy, J	6.173	3.960	2.797
Loaded Shear Energy, J	1.327	0.070	0.283
Total Unloaded Energy, J	5.053	2.723	2.027
Unloaded Compressive Energy, J	4.253	2.720	1.617
Unloaded Shear Energy, J	0.870	0.050	0.187
Total Energy Absorption Ratio	0.317	0.313	0.350
Compressive Energy Absorption Ratio	0.310	0.313	0.350
Shear Energy Absorption Ratio	0.340	0.253	0.340

Table 4.11: Average Absorption Ratios of Wooden Foot on 15-degree Wedge with Pxmallion Insole

	Toe Up	Mid-Stance	Toe Down
Total Loaded Energy, J	7.640	3.837	3.277
Loaded Compressive Energy, J	6.390	3.830	2.927
Loaded Shear Energy, J	1.370	0.063	0.307
Total Unloaded Energy, J	5.243	2.707	2.143
Unloaded Compressive Energy, J	4.430	2.697	1.920
Unloaded Shear Energy, J	0.887	0.047	0.197
Total Energy Absorption Ratio	0.317	0.297	0.343
Compressive Energy Absorption Ratio	0.303	0.297	0.343
Shear Energy Absorption Ratio	0.350	0.283	0.357

Chapter 5: Results and Discussions Pertaining to a Proposed Prosthetic Design

5.1 3D Modeling

One of the objectives of this research thesis was to design an affordable prosthetic foot and use the method of finite element analysis (FEA) in conjunction with experimental tests to improve the prosthetic foot design for transtibial amputees. The process of designing the prosthetic foot involved gathering critical measurements from a standard foot, such as the SACH, including length, height, and width. This information facilitated the creation of the essential components of the prosthetic foot. Two versions of the prosthetic foot were created, each with an upper and lower plate. In the initial version (Figure 5.1), a soft material was used in the heel to absorb the impact experienced by transtibial amputees when the foot is in motion. Additionally, a series of wave springs (Figure 5.2) was incorporated into both the heel and forefoot regions of the shoe design to provide the necessary flexibility required for movements that occur during the gait cycle, such as plantarflexion and dorsiflexion.

Selecting suitable wave springs from the McMaster-Carr catalog resulted in three designs similar to that shown in Figure 5.1. In the following, the three designs are designated as Designs 1, 2, and 3, respectively. The heights of the wave springs in the designs were 10.57, 11.89, and 14.53 mm, respectively. The overall diameters of the wave springs were the same, 10 mm.

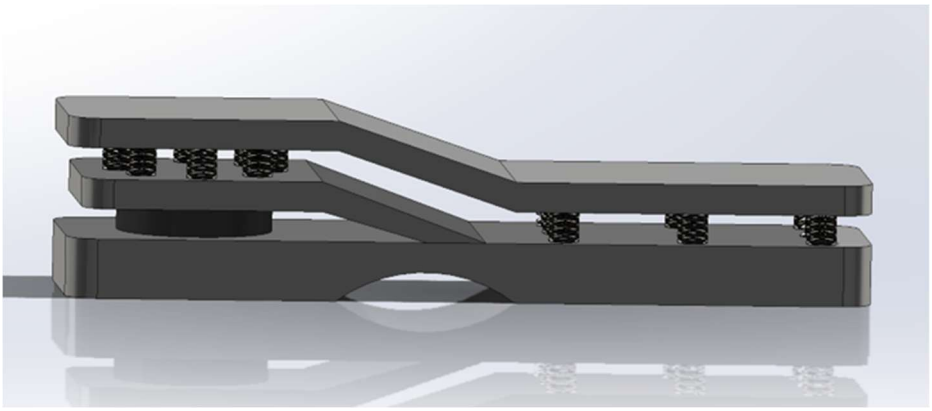

Figure 5.1: Initial Design as Modeled in SolidWorks

Figure 5.2: Wave Springs. https://www.mcmaster.com/products/stacked-disc-springs/corrosion-resistant-stacked-wave-disc-springs/

Due to the complexity and potentially incurred cost of the initial designs, it became necessary to simplify the design to facilitate 3D printing and enhance practicality. Additionally, when the design is implemented in human participants' trials, at least eight copies will need to be produced to ensure that all participants will be tested under the same conditions. These considerations led to the removal of the springs in the initial design. Instead, heel and forefoot pads made of soft materials were to replace the springs to allow for the same flexibility of dorsiflexion

and plantarflexion movements needed by transtibial amputees during the gait cycle. This process resulted in the creation of the final design, which is depicted in Figure 5.3 and designated as Design 4. This design contained a bottom and a top plate, which were 3D-printed with nylon. The plates provided sufficient stiffness and resistance to the applied load and ensured the integrity of the design. The heel and forefoot pads, 3D-printed with thermoplastic polyurethanes (TPUs), provided cushioning for energy absorption and return during the gait cycle.

Nylon and thermoplastic polyurethane (TPU) were selected for their lightweight properties and durability. Nylon is well-known for its exceptional strength, boasting a tensile strength of approximately 50 MPa or higher. This characteristic gives nylon considerable toughness, wear resistance, and impact resistance. As a result, it is particularly effective for shock absorption during the gait cycle when subjected to repeated loading, especially when compared to other materials, such as polyethylene. On the other hand, TPU is ideal for impact absorption at the heel and forefoot due to its low tensile strength, which is approximately 30 MPa (Gomez-Amador et al., 2025). Its high elasticity allows it to deform under load and return to its original shape, making it sufficiently flexible during the gait cycle. TPU exhibits characteristics similar to rubber while maintaining adequate resilience under applied load (Gomez-Amador et al. 2025). These properties make it an excellent choice for the heel and forefoot pads, as well as the insoles.

In terms of costs, the goal of this prosthetic design was to create an affordable solution, addressing the high costs associated with commercial prosthetics available on the market. This included models such as the Wooden SACH Foot, which falls within the range of $1,104 to $2,070 CAD, while the Otto Bock Trias Foot and the Sierra Foot fall within the range of $2,740 to $5,480 CAD (Chen, 2025). However, the material utilized for the new design was significantly more affordable, such as nylon, which fell within the range of $60 - $160 CAD, while TPU fell within

the range of $40 - $95 CAD (Tronxy Global Store, n.d.), which is shown to be more cost-effective than the commercial designs on the Market.

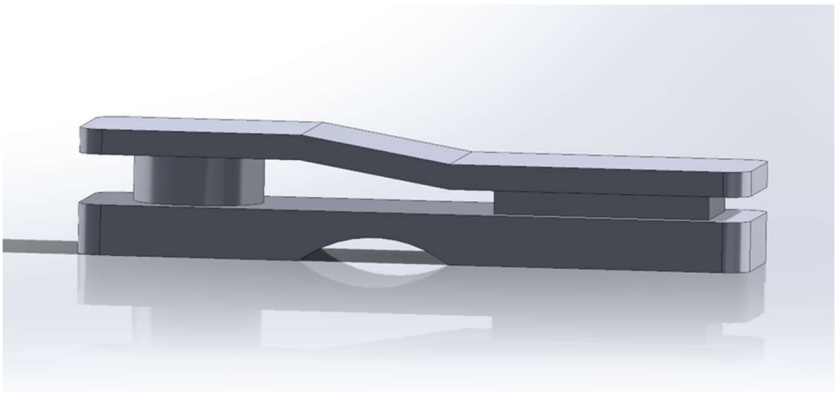

Figure 5.3: Final Design as Modeled in SolidWorks

5.2 FEA Simulations in LISA

Before Design 4 was inputted into LISA for finite element analyses, the geometry was further simplified by removing rounded corners and changing the heel pad from a round disk to a rectangular block. Figure 5.4 shows the geometry being used for FEA. This approach enabled the researcher to use 8-noded brick elements and 6-noded wedge elements, both are believed to be accurate for 3D analyses. Moreover, the aim of the FEA was displacement and stiffness rather than stresses and factors of safety.

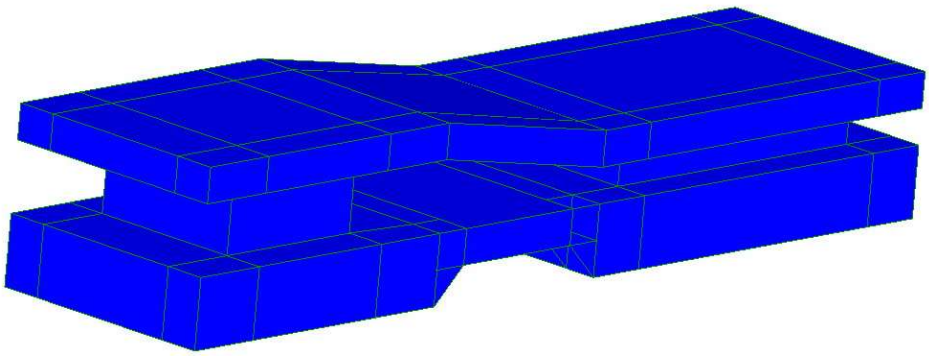

Figure 5.4: Simplified Geometry for the Final Design

5.2.1 Convergence test

To perform the finite element analysis (FEA), the geometry from Figure 5.4 was discretized into a finite element mesh. Using the convergence test, the mesh was progressively refined, allowing the nodal displacement results to be monitored until further refinement produced negligible changes.

In LISA, a rough mesh was constructed by inputting the coordinates of nodes and forming 8-noded brick elements or 6-noded wedge elements (Figure 5.4). Care was taken to ensure that all nodes on an interface were shared by elements on both sides of the interface. This mesh had 50 elements and 144 nodes. Subsequently, the task of refining a mesh (consecutively making the elements smaller and smaller) was performed by applying the option of "Refine ×2". Under this option, one 8-noded brick element becomes eight 8-noded brick elements while one 6-noded wedge element becomes eight 6-noded wedge elements (Figure 5.5). This process was concluded when the computer ran out of memory, including virtual memory. The results demonstrated a relative error as low as 2%, indicating they were very close to convergence. The final mesh contained 38,456 nodes and 32,512 elements. Table 5.1 lists the relation between the number of elements, the number of nodes, and the displacement at a particular node (Figure 5.6). The loading and boundary conditions for the convergence tests are displayed in Figure 5.7.

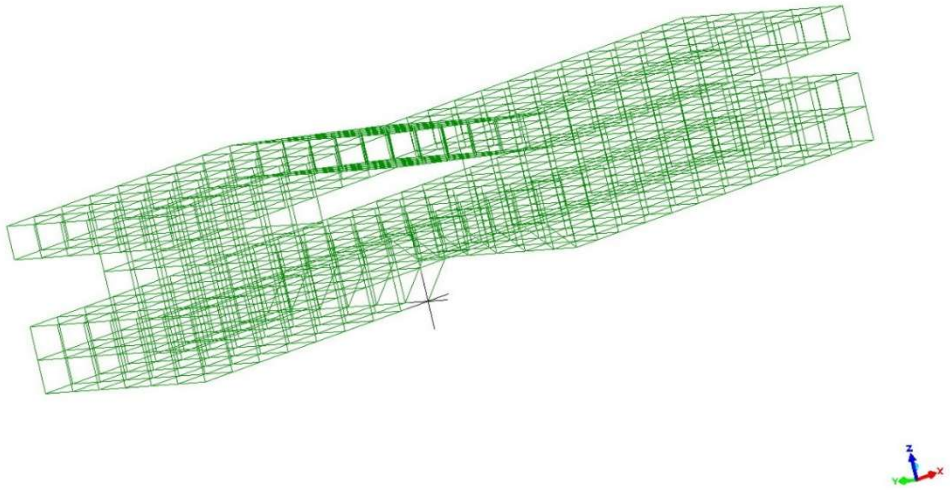

Figure 5.5(a): A Mesh with 508 Elements and 935 Nodes

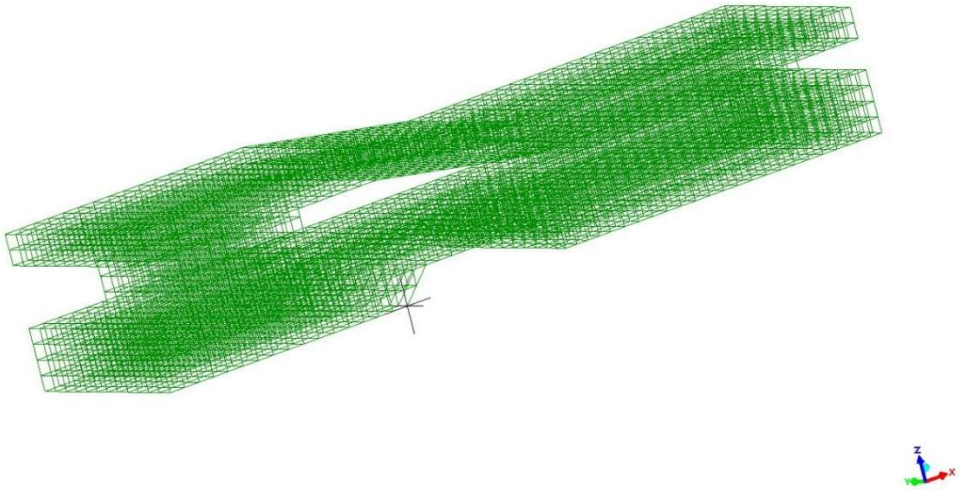

Figure 5.5(b): A Finer Mesh with 4064 Elements and 5648 Nodes

Table 5.1: Convergence Tests

Number of Total Elements	Number of Nodes	Displacement, mm	Relative Error
508	935	-0.0376	-
4,064	5,648	-0.0355	5%
32,512	38,456	-0.0349	2%

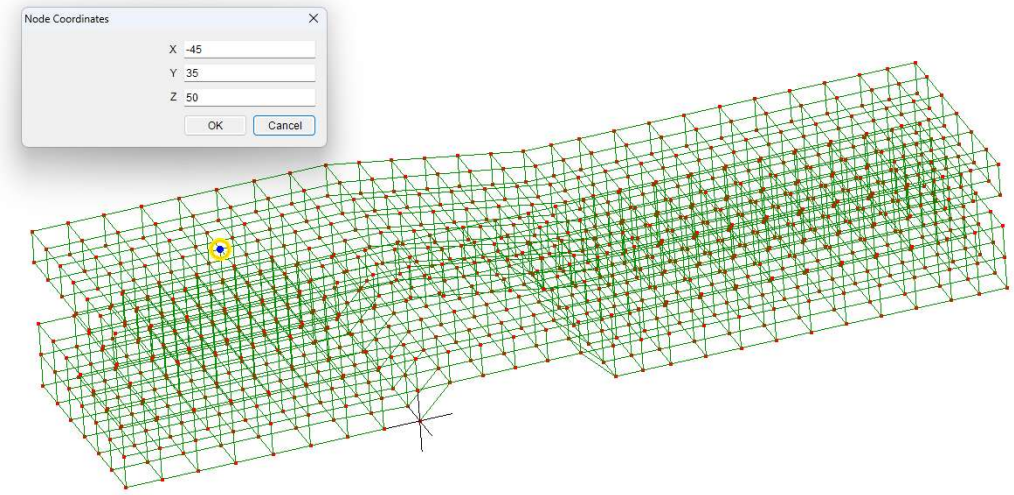

Figure 5.6: Location of the Node for Displacements in Table 1

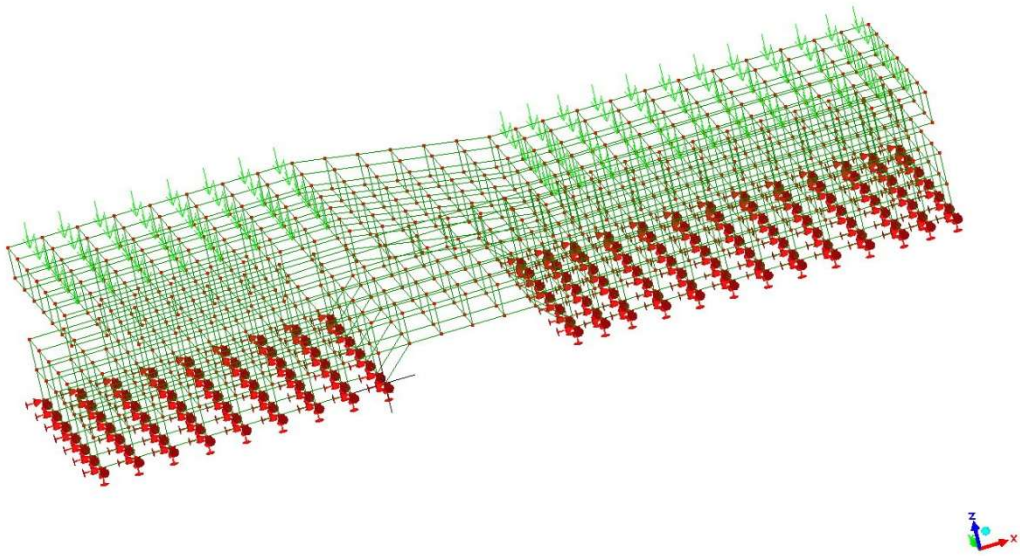

Figure 5.7: Applied Loads and Boundary Conditions for Convergence Tests (Green Arrows: Applied Loads; Red Arrows: Boundary Conditions)

5.2.2 Stiffness calculation

In mechanics, a linear stiffness k is defined as $k = F/X$, the ratio of force F to the corresponding displacement X, where X must be measured in the direction of F and at the same point of application of F (Shigley's Mechanical Engineering Design, 11th Edition, Sec. 4-1). By this definition of linear stiffness, force F would be the force at the selected node and in the same

direction as *X*. While displacement *X* was a direct output from LISA FEA simulation, the challenge arose in determining *F* since the applied loads were uniform pressures (Figure 5.7; also Figure 5.11); that is, force *F* at any node was not given as outputs from LISA. Although force *F* could be estimated manually, it was decided to instead report the applied force and displacement. In the literature, reporting applied loads and displacements at separate selected points was common. Similarly, this thesis also presents the ratios of applied force to displacement. Such ratios, not stiffnesses in the strict sense, can be used to gain insights into the characteristics of the design in question.

5.2.3 Materials and verification of the model

In LISA as in any FEA software, linear static analyses can be conducted using various combinations of materials, especially those commonly found in prosthetic feet, which include, for example, composites consisting of carbon fibers or glass fibers, and other materials such as polyethylene, polypropylene, rubber, and polyurethane, and so on (Kadhim et al., 2022; Oleiwi & Hadi, 2021). Although the intended materials for this research were nylon for the top and bottom plates and TPU for the pads, the properties of these materials were not known, in particular, not known after they were 3D-printed.

In the literature, Saunders et al. (2003) developed an approach that incorporated motion analysis, mechanical properties testing, and FEM to analyze a SACH foot. In terms of mechanical properties, the researchers tested the keel, base, heel, and toe. However, what portions of the SACH foot were the base, keel, etc., were not specified in the article. Nevertheless, the literature provided enough detail for this researcher to use their results to calibrate the FEA model developed in LISA. For example, in the foot flat position (Figure 5.8), the literature reported a heel deflection of 7.07 mm, resulting in a stiffness of 112.4 N/mm. Meanwhile, their experimental results showed a

stiffness of 96.39 N/mm. In addition, experimental results for stiffness in the heel strike and toe off positions were reported as 154.1 and 102.8 N/mm, respectively. But the article did not report computational deflection results for the heel strike and toe off positions.

The LISA FEA model shown in Figure 5.5 was constructed to consist of eight "blocks" of elements that can be assigned block-wise mechanical properties. Figure 5.9 illustrates the material blocks whose properties, as assigned, are listed in Table 5.2. In assigning these properties, references were made to Table II of Saunders et al. (2003) which listed the material properties of the keel (E = 8400 kPa, v = 0.3), base (E = 7.17 kPa, v = 0.4), heel (E = 5.71 kPa, v = 0.44) and toe (E = 18.4 kPa, v = 0.33). Reference was also made to Figure 5.10, which displays the construction of a SACH (Yousif et al., 2018). It should be noted that in Table 5.2, the moduli of elasticity are in terms of MPa, not kPa. This was because using the elastic moduli as given in Saunders et al. (2003) would yield displacements of more than one hundred millimeters in the heel region, which seemed excessive. The material properties listed in Table 5.2 were, in fact, the outcomes of a few iterations on the elastic moduli, after switching the unit to MPa. The load applied to the heel was 794 N (Saunders et al. 2003), which was applied over an area in the heel region, as seen in Figure 5.11(a). Boundary conditions are also shown in Figure 5.11(a). Figure 5.11(b) displays the Z-displacement plot, showing also the selected node. Table 5.3 gives the computed heel deflections and the resulting force-to-displacement ratio. The computed and experimental results on stiffness by Saunders et al. (2003) are also included for easy comparison. The SACH foot simulated in the literature is different from the proposed design in this thesis. Direct comparison may not be meaningful. However, the force-to-displacement ratio from the LISA simulation aligns well with that from the literature. In addition, it is within the experimental stiffnesses that will be reported later (see Tables 5.6 through 5.8).

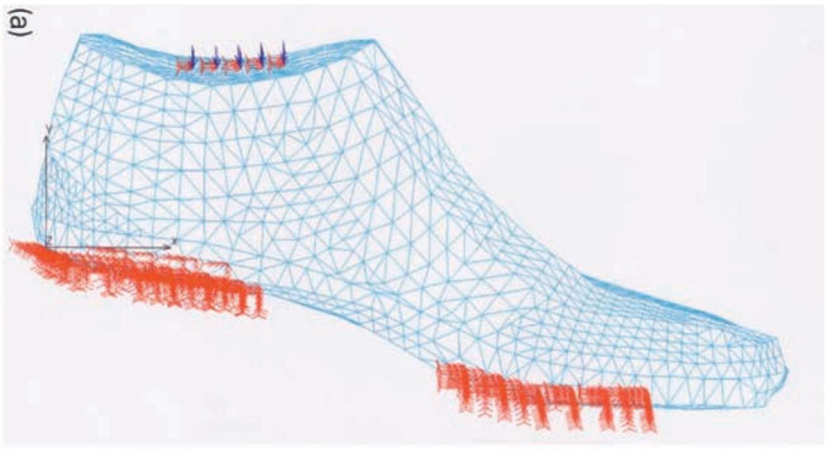

Figure 5.8: Applied Loads (Purple Arrows) and Boundary Conditions (Red Arrows) for Foot Flat Position. Adapted from Saunders, et. al. 2003.

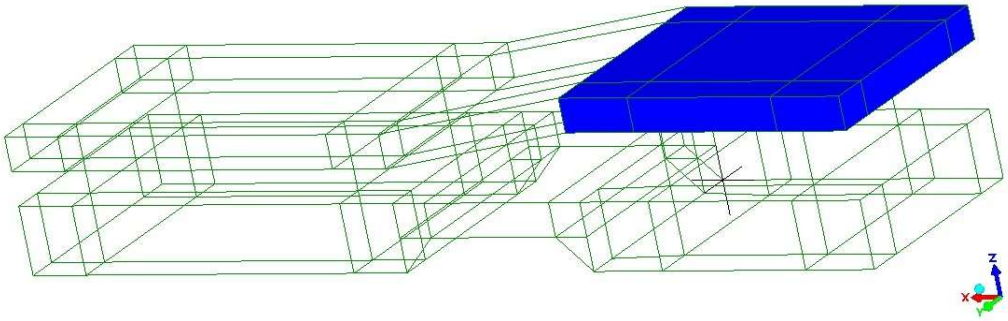

(a) Block 1

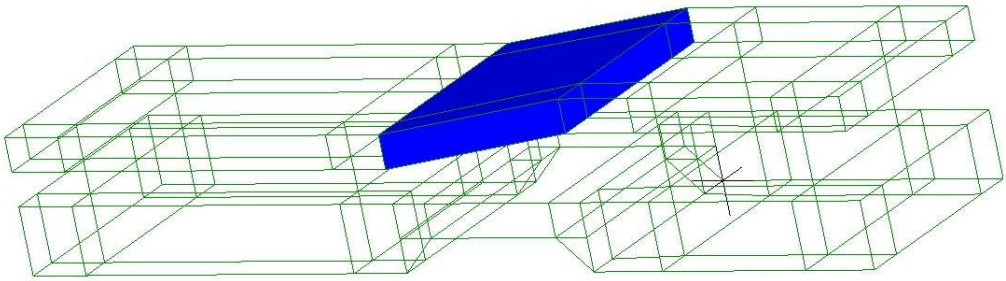

(b) Block 2

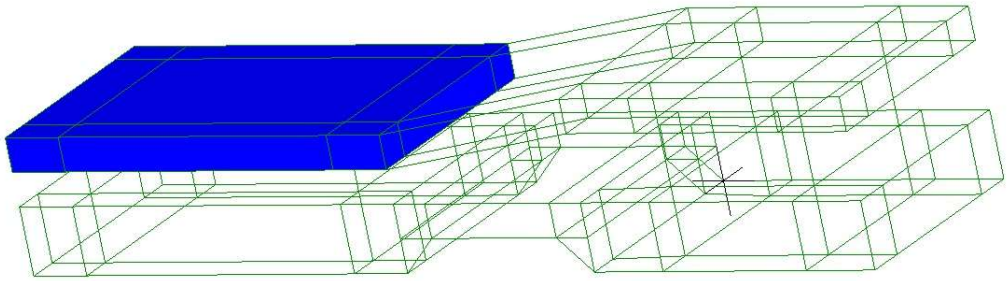

(c) Block 3

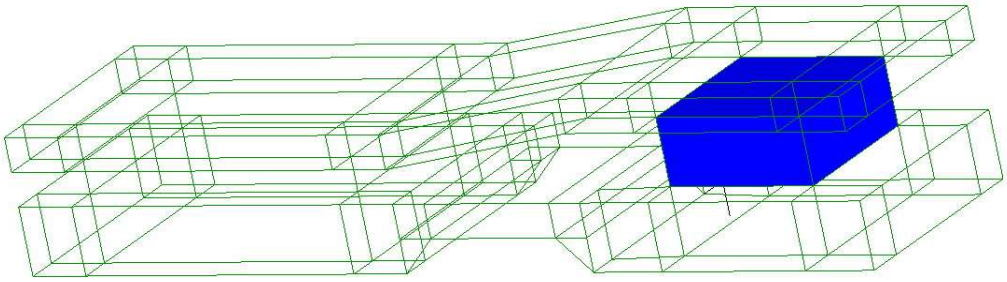

(d) Block 4

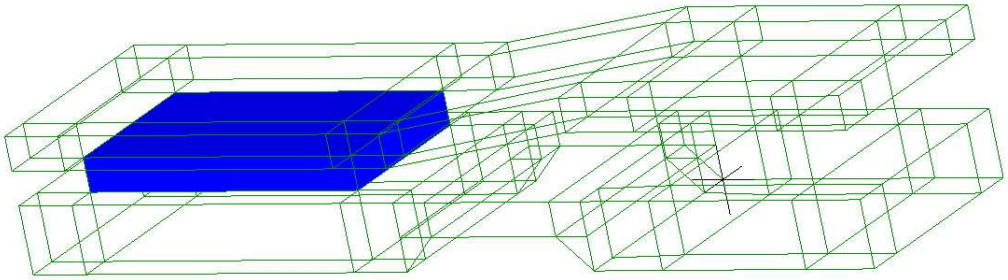

(e) Block 5

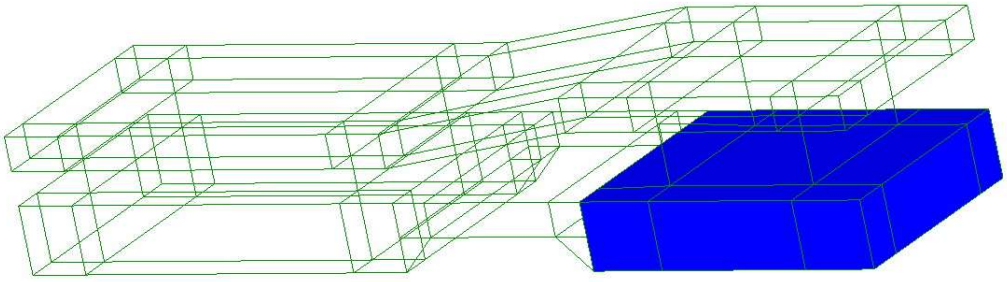

(f) Block 6

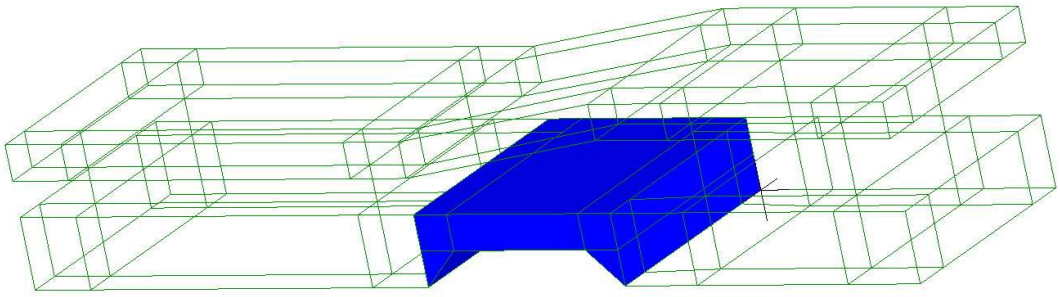

(g) Block 7

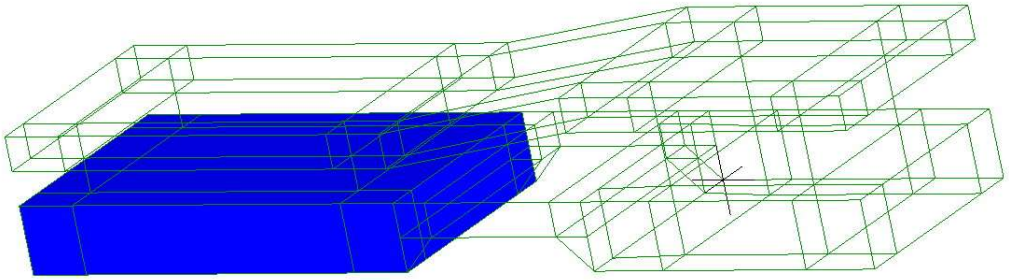

(h) Block 8

Figure 5.9: Material Blocks in the LISA FEA Model

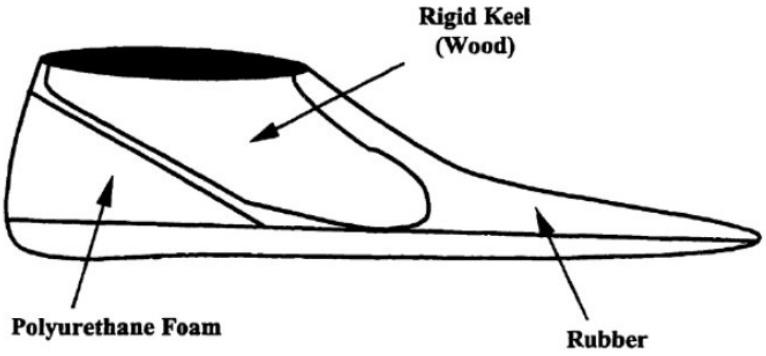

Figure 5.10: Construction of a SACH Foot. Adapted from Figure 1, Yousif et al., 2018.

Table 5.2: Mechanical Properties Used in Verification

Material Block(s)	Modulus of Elasticity, MPa	Poisson's Ratio
1, 2, 3	7.17	0.40
4	1.14	0.44
5	18.40	0.33
6, 7	2,400.00	0.30
8	1,200.00	0.30

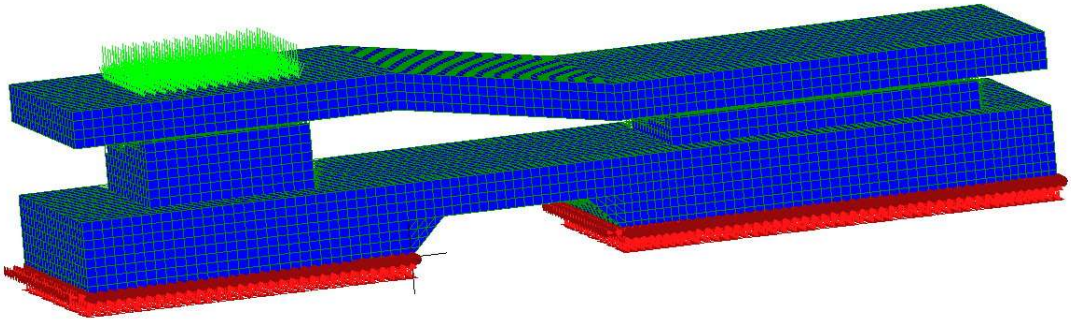

Figure 5.11(a): Applied Loads and Boundary Conditions, for Foot Flat Situation

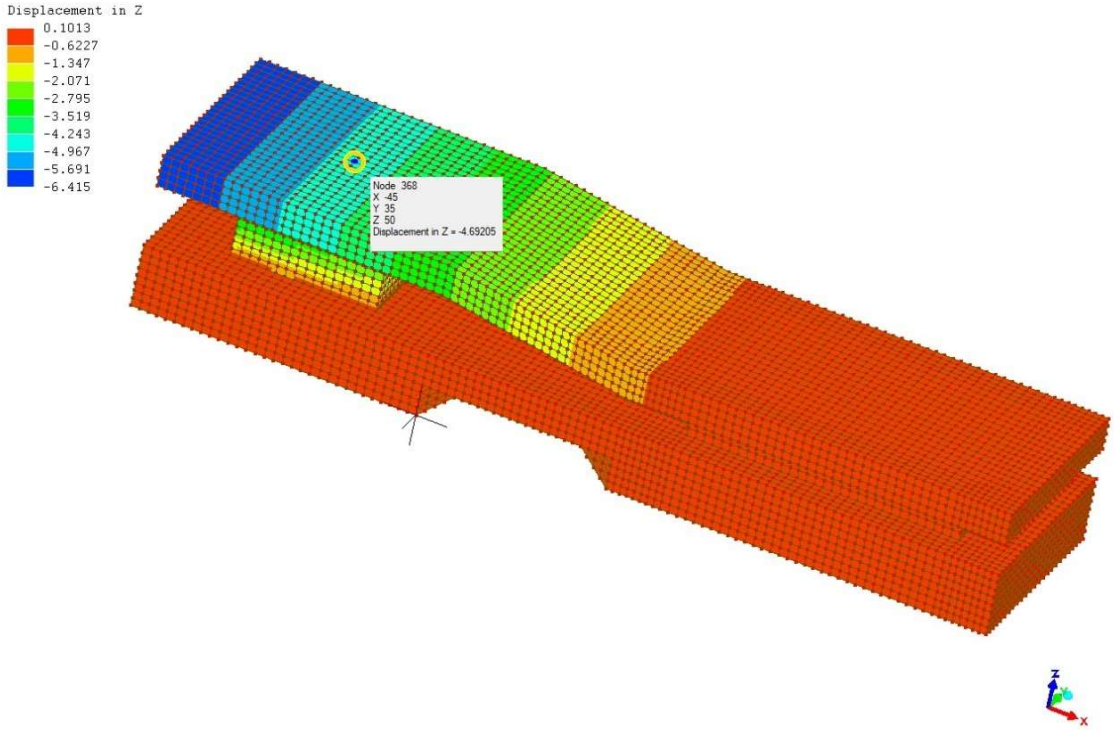

Figure 5.11(b): Deformation in the Z-Direction, for Foot Flat Situation

Table 5.3: Heel Displacements and Stiffnesses (Applied Load = 794 N, or Uniform Pressure = 0.375236 N/mm^2 over an area of 2116 mm^2)

Position	Foot Flat
Heel Deflection at Selected Node, mm	4.69
Force-to-Displacement Ratio, N/mm	169.22
Computed Stiffness*, N/mm	112.40
Experimental Stiffness*, N/mm	96.36

* Saunders et al. (2003)

5.3 FEA Simulations of the Simplified Design 4

5.3.1 Forces and boundary conditions

To accurately simulate a foot's deformation, it became necessary to understand the load that is being applied to the foot when the person is standing. It has been determined that an average male applies a force of approximately 850 N while standing, based on the average weight of adult males. From the perspective of human anatomy, when standing, the heel is to support the body weight, and the toes are to maintain stability. Based on this understanding, 500 N was applied on the heel, while the remaining force of 350 N was exerted on the forefoot. The second reason for splitting the body weight, as mentioned above, had to do with the objective of the FEA. It was to evaluate linear stiffness at selected locations. It was not to compute stresses and factors of safety. Therefore, the amount of force applied was secondary to the geometric shapes and dimensions of the design, as well as the properties of the materials. This insight led to the application of a 500-N force on the heel, and simultaneously a 350-N force on the forefoot. Both forces were uniformly distributed across the heel and forefoot regions when conducting the simulations, as demonstrated by the green arrows on the top plate as seen in Figure 5.12. Two more situations were simulated, (1) heel loading where an 850 N force was applied as a uniform pressure over the heel region and the only the heel region of the bottom plate was constrained; and (2) forefoot loading where an 850 N force was applied as a uniform pressure over the forefoot region and the forefoot region of the bottom plate was constrained.

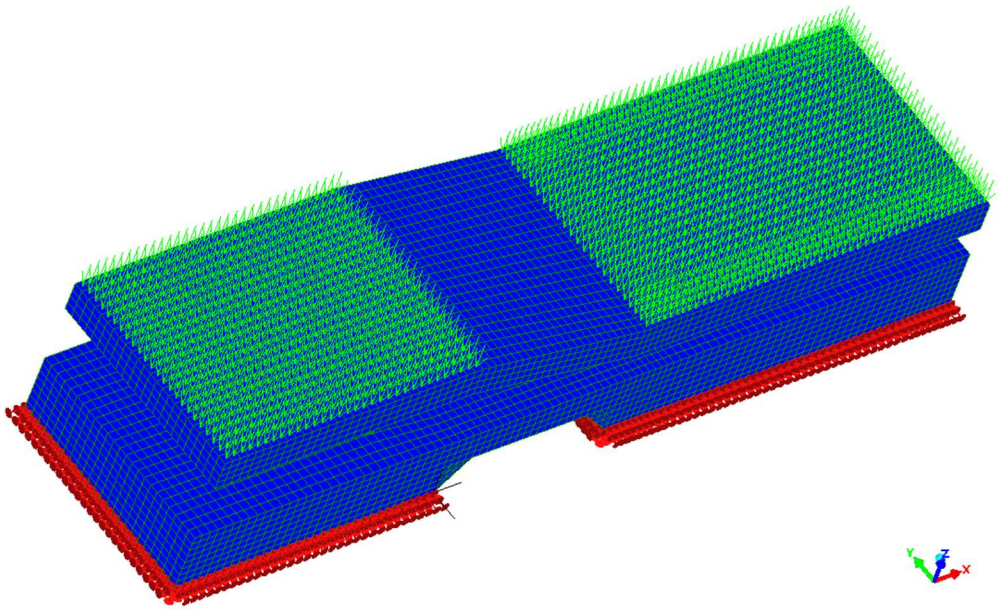

Figure 5.12: Applied Loads and Boundary Conditions for the Simplified Design

As shown in Figure 5.12, the fixed boundary conditions represented by the red arrows were applied on the bottom surface of the bottom plate across the heel and forefoot regions to simulate the situation when the entire foot is pressed on the ground. The fixed boundary conditions will keep the heel and forefoot regions on the bottom surface from translating in any direction. This approach allowed the researcher to apply FEA to gain a better understanding of how the designs (including material selections) respond to a certain static load.

Stiffness was chosen to represent the response of a design and its materials to a statically applied load. With stiffness known, the designs can be compared to stiffness values reported in the literature, some of which were included in the discussion portion of Section 4.1.3 and in Saunders et al. (2003), for example. The computation of stiffness using FEA will help examine the effect of the applied loads on various material combinations, gaining valuable insights into the flexibility (stiffness not being too high) and stability (stiffness not being too low) of the prosthetic designs.

5.3.2 Materials properties

Table 5.4 below gives the mechanical properties used in the LISA FEA simulations of the simplified design 4. They are different from those used for verification (see Table 5.2). For Blocks 1 to 3 (the bottom plate) and 6 to 8 (the top plate), the properties are close to those of nylon. Block 5 is assigned an elastic modulus at approximately 50% of that for polyurethane; Finally, Block 4 is made 50% softer than Block 5.

Table 5.4: Mechanical Properties Used in the Simulations

Material Block	Modulus of Elasticity, MPa	Poisson's Ratio
1, 2, 3	400.00	0.3
4	0.90	0.4
5	1.80	0.4
6, 7, 8	400.00	0.3

5.3.3 Simulation results and discussions

Figures 5.13 through 5.15 show the Z-displacements of the standing, heel loading, and forefoot loading cases. Table 5.5 lists the displacements at selected nodes and the corresponding force-to-displacement ratios. It is interesting to note that, examining the force-to-displacement ratios for the standing position and for loading at the heel region, the ratios are very close, at 139.743 versus 139.964 N/mm, which are above the stiffness values reported by Saunders et al. (2003) but within the experimental results to be reported later (see Tables 5.6 through 5.8). The force-to-displacement ratios for the standing position and for loading at the forefoot region are larger and not as close as the ratios for the heel. As discussed in previous sections, a large stiffness may assist in propelling the foot and body forward, while a small stiffness may benefit from absorbing impacts at heel strike.

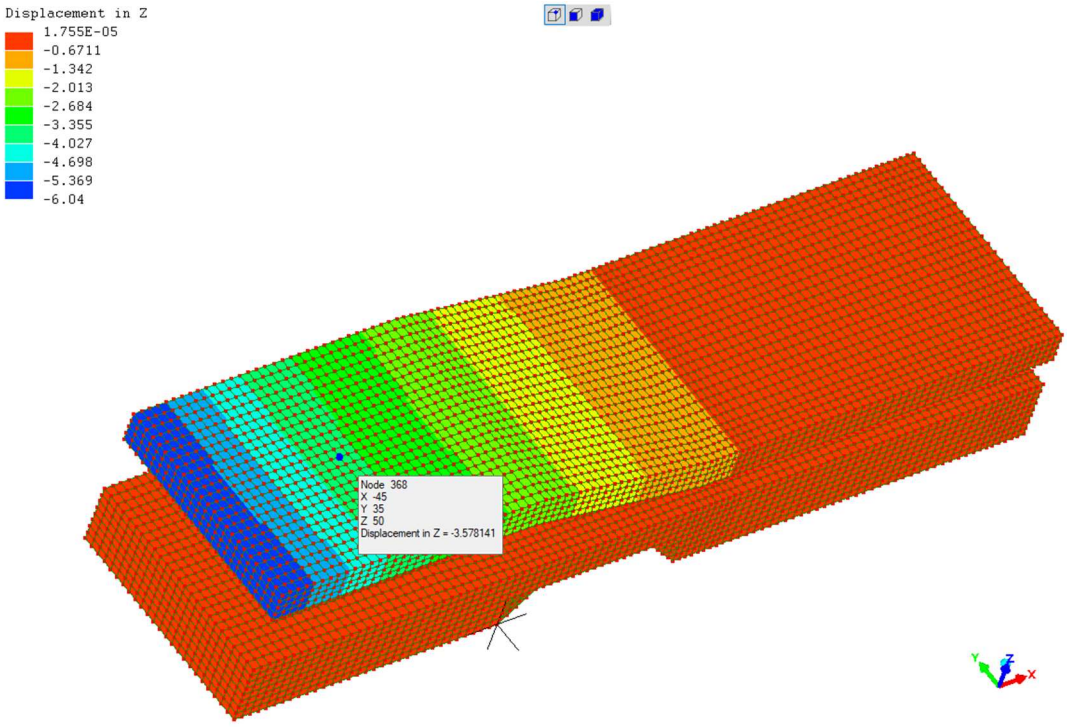

Figure 5.13: Displacements in the Z-Direction, Standing Position.

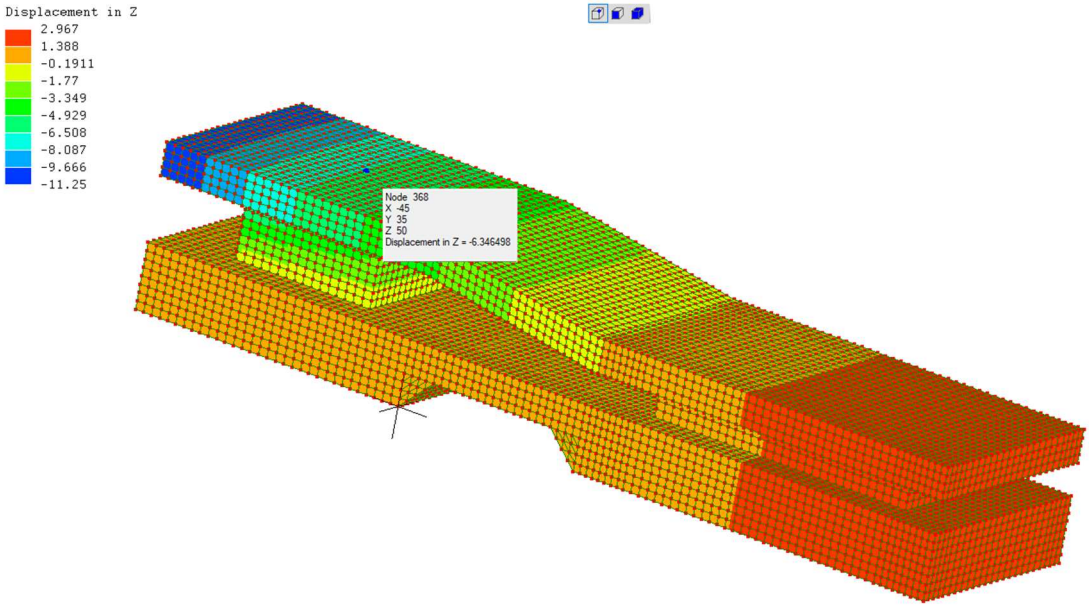

Figure 5.14: Displacements in the Z-Direction, Loaded at the Heel.

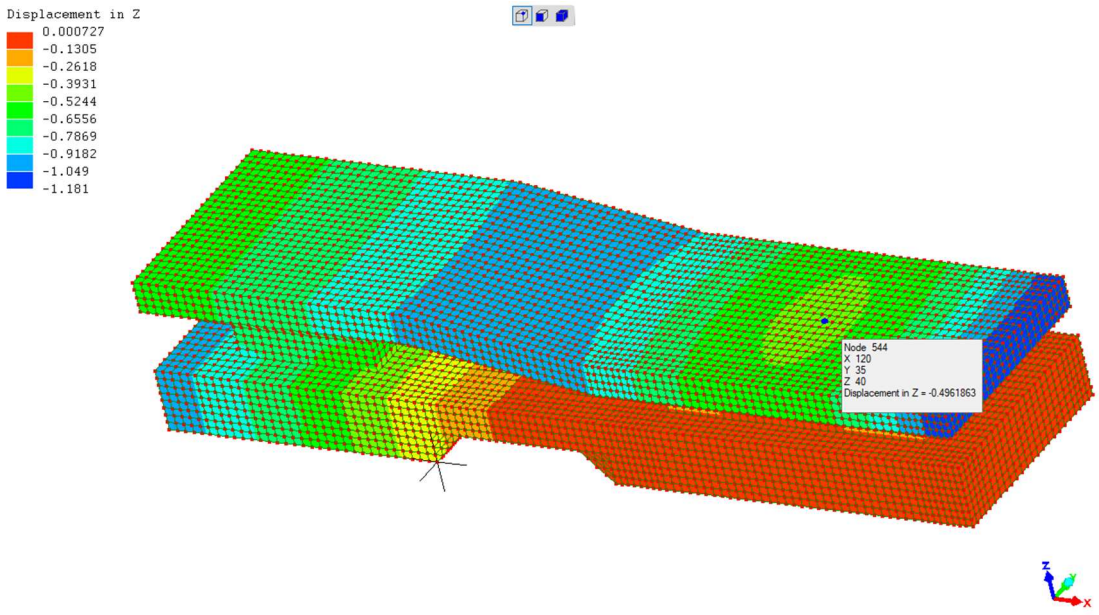

Figure 5.15: Displacements in the Z-Direction, Loaded at the Forefoot.

Table 5.5: Displacements and Force-to-Displacement Ratios

Position	Standing (500 N on the heel and 350 N on the forefoot)	Heel (850 N on the heel)	Forefoot (850 N on the forefoot)
Heel Deflection, mm	3.578	6.073	-
Forefoot Deflection, mm	0.186	-	0.496
Force-to-Displacement Ratio at the Heel, N/mm	139.743	139.964	-
Force-to-Displacement Ratio at the Forefoot, N/mm	1881.720	-	1713.710
Heel Stiffness*, N/mm	96.360 – 12.400	-	-

* Saunders et al. (2003)

5.4 Experimental Results for the Final Design

The static testing protocol, specifically the CC test, was conducted to evaluate the response of the new foot design created with SolidWorks and 3D printing technology. For this foot design, the researcher used nylon for both the top and lower plates to improve the durability of the foot structure. Additionally, two brands of TPU material were used for the heel and forefoot pads,

namely Tronxy and Polyflex. A series of tests was conducted to identify the best material combination to use in walking that can absorb more energy at heel strike than at push-off to allow a transtibial amputee to propel forward during the gait cycle and acquire a more symmetrical walking pattern (Houdijk et al., 2009; Verdini et al., 2006). For instance, as illustrated in Figure 5.16, the design of the new foot, featuring the Tronxy material at the heel and forefoot, is positioned on the force tester where the load is applied, allowing the necessary data, such as energy and stiffness, to be computed.

Figure 5.16: Final Design with the Tronxy Material for the Heel and Forefoot

5.4.1 Final design without insoles

For individual trials, Tables B.1 and B.2 contain the ratios of energy absorption and stiffness values at both high and low loads for the Polyflex and Tronxy materials tested at the heel and forefoot with the nylon plates and without the use of insoles. Table 5.6 contains the average

ratios of energy absorption and stiffness values at both high and low loads calculated from the three trials presented in Tables B.1 and B.2 at both heel and forefoot.

5.4.1.1 Energy absorptions

The data presented in Table 5.6 shows that, for the heel area, the Tronxy has an energy absorption ratio of 0.448, while the Polyflex has an energy absorption ratio of 0.320. This outcome suggests that the Tronxy absorbs more energy at the heel than the Polyflex when compressed with the same amount of force. This result seems promising in identifying a material that absorbs the most energy during heel strike for a transtibial amputee. In the forefoot area, the situation is reversed, as the Tronxy has an energy absorption ratio of 0.187, but the PolyFlex has a higher energy absorption ratio of 0.247. These outcomes are desirable and suggest Tronxy is a better choice of material for the heel and forefoot pads. The rationale behind this is as follows. The Tronxy absorbs 44.8% of the energy “at heel strike” and returns 81.3% of the energy “during toe-off”. In contrast, the Polyflex absorbs 32.0% and returns 75.3%. Absorbing more energy at heel strike than at push-off allows a transtibial amputee to propel forward during the gait cycle and acquire a more symmetrical walking pattern (Houdijk et al., 2009; Verdini et al., 2006). As stated by Hafner et al. (2002), the prosthetic foot must mimic the two phases of loading and unloading that are seen during normal gait by dissipating high impact forces, storing energy during the loading and midstance phases, and returning the energy during late stance until toe-off. That is, the less energy is absorbed during the late stance, the better a prosthetic foot can mimic the gait pattern of non-amputees.

Table 5.6: Average Values for the Final Design without Insoles

Material	Polyflex		Tronxy	
Foot Area	Heel	Forefoot	Heel	Forefoot
Ratio of Absorption	0.320	0.247	0.448	0.187
k for high load in loading, N/mm	486.996	256.275	520.783	857.828
k for high load in unloading, N/mm	998.599	852.124	1273.633	1474.633
k for low load in loading, N/mm	4.403	329.410	19.054	275.797
k for low load in unloading, N/mm	6.400	349.061	9.681	341.197

5.4.1.2 Stiffness at high load

For the stiffness values listed in Table 5.6, the loading condition has lower stiffness values than the unloading condition, similar to the results presented in Section 4.1.3, for example. This outcome is due to the strain-induced stiffness of the TPU material. That is, when the material is stretched during loading, its internal polymer chain starts loose and gradually aligns in the direction of the force to make the material stiffer (Scetta et al., 2021). During the unloading condition, however, the aligned chain resists deformation, making the stiffness values higher than the values obtained during the loading phase (Scetta et al., 2021).

In regard to the compressive behavior of 3D printed TPUs, Iacob et al. (2024) tested samples that were printed at different temperatures, infill densities, and patterns. Figure 5.17, or Figure 4c of Iacob et al. (2024), shows the test result of a sample under four cycles of loading and unloading, where the first cycle has noticeably different behaviors than the remaining ones. Experimental tests run in this thesis exhibited the same phenomenon. 3D-printed samples, when coming off the printers, typically have some remnant support materials attached to the samples. The first loading-unloading cycle would break off the bonds between the sample and remnant support materials, hence showing a different behavior than the cycles that follow.

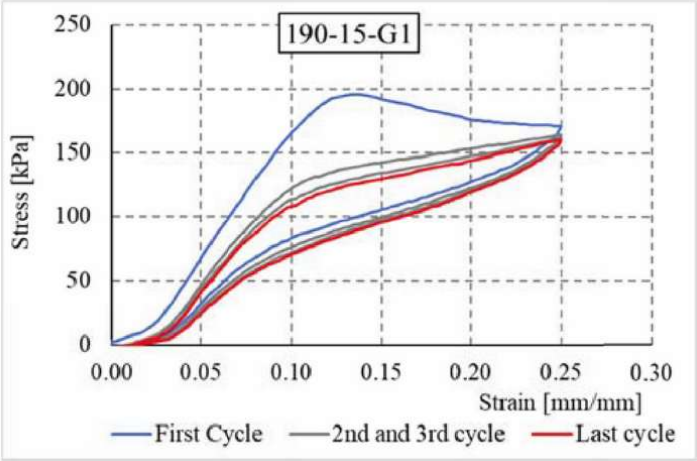

Figure 5.17: Stress-Strain Plot of a 3D Printed TPU Sample. Adapted from Iacob et al., 2024.

In both the loading and unloading conditions under high loads, the Tronxy material shows a higher stiffness than the PolyFlex at the heel as well as at the forefoot. For example, the Tronxy material achieved a stiffness value of 520.78 N/mm under the high-load loading condition and a stiffness value of 1273.63 N/mm under the high-load unloading condition at the heel. In comparison, the Polyflex material achieved lower stiffness values with scores of 486.99 N/mm for high-load loading and 998.59 N/mm for high-load unloading at the heel. At the forefoot, the stiffness values were, for the Tronxy insole, 857.828 and 1474.633 N/mm for high-load loading and unloading, respectively. The Polyflex had substantially lower high-load stiffnesses. These differences suggest that, in the high load situation and during both the “heel strike” and “toe off”, the Tronxy material deforms less than the Polyflex material and more easily returns to its original form upon release of the load.

This outcome suggests that the Tronxy is the material that appears to be the most promising to store energy to help the body propel forward to acquire better walking symmetry for a transtibial amputee.

5.4.1.3 Stiffness at low loads

When examining the stiffness values for the Tronxy and Polyflex materials in the low-load condition during loading and unloading at the heel, as shown in Table 5.6, the results indicate higher stiffness values of 19.054 N/mm during loading and 9.681 N/mm during unloading for the Tronxy material when compared to the Polyflex material with stiffness values of 4.403 N/mm during loading and 6.400 N/mm during unloading. However, when examining the low-load stiffness values for the Tronxy and Polyflex materials in the loading and unloading conditions at the forefoot, as shown in Table 5.6, the results indicate lower stiffness values of 275.797 N/mm during loading and 341.197 N/mm for the Tronxy material when compared to the Polyflex material with stiffness values of 329.410 N/mm during loading and 349.061 N/mm during unloading. That is, the Tronxy had higher low-load stiffnesses at the heel than the Polyflex, which suggests that the Polyflex material deforms more than the Tronxy material under the same load at the heel for a low load. The Tronxy material, on the other hand, had slightly lower low-load stiffness values at the forefoot. In particular, stiffness was 341.197 N/mm for Tronxy and 349.061 N/mm for Polyflex under the low load unloading condition. Keeping in mind that too soft a cushion would feel like "walking on squish gels," which may cause loss of stability and balance when walking, the Tronxy seems to be attractive for use in the prosthetic foot's design to help the transtibial amputee propel forward during the gait cycle.

In summary, considering energy absorptions, the Tronxy stands as a better choice of material for the heel and forefoot pads. On the other hand, from the stiffness perspective, especially the high-load stiffness perspective, the Tronxy seems to be more promising to store the energy to help the body propel forward.

5.4.2 Final design with insoles

Again, for individual trials, Tables B.3 through B.6 contain the ratios of energy absorption and stiffness values at both high and low loads for the Polyflex and Tronxy materials, with Polyflex and Tronxy insoles tested at the heel and forefoot using nylon plates. Table 5.7 lists the average ratios of energy absorption and stiffness values at both high and low loads, calculated from the three trials presented in Tables B.3 through B.6, for both the heel and forefoot. Figure 5.18 displays an experimental setup featuring Tronxy heel and forefoot pads, as well as an insole.

Table 5.7: Average Values for the Final Design with Insoles

Insole	Tronxy			
Heel pad and forefoot pad material	Polyflex		Tronxy	
Foot area	Heel	Forefoot	Heel	Forefoot
Ratio of absorption	0.328	0.323	0.446	0.210
k for high load in loading, N/mm	233.824	221.893	296.478	692.085
k for high load in unloading, N/mm	750.780	719.462	911.275	1268.933
k for low load in loading, N/mm	4.218	202.277	5.681	223.251
k for low load in unloading, N/mm	6.845	182.881	28.591	272.083

Table 5.7 (continued): Average Values for the Final Design with Insoles

Insole	Polyflex			
Heel pad and forefoot pad material	Polyflex		Tronxy	
Foot area	Heel	Forefoot	Heel	Forefoot
Ratio of absorption	0.354	0.318	0.436	0.201
k for high load in loading, N/mm	347.676	224.412	358.012	489.119
k for high load in unloading, N/mm	784.177	654.168	903.569	999.478
k for low load in loading, N/mm	3.506	193.806	5.270	222.993
k for low load in unloading, N/mm	6.327	164.094	24.018	242.182

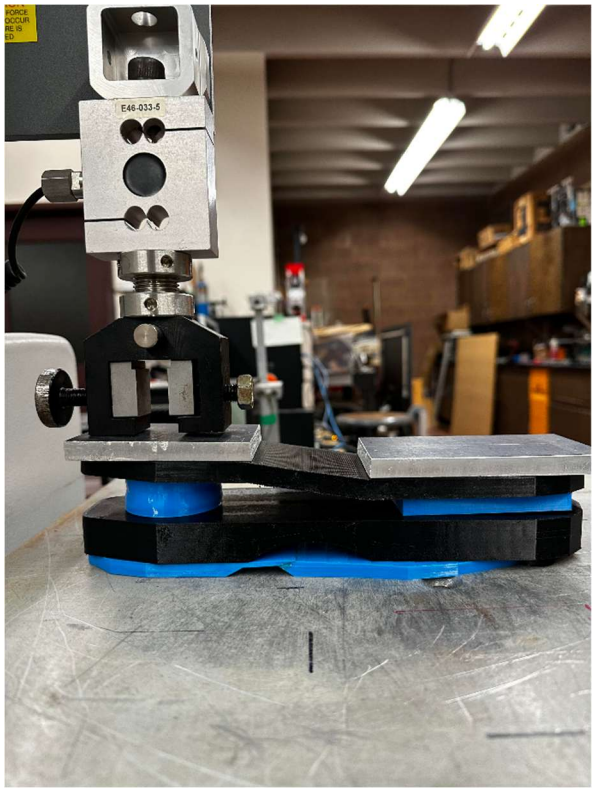

Figure 5.19: Final Design with Tronxy Material for Heel, Forefoot, and Insole

When comparing the average values in Table 5.7, the Tronxy pads combined with the Tronxy insole show the most promising results at the heel and forefoot. This configuration of the Tronxy pads with the Tronxy insole yields an average energy absorption ratio of 0.446 at the heel and 0.210 at the forefoot. It is interesting to note that, without the insole, the Tronxy heel and forefoot pads produced an absorption ratio of 0.448 at the heel and 0.187 at the forefoot (Table 5.6). That is, the Tronxy insole benefited energy absorption at the forefoot. This outcome suggests an improvement in energy absorption at the forefoot for the Tronxy heel and forefoot pads when used with the Tronxy insole, with a lower energy absorption ratio at the forefoot, which aligns better with the concept of force and energy absorption to improve symmetry of walking in a transtibial amputee, as stated by Houdijk et al. (2009) and Verdini et al. (2006).

For further verification, the average stiffness values for high and low loads from both the loading and unloading conditions were obtained and compared in Table 5.7. In examining the stiffness under high load, the combination of Tronxy pads with Tronxy insole yielded the highest stiffness values for unloading at the forefoot. At the heel, for loading in high load, both the combination of Tronxy pads and Tronxy insole, and the combination of Tronxy pads and Polyflex insole seemed to show high stiffness, suggesting that the pads may play a more crucial role than the insole in the high-load stiffness during loading. For low-load stiffness at the forefoot, the combination of Tronxy pads with Tronxy insole also yielded the highest stiffness values.

The above outcomes suggest that the combination of Tronxy heel and forefoot pads with Tronxy insole may have a superior ability to absorb energy while maintaining sufficient stiffness to ensure stability and balance during gait. The outcomes also align with the earlier results and discussions comparing various materials without insoles. The outcomes are also supported by the properties of TPU material, which is known to exhibit the Mullins effect (Figure 5.18), which allows it to absorb energy through a phenomenon called strain-induced softening. This effect is characterized by a reduction in stiffness during the first loading cycle, followed by a smaller hysteresis loop in subsequent cycles (Miao et al., 2019).

5.4.3 Final design with parts glued

This protocol entailed gluing the plates to the heel and forefoot pads to obtain a complete final design and to test for more accurate data on the design. Based on data from the previous protocol, the Tronxy was identified as the desirable material for the prosthetic foot design; therefore, it was also applied as the material for the plates, resulting in two test models (Figure 5.20). The first one used nylon for the plates, the Tronxy for the heel and forefoot pads. The second model used Tronxy for the top and bottom plates as well as the heel and forefoot pads. The Tronxy

plates were printed with 25% infill density in contrast to the 10% and 15% infill densities for the heel pad and forefoot pad, respectively. This approach enabled the comparison of the two models to assess the effects of materials on energy absorption and stiffness when the plates are glued to the heel and forefoot pads, as shown in Figure 5.20.

The experiment was conducted with the CC test being performed again. This test involved applying a load of 1230 N on the prosthetic foot using a force tester, followed by the removal of the load for a total of 16 cycles of loading and unloading. This process was repeated for three trials to ensure an accurate comparison of the data for both the heel and forefoot of each model.

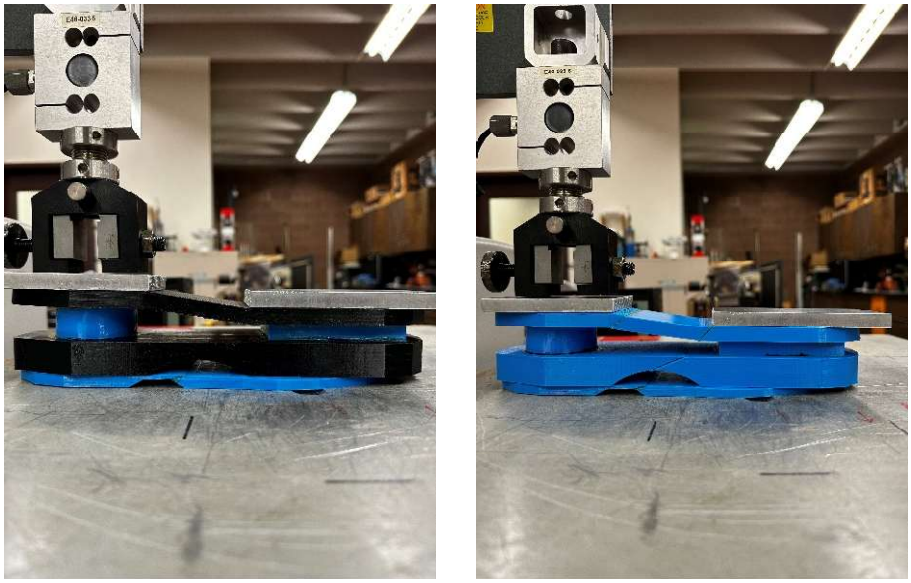

Figure 5.20: Experimental Setups (Left: Nylon Plates Model; Right: Tronxy Plates Model).

5.4.3.1 Energy absorption

The results shown in Table 19 highlight notable differences between the models in terms of their performance. For instance, during heel strike, the nylon model has an energy absorption ratio of 0.475, higher than the Tronxy model with an energy absorption ratio of 0.441. At toe off, the nylon model absorbed 24.5% of the energy while the Tronxy model absorbed 28.5%. This

outcome seems to suggest that the nylon model may provide an easier push off to propel the foot forward during walking while it absorbs more energy at heel strike, making the nylon model a better choice. By absorbing more energy at heel strike, the prosthetic foot will reduce the impact experienced by an amputee. The nylon model also helps the foot maintain a more natural gait by returning more of the stored energy to propel the foot and body forward in a gait. According to Hafner et al. (2002), prosthetic feet must effectively mimic both the loading and unloading phases. This concept involves reducing impact force, storing energy during the loading and mid-stance phases, and returning that energy during the late stance to propel the foot forward. Additionally, less energy absorption during the late stance of the forefoot generally indicates a better ability of the foot to replicate natural walking motion based on Childers et al. (2018).

Table 5.8: Average Values for Final Design Printed with Different Plate Materials

Material for the plates	Tronxy		Nylon	
Foot area	Heel	Forefoot	Heel	Forefoot
Ratio of absorption	0.441	0.285	0.475	0.245
k for high load in loading, N/mm	226.637	214.545	202.067	336.044
k for high load in unloading, N/mm	631.199	621.363	704.883	839.241
k for low load in loading, N/mm	2.149	185.257	20.592	199.082
k for low load in unloading, N/mm	32.465	171.214	29.196	227.635

5.4.3.2 Stiffness at high load

As in previous experiments, stiffness was determined at low and high loads and during two phases: the loading phase, when the load was applied, and the unloading phase, when the load was removed.

In the loading phase under a high load at the heel, the Tronxy model demonstrated greater stiffness, measuring 226.637 N/mm, compared to the nylon model, which had a stiffness value of 202.067 N/mm. However, the situation changed during the unloading phase at the heel. The nylon

model exhibited a stiffness of 704.883 N/mm, higher than the unloading stiffness of the Tronxy model at 631.199 N/mm. When focusing on the forefoot under the high load, the nylon model consistently showed higher stiffness values for both the loading and unloading phases, measuring at 336.044 and 839.241 N/mm, respectively. These outcomes suggest that the nylon model not only has sufficient resistance to deformation when a load is applied to the heel or forefoot but also allows the foot to return to its original shape more easily during the toe off.

5.4.3.3 Stiffness at low load

Under the low load, the nylon model demonstrated significantly better resistance to deformation at both the heel and forefoot during the loading phase compared to the Tronxy model. This is evident from the average stiffness values listed in Table 5.8, where the nylon model had values of 20.592 and 199.082 N/mm at the heel and forefoot, respectively, while the Tronxy model showed lower stiffness values of 2.149 and 185.257 N/mm at the heel and forefoot, respectively. However, in the unloading phase, when the load is removed, the scenario changed. The stiffness of the Tronxy model was higher than that of the nylon model, with values of 32.465 N/mm for the Tronxy and 29.196 N/mm for the nylon.

As the Tronxy model had very low stiffness, 2.149 N/mm, at the heel during the loading phase when the load was light, it may not be beneficial for maintaining stability and balance in gait. The nylon model, however, had higher stiffnesses in the forefoot region during both the loading and unloading phases. In addition, the stiffnesses of the nylon model at the heel did not reach values as low as 2.149 N/mm during loading or unloading. This characteristic, together with the nylon model's more desirable energy absorption ability, makes it a winner over the Tronxy model.

In passing, it may be worthwhile to mention that, due to the sizes of the hot plate, the Tronxy top plate, as well as the bottom plate, were each 3D-printed as two separate pieces and then glued together as a plate. The nylon plates, however, were printed as single pieces. It is currently unknown whether printing the components separately had any effect on the outcome, or to what extent. Further testing with additional samples will be required to determine this. Changing the infill density when printing the Tronxy plates will no doubt change the characteristics of the Tronxy model to match or surpass those of the nylon model. This may be advantageous in the long run as TPU filaments are generally more cost-effective than nylon filaments. Compared to TPUs, nylon also requires specialized 3D printers to print.

Chapter 6: Findings and Recommendations for Future Work

This chapter presents the key observations from both the experimental and simulation aspects of this study. The objective of this research was to develop an affordable alternative prosthetic foot design that offers adaptability for the user. The study analyzed three different commercial models (Wooden Foot, Otto Bock Trias, and Sierra Foot) alongside a prosthetic foot design created in SolidWorks. This analysis employed Finite Element Analysis, which examined node forces and node displacements within the simulations for the proposed design. Additionally, energy absorption and stiffness were computed for both the commercial models and the new design.

6.1 Key Findings

6.1.1 Chapter 4 Findings

Chapter 4 primarily focuses on evaluating the commercial prosthetics using three protocols with the force tester.

Commercial Prosthetic with no Insoles

The Wooden foot demonstrated higher energy absorption. This type of prosthetic foot, however, is known to return less energy during the gait cycle, resulting in asymmetrical walking patterns. Among the two ESAR feet, the Otto Bock Trias exhibited slightly more energy retention than the Sierra.

Regarding stiffness under high load, the Otto Bock Trias showed the highest stiffness during the loaded stage, while the Wooden foot held the highest stiffness in the unloaded stage. The Sierra exhibited the lowest stiffness in both stages, indicating it is less resistant to loads.

For low-load stiffness, the Wooden foot maintained the highest stiffness, with loaded stiffness exceeding that of the unloaded stiffness. In contrast, both the Otto Bock Trias and Sierra prosthetics had higher unloaded stiffness than loaded stiffness.

Wooden Foot with TPU Insoles

The Wooden Foot with the Tronxy TPU insole ended up having the highest energy absorption and the highest stiffness level for both the high and low load cases. This outcome revealed an improvement in energy absorption when compared to the no insole protocol. The Wooden Foot with the Polyflex TPU insole was found to be the material with the lowest stiffness. The variation in stiffness among TPU materials was attributed to the Mullins effect.

Commercial Prosthetics with a 15-degree wedge

All commercial prosthetic feet were shown to have more loaded energy during the plantar flexion stance, followed by midstance, and then dorsiflexion stance. The Sierra foot was revealed to have the highest loaded energy during all three stances.

In terms of energy absorption, the wooden foot absorbed the most energy. Between the Otto Bock Trias and Sierra, the Sierra absorbed more energy during the plantarflexion, while the Otto Bock absorbed more energy during dorsiflexion.

When the wooden foot was tested with the insoles, the plantarflexion and midstance foot positions had more loaded energy, but less in the dorsiflexion position. In terms of energy absorption, however, the wooden foot with the Tronxy and Polyflex insoles had higher energy absorption during the dorsiflexion foot position. Finally, the wooden foot with the Sain Smart and Pxmallion insoles also had high loaded energy during dorsiflexion and plantarflexion. The loaded energy, however, was lower in the midstance foot position.

6.1.2 Chapter 5 Findings

Chapter 5 presented the design created in SolidWorks, tested with and without insoles, and when parts are glued.

Simulations Results

Overall, the simulations revealed that the prosthetic foot exhibits similar stiffness values in the standing and heel-loading positions, as shown in Table 5.5. These values are reported to be higher than the stiffness value from Saunders et al. (2003) but falling within the range of the experimental results. The stiffness values for the standing position and the forefoot region were shown to be larger than the heel, but not similar.

Final design Experimental results

In the no-insole condition, the Tronxy foot design absorbed the most energy during heel strike and returned the most energy during the toe off stance, when compared to the Polyflex foot design. In terms of stiffness, the Tronxy showed the highest stiffness for the loading and unloading conditions for both the high-load and low-load, making it the preferred choice for the heel and forefoot pads.

With the addition of the TPU insoles, the Tronxy again produced the highest energy absorption value for both pads and insoles. When comparing this outcome to the results with no insole, an improvement was observed in the forefoot. With regards to the stiffness measures, the results for the high-load and low-load seem to suggest that the Tronxy pads and insole are the preferred choice for the design.

When the Tronxy heel and forefoot pads were glued to the plates for a complete design and tested with the CC test, the model with the Nylon plates absorbed more energy at the heel and less energy during the toe off. This outcome suggests that the Nylon model is the best option for the foot to propel forward during the gait cycle. With respect to stiffness, the Nylon configuration remains the best option to resist deformation during the high-load and low-load phases.

6.2 Recommendations for Future Work

In the future, instead of solely relying on the force tester to simulate the effect of a load on the prosthetic foot, the next step will be to involve human participants. This approach will provide more accurate data for comparing both the commercial design and the custom-designed prosthetic foot. The first step will be to recruit non-amputee participants and use devices that simulate transtibial amputation, as finding actual amputees may prove to be more challenging. Another interesting aspect that can be explored in this research would be to examine the impact that an amputee's leg can have on the healthy leg during the gait cycle.

Additionally, if an amputee can also be found, the same test could be performed to determine the effectiveness of each design and compare them to the created design to gain feedback on what could be improved in the creative design.

It may be beneficial to use a different software tool to conduct simulations on the model. While SolidWorks was effective for 3D modeling, it has limitations regarding simulation, particularly in analyzing nodes. For instance, certain information, such as node force, cannot be directly obtained from SolidWorks.

This study notes that a previous model was designed with springs applied to the heel and forefoot. Therefore, additional funding could be sought to construct the original model with

springs. This approach could potentially allow more flexibility and improve impact absorption during human participant trials.

References

Adamczyk, P. G., Roland, M., & Hahn, M. E. (2017). Sensitivity of biomechanical outcomes to independent variations of hindfoot and forefoot stiffness in foot prostheses. Human movement science, 54, 154-171. https://doi-org.ezproxy.lakeheadu.ca/10.1016/j.humov.2017.04.005

American Orthotic Prosthetic Association. (2010). AOPA'S Prosthetic Foot Project: What It Is. What It Is Not, and What Patient Care Facility Providers/Practitioners Need to Know.

Arun, S., & Kanagaraj, S. (2015). Performance enhancement of epoxy-based sandwich composites using multiwalled carbon nanotubes for the application of sockets in trans-femoral amputees. *Journal of Mechanical Behavior of Biomedical Materials, 59*, 1–10. http://doi.org/cv6h

Berry, C. (2022). Comparing the symmetry of walking in transtibial amputees: biomechanical differences of prosthetic heel lifts. https://knowledgecommons.lakeheadu.ca/handle/2453/5005

Baines, P. M., Schwab, A. L., & Van Soest, A. J. (2018). Experimental estimation of energy absorption during heel strike in human barefoot walking. *PloS one*, *13*(6), e0197428. https://doi.org/10.1371/journal.pone.0197428

Budynas, R. G., Nisbett, J. K., & Shigley, J. E. (2020). Shigley's mechanical engineering design (11th ed.). McGraw-Hill Education. Sec. 4-1.

Bari, M. A., Mir, H. N., Parrey, J. A., Ateeq, A., Ajhar, A., Al Muslem, W. H., Nuhmani, S., Alduhishy, A., & Alsubaiei, M. E. (2023). Exploring variations in gait patterns and joint

motion characteristics in school-aged children across different walking speeds: A comprehensive motion analysis study. Journal of Taibah University Medical Sciences, 18(5), 765–776. https://doi.org/10.1016/j.jtumed.2023.07.006

Berge, J. S., Czerniecki, J. M., & Klute, G. K. (2005). Efficacy of shock-absorbing versus rigid pylons for impact reduction in transtibial amputees based on laboratory, field, and outcome metrics. *Journal of Rehabilitation Research and Development*, *42*(6), 795–808. https://doi.org/10.1682/jrrd.2005.02.0034

Bicchi, A., Gabiccini, M., & Santello, M. (2011). Modelling natural and artificial hands with synergies. *Philosophical Transactions of the Royal Society B: Biological Sciences, 366*(1581), 3153–3161. https://www.jstor.org/stable/23035690

Bonnet, X., Pillet, H., Fode, P., Lavaste, F., & Skalli, W. (2012). Finite element modelling of an energy-storing prosthetic foot during the stance phase of transtibial amputee gait. *Journal of Engineering in Medicine, 226(1)*, 70–75. 10.1177/0954411911429534

Burger, H., & Marinček, Č. (1997). The lifestyle of young persons after lower limb amputation caused by injury. *Prosthetics and Orthotics International, 21*(1), 35–39. https://journals.sagepub.com/doi/pdf/10.3109/03093649709164528

Burnfield, J. M., Eberly, V. J., Gronely, J. K., Perry, J., Yule, W. J., & Mulroy, S. J. (2012). Impact of stance phase microprocessor-controlled knee prosthesis on ramp negotiation and community walking function in K2 level transfemoral amputees. *Prosthetics and Orthotics International, 36*(1), 95–104. https://doi.org/10.1177/0309364611431611

Chen, M. (2025, December 15). How to choose the best carbon fiber prosthetic foot: A complete buying guide. Alibaba Plantin. https://plantin.alibaba.com/buyingguides/carbon-fiber-prosthetic-foot

Childers, W. L., & Takahashi, K. Z. (2018). Increasing prosthetic foot energy return affects whole-body mechanics during walking on level ground and slopes. Scientific reports, 8(1), 5354. 10.1038/s41598-018-23705-8

Chin, T., Machida, K., Sawamura, S., Shiba, R., Oyabu, H., Nagakura, Y., et al. (2006). Comparison of different microprocessor-controlled knee joints on the energy consumption during walking in trans-femoral amputees: Intelligent Knee Prosthesis (IP) versus C-Leg. *Prosthetics and Orthotics International, 30*(1), 73–80. https://doi.org/10.1080/03093640500533414

Collins, J. J., & Whittle, M. W. (1989). Impulsive forces during walking and their clinical implications. *Clinical Biomechanics*, *4*(3), 179-187. https://doi.org/10.1016/0268-0033(89)90023-5

Cook, R. D., Malkus, D. S., Plesha, M. E., & Witt, R. J. (2002). Concepts and applications of finite element analysis (4th ed.). John Wiley & Sons.

Davis, S., & Caldwell, D. G. (2010). The design of an anthropomorphic dexterous humanoid foot. In *Intelligent Robots and Systems (IROS), 2010 IEEE/RSJ International Conference on* (pp. 2200–2205). IEEE. 10.1109/IROS.2010.5649756

Dede, A. (2012). *Prosthetic End-User Usability Survey* (Doctoral dissertation, Worcester Polytechnic Institute).

Dillingham, T. R., Pezzin, L. E., & MacKenzie, E. J. (2002). *Limb amputation and limb deficiency: epidemiology and recent trends in the United States*. Southern Medical Journal, 95(8), 875-883.

El-Mohandes, M. S., & Ibrahem, M. E. H. (2014, December). Stiffness analyses of modified niagara prosthetic feet using finite element modelling. In *2014 Cairo International Biomedical Engineering Conference (CIBEC)* (pp. 19-23). IEEE. 10.1109/CIBEC.2014.7020953

Ehde, D. M., Czerniecki, J. M., Smith, D. G., Campbell, K. M., Edwards, W. T., Jensen, M. P., & Robinson, L. R. (2000). Chronic phantom sensations, phantom pain, residual limb pain, and other regional pain after lower limb amputation. *Archives of Physical Medicine and Rehabilitation, 81* (8), 1039-1044. https://doi.org/10.1053/apmr.2000.7583

Figueroa, R., & Müller-Karger, C. M. (2009). Using FE for dynamic energy return analysis of prosthetic feet during design process. In A. J. McGoron, C. Z. Li, & W. C. Lin (Eds.), *25th Southern Biomedical Engineering Conference 2009, 15–17 May 2009, Miami, Florida, USA* (IFMBE Proceedings, Vol. 24). Springer, Berlin, Heidelberg. https://doi.org/10.1007/978-3-642-01697-4_101

Fosse, S., Hartemann-Heurtier, A., Jacqueminet, S., Van Ha, G., Grimaldi, A., & Fagot-Campagna, A. (2009). Incidence and characteristics of lower limb amputations in people with diabetes. *Diabetic Medicine, 26*(4), 391–396. https://doi-org.ezproxy.lakeheadu.ca/10.1111/j.1464-5491.2009.02698.x

Gailey, R., Allen, K., Castles, J., Kucharik, J., & Roeder, M. (2008). Review of secondary physical conditions associated with lower-limb amputation and long-term prosthesis use. *Journal of*

Rehabilitation Research and Development, *45*(1), 15–29. https://doi.org/10.1682/jrrd.2006.11.0147

Gardinier, E. S., Kelly, B. M., Wensman, J., & Gates, D. H. (2018). A controlled clinical trial of a clinically-tuned powered ankle prosthesis in people with transtibial amputation. *Clinical Rehabilitation, 32*(3), 319–329.

Gholizadeh, H., Lemaire, E. D., & Eshraghi, A. (2016). The evidence-base for elevated vacuum in lower limb prosthetics: Literature review and professional feedback. *Clinical Biomechanics, 37*, 108–116. https://doi-org.ezproxy.lakeheadu.ca/10.1016/j.clinbiomech.2016.06.005

Gómez-Amador, A. M., Pérez-Carrera, C., Prieto-Fernández, L., & Rubio-Alonso, H. (2025). 3D-printed prosthetic foot design: Mechanical similarity and testing. Materials & Design, 253, 113918. https://doi.org/10.1016/j.matdes.2025.113918

Houdijk, H., Pollmann, E., Groenweold, M., Wiggerts, H., & Polomski, W. (2009). The energy cost for the step-to-step transition in amputee walking. Gait & Posture, 30(1), 35-40. https://doi.org/10.1016/j.gaitpost.2009.02.009

Halsne, E. G., Curran, C. S., Caputo, J. M., Hansen, A. H., Hafner, B. J., & Morgenroth, D. C. (2022). Emulating the effective ankle stiffness of commercial prosthetic feet using a robotic prosthetic foot emulator. Journal of Biomechanical Engineering, 144(11), 111009. https://doi.org/10.1115/1.4054834

Hafner, B. J., Sanders, J. E., Czerniecki, J. M., & Fergason, J. (2002). Transtibial energy-storage-and-return prosthetic devices: a review of energy concepts and a proposed nomenclature. Journal of Rehabilitation Research & Development, 39(1).

http://ezproxy.lakeheadu.ca/login?url=https://www.proquest.com/scholarly-journals/transtibial-energy-storage-return-prosthetic/docview/215291206/se-2?accountid=11956

Hafner, B. J. (2005). Clinical prescription and use of prosthetic foot and ankle mechanisms: A review of the literature. *Journal of Prosthetics and Orthotics, 17(4)*, 5–11.

Hamzah, M., & Gatta, A. (2018). Design of a novel carbon-fiber ankle-foot prosthetic using finite element modeling. IOP Conference Series. *Materials Science and Engineering, 433(012056)*, 10-1088.

Hansen, A. H., Childress, D. S., & Knox, E. H. (2004). Roll-over shapes of human locomotor systems: Effects of walking speed. *Clinical Biomechanics, 19*, 407–414. https://doi-org.ezproxy.lakeheadu.ca/10.1016/j.clinbiomech.2003.12.001

Hicks, J. H. (1954). The mechanics of the foot: II. The plantar aponeurosis and the arch. *Journal of Anatomy, 88*(Pt 1), 25.

Highsmith, J. T., & Highsmith, M. J. (2007). Common skin pathology in LE prosthesis users. *JAAPA: Journal of the American Academy of Physician Assistants, 20*(11), 33–37.

Hsu, J. D., Michael, J. W., & Fisk, J. R. (2008). *AAOS atlas of orthoses and assistive devices* (4th ed.). Mosby Elsevier.

Houdijk, H., Pollmann, E., Groenweold, M., Wiggerts, H., & Polomski, W. (2009). The energy cost for the step-to-step transition in amputee walking. Gait & Posture, 30(1), 35-40. https://doi.org/10.1016/j.gaitpost.2009.02.009

Iacob, M. C., Popescu, D., Stochioiu, C., Baciu, F., & Hadar, A. (2024). Compressive behavior of thermoplastic polyurethane with an active agent foaming for 3D-printed customized comfort insoles. Polymer Testing, 137, 108517. https://doi.org/10.1016/j.polymertesting.2024.108517

Imam, B., Miller., W., Eng, J., & Finlayson, H. (2017). Incidence of lower limb amputations in Canada. *Canadian Journal of Public Health, 108*(4), 374. https://doi.org/10.17269/cjph.108.6093

John, C. T., Seth, A., Schwartz, M. H., & Delp, S. L. (2012). Contributions of muscles to mediolateral ground reaction force over a range of walking speeds. Journal of Biomechanics, 45(14), 2438–2443. https://doi.org/10.1016/j.jbiomech.2012.06.037

Kadhim, F. M., Hasan, S. F., & Sadiq, S. E. (2022). Optimal Material Selection for Manufacturing Prosthetic Foot. Pertanika Journal of Science & Technology, 30(4). http://119.40.116.186/resources/files/Pertanika%20PAPERS/JST%20Vol.%2030%20(4)%20Oct.%202022/03%20JST-3410-2022.pdf

Kelly, L. A., Cresswell, A. G., & Farris, D. J. (2018). The energetic behaviour of the human foot across a range of running speeds. Scientific reports, 8(1), 10576. https://www.nature.com/articles/s41598-018-28946-1

Kang, H.-J., Hashimoto, K., Kondo, H., Hattori, K., Nishikawa, K., Hama, Y., Lim, H.-O., Takanishi, A., Suga, K., & Kato, K. (2010). Realization of biped walking on uneven terrain by new foot mechanism capable of detecting ground surface. In *Robotics and Automation (ICRA), 2010 IEEE International Conference on* (pp. 5167–5172). IEEE. 10.1109/ROBOT.2010.5509348

Kaufman, K. R., Levine, J. A., Brey, R. H., Iverson, B. K., McCrady, S. K., Padgett, D. J., et al. (2007). Gait and balance of transfemoral amputees using passive mechanical and microprocessor-controlled prosthetic knees. *Gait & Posture, 26*(4), 489–493. https://doi.org/10.1016/j.gaitpost.2007.07.011

Kaufman, K. R., Levine, J. A., Brey, R. H., McCrady, S. K., Padgett, D. J., & Joyner, M. J. (2008). Energy expenditure and activity of transfemoral amputees using mechanical and microprocessor-controlled prosthetic knees. *Archives of Physical Medicine and Rehabilitation, 89*(7), 1380–1385. https://doi.org/10.1016/j.apmr.2007.11.053

Kharb, A., Saini, V., Jain, Y. K., & Dhiman, S. (2011). A review of the gait cycle and its parameters. IJCEM International Journal of Computational Engineering & Management, 13(01). https://www.researchgate.net/profile/Surender-Dhiman/publication/268423123_A_review_of_gait_cycle_and_its_parameters/links/582f259108ae138f1c035005/A-review-of-gait-cycle-and-its-parameters.pdf?tg=SEO&tag1=Entail&tag2=Entail

Klodd, E., Hansen, A., Fatone, S., & Edwards, M. (2010). Effects of prosthetic foot forefoot flexibility on oxygen cost and subjective preference rankings of unilateral transtibial prosthesis users. *Journal of Rehabilitation Research and Development, 47*(6), 543–552. https://www.proquest.com/docview/752917585?pq-origsite=gscholar&fromopenview=true&sourcetype=Scholarly%20Journals

Kuehn, D., Beinersdorf, F., Bernhard, F., Fondahl, K., Schilling, M., Simnofske, M., Stark, T., & Kirchner, F. (2012). Active spine and feet with increased sensing capabilities for walking

robots. In *International Symposium on Artificial Intelligence, Robotics and Automation in Space (iSAIRAS-12)* (pp. 4–6).

Lestari, W. D., & Adyono, N. (2022). Analysis of Ankle Foot Design for Transtibial Prosthesis Components using the Finite Element Method. Teknik, 43(3), 272-279. https://doi.org/10.14710/teknik.v43i3.48653

Laferrier, J. Z., & Gailey, R. (2010). Advances in lower-limb prosthetic technology. *Physical Medicine and Rehabilitation Clinics of North America, 21*(1), 87–110. http://doi.org/bwpj2v

Legro, M. W., Reiber, G., Del Aguila, M. D., Ajax, M. J., Boone, D. A., Larsen, J. A., et al. (1999). Issues of importance reported by persons with lower limb amputations and prostheses. *Journal of Rehabilitation Research and Development, 36*(3), 155–163.

Lehmann, J. F., Price, R., Boswell-Bessette, S., Dralle, A., & Questad, K. (1993). Comprehensive analysis of dynamic elastic response feet: Seattle Ankle/Lite Foot versus SACH foot. *Archives of Physical Medicine and Rehabilitation, 74*(8), 853–861. https://doi.org/10.1016/0003-9993(93)90013-Z

Lamkin-Kennard, K., & Popovic, M. (2019). Biomechatronics. Academic Press. https://doi.org/10.1016/B978-0-12-812939-5.00004-5

Li, J., Huang, Q., Zhang, W., Yu, Z., & Li, K. (2008). Flexible foot design for a humanoid robot. In *Automation and Logistics, 2008. ICAL 2008. IEEE International Conference on* (pp. 1414–1419). IEEE. 10.1109/ICAL.2008.4636375

Lin, T., Lou, C., & Lin, J. (2016). The effects of thermoplastic polyurethane on the structure and

mechanical properties of modified polypropylene Blends. Applied Sciences, 7(12), 1254. https://doi.org/10.3390/app7121254

Miao, Y., He, H., & Li, Z. (2019). Strain hardening behaviors and mechanisms of polyurethane under various strain rate loading. Polymer Engineering & Science, 60(5), 1083–1092. https://doi.org/10.1002/pen.25364

Major, M. J., Twiste, M., Kenney, L. P., & Howard, D. (2011). Amputee Independent Prosthesis Properties—A new model for description and measurement. Journal of biomechanics, 44(14), 2572-2575. https://doi.org/10.1016/j.jbiomech.2011.07.016

Manz, S., Valette, R., Damonte, F., Avanci Gaudio, L., Gonzalez-Vargas, J., Sartori, M., ... & Rietman, J. (2022). A review of user needs to drive the development of lower limb prostheses. Journal of neuroengineering and rehabilitation, 19(1), 119. https://link.springer.com/article/10.1186/s12984-022-01097-1

Marasovic, T., Cecic, M., & Zanchi, V. (2009). Analysis and interpretation of ground reaction forces in normal gait. *WSEAS Transactions on Systems Archive, 8*, 1105-1114. http://www.wseas.us/e-library/transactions/systems/2009/29-755.pdf

Najmuddin, A., Fukuoka, Y., & Ochiai, S. (2012). Experimental development of stiffness adjustable foot sole for use by bipedal robots walking on uneven terrain. In *System Integration (SII), 2012 IEEE/SICE International Symposium on* (pp. 248–253). IEEE. 10.1109/SII.2012.6426940

Oleiwi, J. K., & Hadi, A. N. (2021, February). Properties of materials and models of prosthetic feet: A review. In IOP Conference Series: Materials Science and Engineering (Vol. 1094,

No. 1, p. 012151). IOP Publishing. https://iopscience.iop.org/article/10.1088/1757-899X/1094/1/012151/meta

Pelayo, F., Blanco, D., Fernández, P., González, J., & Beltrán, N. (2021). Viscoelastic Behaviour of Flexible Thermoplastic Polyurethane Additively Manufactured Parts: Influence of Inner-Structure Design Factors. Polymers, 13(14), 2365. https://doi.org/10.3390/polym13142365

Postema, K., Hermens, H. J., De Vries, J., Koopman, H. F., & Eisma, W. H. (1997). Energy storage and release of prosthetic feet Part 1: Biomechanical analysis related to user benefits. Prosthetics and Orthotics International, 21(1), 17-27. https://doi.org/10.3109/03093649709164526

Prince, F., Winter, D. A., Sjonnesen, G., & Wheeldon, R. K. (1994). A new technique for the calculation of the energy stored, dissipated, and recovered in different ankle-foot prostheses. IEEE Transactions on Rehabilitation Engineering, 2(4), 247-255. 10.1109/86.340873

Paternò, L., Ibrahimi, M., Gruppioni, E., Menciassi, A., & Ricotti, L. (2018). Sockets for limb prostheses: A review of existing technologies and open challenges. *IEEE Transactions on Biomedical Engineering,* *65*(9), 1996–2010. https://ieeexplore.ieee.org/abstract/document/8267041

Piazza, C., Della Santina, C., Gasparri, G. M., Catalano, M. G., Grioli, G., Garabini, M., & Bicchi, A. (2016, November). Toward an adaptive foot for natural walking. In 2016 IEEE-RAS 16th International Conference on Humanoid Robots (Humanoids) (pp. 1204-1210). IEEE. https://ieeexplore.ieee.org/abstract/document/7803423

Pirker, W., Pirker, W., Katzenschlager, R., & Katzenschlager, R. (2017). Gait disorders in adults and the elderly: A clinical guide. *Wiener Klinische Wochenschrift*, *129*(3), 81–95. https://link.springer.com/article/10.1007/s00508-016-1096-4

Pitkin, M. (2009). *Biomechanics of lower limb prosthetics.* Springer. https://doi.org/10.1007/978-3-642-03016-1

Preatoni, G., Valle, G., Petrini, F. M., & Raspopovic, S. (2021). Lightening the perceived prosthesis weight with neural embodiment promoted by sensory feedback. *Current Biology, 31*(5), 1065–1071. https://www.cell.com/current-biology/fulltext/S0960-9822(20)31782-6

Prendergast, P. J. (1997). Finite element models in tissue mechanics and orthopaedic implant design. *Clinical Biomechanics*, *12(6)*, 343–366. https://doi.org/10.1016/S0268-0033(97)00018-1

Raschke, S. U., Orendurff, M. S., Mattie, J. L., Kenyon, D. E. A., Jones, O. Y., Moe, D., ... & Kobayashi, T. (2015). Biomechanical characteristics, patient preference and activity level with different prosthetic feet: A randomized double-blind trial with laboratory and community testing. *Journal of Biomechanics,* *48*(1), 146–152. https://doi.org/10.1016/j.jbiomech.2014.10.002

Ros, J., Font-Llagunes, J. M., Plaza, A., & Kövecses, J. (2015). Dynamic considerations of heel-strike impact in human gait. Multibody system dynamics, 35(3), 215-232. https://link-springer-com.ezproxy.lakeheadu.ca/article/10.1007/s11044-015-9460-0

Sanders, J. E., Nicholson, B. S., Zachariah, S. G., Cassisi, D. V., Karchin, A., & Fergason, J. R. (2004). Testing of elastomeric liners used in limb prosthetics: Classification of 15 products

by mechanical performance. *Journal of Rehabilitation Research and Development, 41*(2), 175–186. http://doi.org/cpbfn8

Saunders, M. M., Schwentker, E. P., Kay, D. B., Bennett, G., Jacobs, C. R., Verstraete, M. C., & Njus, G. O. (2003). Finite element analysis as a tool for parametric prosthetic foot design and evaluation. Technique development in the solid ankle cushioned heel (SACH) foot. Computer Methods in Biomechanics & Biomedical Engineering, 6(1), 75-87. https://doi.org/10.1080/1025584021000048974

Schaffalitzky, E., Gallagher, P., Maclachlan, M., & Ryall, N. (2011). Understanding the benefits of prosthetic prescription: exploring the experiences of practitioners and lower limb prosthetic users. *Disability and rehabilitation, 33*(15-16), 1314-1323. https://doi.org/10.3109/09638288.2010.529234

Scholz, M. S., Blanchfield, J. P., Bloom, L. D., Coburn, B. H., Elkington, M., Fuller, J. D., et al. (2011). The use of composite materials in modern orthopedic medicine and prosthetic devices: A review. *Composites Science and Technology, 71*(16), 1791–1803. http://doi.org/bhmr26

Schuller-Götzburg, P., & Krenkel, C. (1999). 2D-finite element analyses and histomorphology of lag screws with and without a biconcave washer. *Journal of Biomechanics, 32(5)*, 511–520. https://doi.org/10.1016/S0021-9290(98)00156-0

Seo, J.-T., & Yi, B.-J. (2009). Modeling and analysis of a biomimetic foot mechanism. In *2009 IEEE/RSJ International Conference on Intelligent Robots and Systems* (pp. 1472–1477). IEEE. 10.1109/IROS.2009.5354153

Seymour, R., Engbretson, B., Kott, K., Ordway, N., Brooks, G., Crannell, J., et al. (2007). Comparison between the C-leg® microprocessor-controlled prosthetic knee and non-microprocessor control prosthetic knees: A preliminary study of energy expenditure, obstacle course performance, and quality of life survey. *Prosthetics and Orthotics International, 31*(1), 51–61. https://doi.org/10.1080/03093640600982

Siegert, R. J., & Taylor, W. J. (2004). Theoretical aspects of goal-setting and motivation in rehabilitation. *Disability and Rehabilitation, 26*, 1–8. https://doi.org/10.1080/09638280410001644932

Scetta, G., Ju, J., Selles, N., Heuillet, P., Ciccotti, M., & Creton, C. (2021). Strain-induced strengthening of soft thermoplastic polyurethanes under cyclic deformation. Journal of Polymer Science, 59(8), 741–749. https://doi.org/10.1002/pol.20210060

Turner, A. T., Halsne, E. G., Caputo, J. M., Curran, C. S., Hansen, A. H., Hafner, B. J., & Morgenroth, D. C. (2022). Prosthetic forefoot and heel stiffness across consecutive foot stiffness categories and sizes. PLoS One, 17(5), e0268136. https://doi.org/10.1371/journal.pone.0268136

Tronxy Global Store. (n.d.). Home. Tronxy Global Store. https://tronxyglobal.com/products/tronxy-3d-printer-3d-flexible-blue-tpu-filament-1-75-mm-2-2-lbs-1kg?utm_source

Taboga, P., & Grabowski, A. M. (2017). Axial and torsional stiffness of pediatric prosthetic feet. Clinical Biomechanics, 42, 47-54. https://doi.org/10.1016/j.clinbiomech.2017.01.005

Thompson, D. M., & Haran, D. (1984). Living with an amputation. *International Journal of Rehabilitation Research, 7*(3), 283–292.

Tsagarakis, N. G., Li, Z., Saglia, J., & Caldwell, D. G. (2011). The design of the lower body of the compliant humanoid robot "ccub". In *Robotics and Automation (ICRA), 2011 IEEE International Conference on* (pp. 2035–2040). IEEE. 10.1109/ICRA.2011.5980130

Verdini, F., Marcucci, M., Benedetti, M., & Leo, T. (2006). Identification and characterization of heel strike transient. Gait and Posture, 24(1), 77-84. https://doi.org/10.1016/j.gaitpost.2005.07.008

Vaverka, F., Elfmark, M., Svoboda, Z., & Janura, M. (2015). System of gait analysis based on ground reaction force assessment. *Acta Gymnica*, *45*(4), 187–193. https://doi.org/10.5507/ag.2015.022

Van der Spoel, E., Rozing, M. P., Houwing-Duistermaat, J. J., Slagboom, P. E., Beekman, M., de Craen, A. J., et al. (2015). Association analysis of insulin-like growth factor-1 axis parameters with survival and functional status in nonagenarians of the Leiden Longevity Study. *Aging (Albany NY), 7*(11), 956–963. http://doi.org/cv6j

Van Schaik, L., Hoeksema, S., Huvers, L. F., Geertzen, J. H. B., Dijkstra, P. U., & Dekker, R. (2022). The most important activities of daily functioning: The opinion of persons with lower limb amputation and healthcare professionals differ considerably. *International Journal of Rehabilitation Research, 43*(1), 82–89. https://journals.lww.com/intjrehabilres/fulltext/2020/03000/the_most_important_activities_of_daily.13.aspx

Whittle, M. W. (1999). [Rev. of Generation and attenuation of transient impulsive forces beneath the foot: a review]. Gait & Posture, 10(3), 264–275. https://doi.org/10.1016/S0966-6362(99)00041-7

Warder, H. H., Fairley III, J. K., Coutts, J., Glisson, R. R., & Gall, K. (2018). Examining the viability of carbon fiber reinforced three-dimensionally printed prosthetic feet created by composite filament fabrication. Prosthetics and orthotics international, 42(6), 644-651. https://doi.org/10.1177/0309364618785572

Webber, C. M., & Kaufman, K. (2017). Instantaneous stiffness and hysteresis of dynamic elastic response prosthetic feet. Prosthetics and Orthotics International, 41(5), 463-468. https://doi.org/10.1177/0309364616683980

Womac, N. D., Neptune, R. R., & Klute, G. K. (2019). Stiffness and energy storage characteristics of energy storage and return prosthetic feet. Prosthetics and orthotics international, 43(3), 266-275. https://doi.org/10.3109/03093649709164526

Weerakkody, T. H., Lalitharatne, T. D., & Gopura, R. A. R. C. (2017). Adaptive Foot in Lower-Limb Prostheses. Journal of Robotics, 2017(1), 9618375. https://doi.org/10.1155/2017/9618375

White, A., & Harold, N. (2024, March). New data: Over 5.6 million Americans living with limb loss & limb difference. *THRIVE - Amputee Coalition Blog*. https://blog.amputee-coalition.org/inmotion/issue/mar-apr-2024/new-data-over-5-6-million-americans-living-with-limb-loss-limb-difference/

Winter, D. A. (1991). *The biomechanics and motor control of human gait: normal, elderly, and pathological*. University of Waterloo Press

Wise, D. L., Trantolo, D. J., Altobelli, D. E., Yaszemski, M. J., & Gresser, J. D. (1996). *Human biomaterials applications: Part III biomedical applications of biomaterials*. Humana Press.

Wong, C. K., & Edelstein, J. E. (2020). Advanced rehabilitation for people with microprocessor knee prostheses. In K. K. Chui, M. Jorge, S.-C. Yen, & M. M. Lusardi (Eds.), *Orthotics and prosthetics in rehabilitation* (4th ed., pp. 704–723). Elsevier.

Yousif, L. E., Resan, K. K., & Fenjan, R. M. (2018). Temperature effect on mechanical characteristics of a new design prosthetic foot. International Journal of Mechanical Engineering and Technology, 9(13), 1431-1447. https://www.researchgate.net/profile/Kadhim-Resan/publication/330262184_Temperature_effect_on_mechanical_characteristics_of_a_new_design_prosthetic_foot/links/5c3643fd299bf12be3ba695a/Temperature-effect-on-mechanical-characteristics-of-a-new-design-prosthetic-foot.pdf

Yazji, M., Raison, M., Aubin, C., Labelle, H., Detrembleur, C., Mahaudens, P., & Mousny, M. (2015). Are the mediolateral joint forces in the lower limbs different between scoliotic and healthy subjects during gait? *Scoliosis 10*(3). https://doi.org/10.1186/1748-7161-10-S2-S3

Zelik, K. E., Collins, S. H., Adamczyk, P. G., Segal, A. D., Klute, G. K., Morgenroth, D. C., ... Kuo, A. D. (2011). Systematic variation of prosthetic foot spring affects center-of-mass mechanics and metabolic cost during walking. Neural Systems and Rehabilitation Engineering, IEEE Transactions on, 19(4), 411–419. 10.1109/TNSRE.2011.2159018

Zhang, M., Mak, A., & Roberts, V. C. (1998). Finite element modeling of a residual lower-limb in a prosthetic socket: A survey of the development in the first decade. *Medical Engineering & Physics, 20(5)*, 360–373. https://doi.org/10.1016/S1350-4533(98)00027-7

Appendix A: Plots and Tables for Experimental Trials Conducted for and Included in Chapter 4

Figure A.1: Wooden Foot on Force Tester

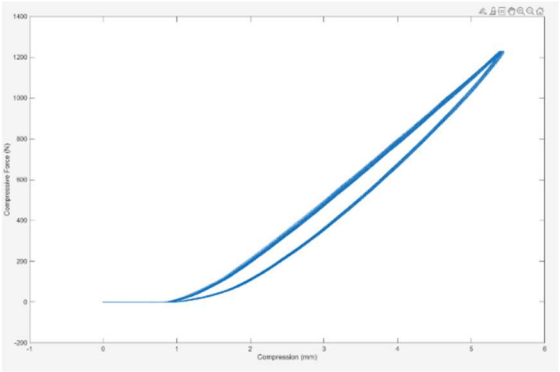

Figure A.2: CC test, Trial 2, wooden foot

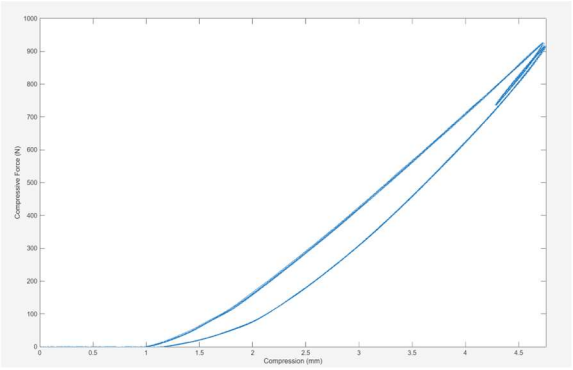

Figure A.3: M5 test, Trial 2, wooden foot

Table A.1: Wooden Foot without Insole

Prosthetic Foot	Wooden Foot					
Type of Tests	CC			M5		
Trials	1	2	3	1	2	3
Loaded Energy, J	2.579	2.477	2.499	1.506	1.513	1.517
Unloaded Energy*, J	-2.154	-2.098	-2.108	-1.236	-1.239	-1.239
Absorbed Energy, J	0.424	0.378	0.391	0.271	0.274	0.271
Ratio of Absorption	0.163	0.153	0.156	0.179	0.181	0.179
Stiffness for High-Load in Loading, N/mm	309.028	311.013	302.713	-	-	-
Stiffness for High-Load in Unloading, N/mm	468.644	443.729	421.783	-	-	-
Stiffness for Low-Load in Loading, N/mm	189.651	195.631	194.573	-	-	-
Stiffness for Low-Load in Unloading, N/mm	170.545	187.736	181.379	-	-	-

* Energy is a positive quantity. The "-" signs here are to denote the unloaded nature of energy.

Figure A.4: Otto Bock Trias Foot on Forcer Tester

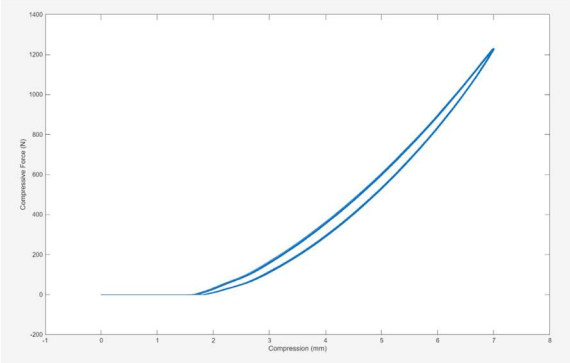

Figure A.5: CC test, Trial 2, Otto Bock Trias foot

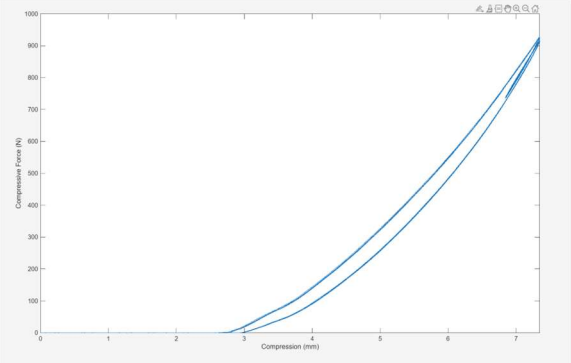

Figure A.6: M5 test, Trial 2, Otto Bock Trias foot

Table A.2: Otto Bock Trias without Insole

Prosthetic Foot	Otto Bock Trias Foot					
Type of Tests	CC			M5		
Trials	1	2	3	1	2	3
Loaded Energy, J	2.623	2.619	2.613	1.718	1.715	1.709
Unloaded Energy*, J	-2.351	-2.352	-2.346	-1.493	-1.492	-1.489
Absorbed Energy, J	0.271	0.268	0.267	0.225	0.223	0.219
Ratio of Absorption	0.103	0.102	0.102	0.131	0.130	0.129
Stiffness for High-Load in Loading, N/mm	341.833	343.345	344.874	-	-	-
Stiffness for High-Load in Unloading, N/mm	439.920	440.394	442.377	-	-	-
Stiffness for Low-Load in Loading, N/mm	132.572	134.149	135.321	-	-	-
Stiffness for Low-Load in Unloading, N/mm	140.744	141.282	141.483	-	-	-

* Energy is a positive quantity. The "-" signs here are to denote the unloaded nature of energy.

Figure A.7: Sierra Foot on Force Tester

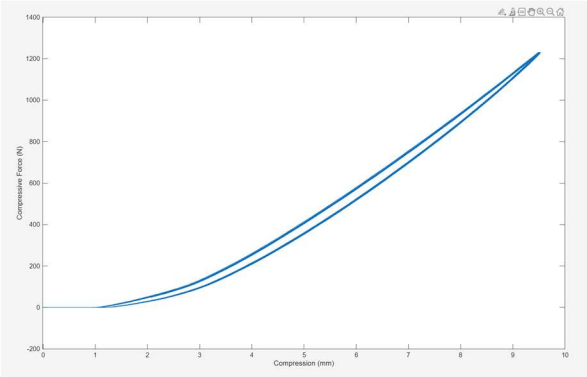

Figure A.8: CC test, Trial 2, Sierra foot

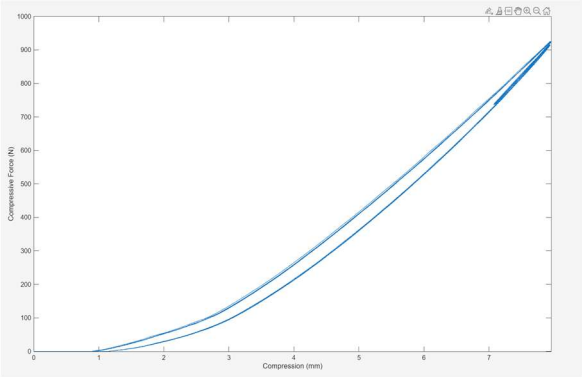

Figure A.9: M5 test, Trial 2, Sierra foot

Table A.3: Sierra Foot without Insole

Prosthetic Foot	Otto Bock Trias Foot					
Type of Tests	CC			M5		
Trials	1	2	3	1	2	3
Loaded Energy, J	4.257	4.246	4.243	2.595	2.591	2.585
Unloaded Energy*, J	-3.938	-3.932	-3.931	-2.333	-2.329	-2.324
Absorbed Energy, J	0.319	0.313	0.311	0.262	0.262	0.261
Ratio of Absorption	0.075	0.074	0.073	0.101	0.101	0.101
Stiffness for High-Load in Loading, N/mm	185.616	198.139	198.104	-	-	-
Stiffness for High-Load in Unloading, N/mm	222.407	235.989	235.202	-	-	-
Stiffness for Low-Load in Loading, N/mm	83.017	87.880	88.749	-	-	-
Stiffness for Low-Load in Unloading, N/mm	91.794	94.191	94.739	-	-	-

* Energy is a positive quantity. The "-" signs here are simply to denote the unloaded nature of the energy.

Figure A.10: Wooden Foot with Tronxy Insole

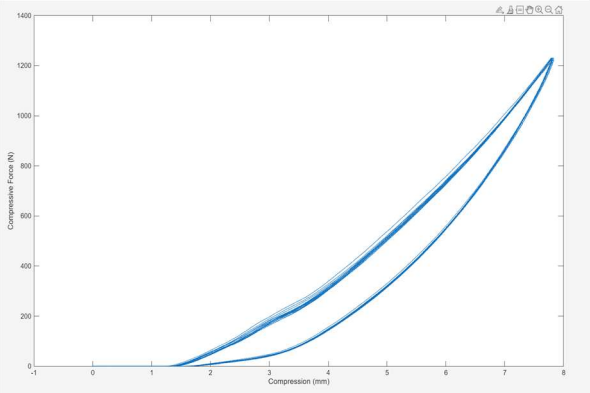

Figure A.11: CC Test for Tronxy Insole

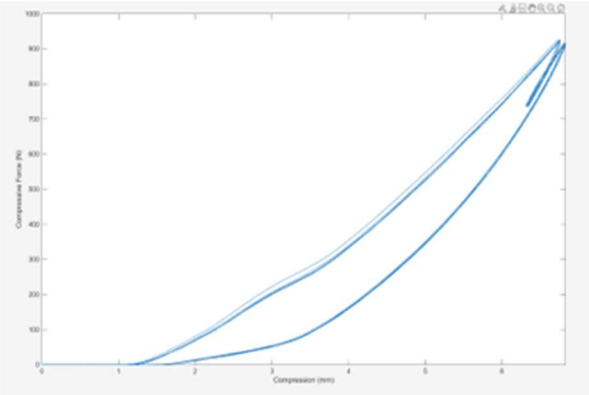

Figure A.12: M5 Test for Tronxy Insole

Table A.4: Wooden Prosthetic with Tronxy Insole

Prosthetic Foot	Tronxy Insole					
Type of Tests	CC			M5		
Trials	1	2	3	1	2	3
Loaded Energy, J	3.377	3.152	3.100	2.132	2.115	2.102
Unloaded Energy*, J	-2.392	-2.299	-2.278	-1.458	-1.455	-1.443
Absorbed Energy, J	0.985	0.853	0.822	0.647	0.660	0.659
Ratio of Absorption	0.291	0.271	0.265	0.316	0.312	0.313
Stiffness for High-Load in Loading, N/mm	282.987	295.613	296.577	-	-	-
Stiffness for High-Load in Unloading, N/mm	539.059	527.209	503.328	-	-	-
Stiffness for Low-Load in Loading, N/mm	121.056	113.125	109.332	-	-	-
Stiffness for Low-Load in Unloading, N/mm	107.223	117.923	115.893	-	-	-

* Energy is a positive quantity. The "-" signs here are to denote the unloaded nature of the energy.

Figure A.13: Wooden Foot with Polyflex Insole

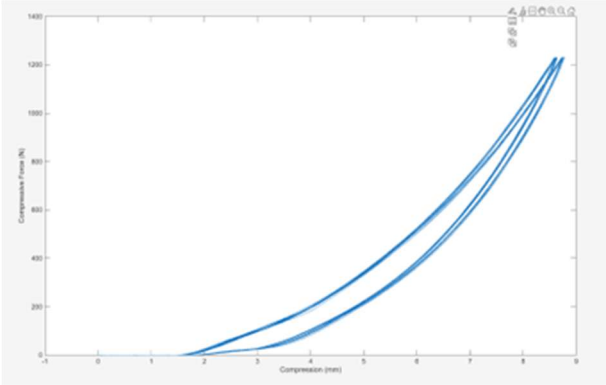

Figure A.14: CC Test for Polyflex Insole

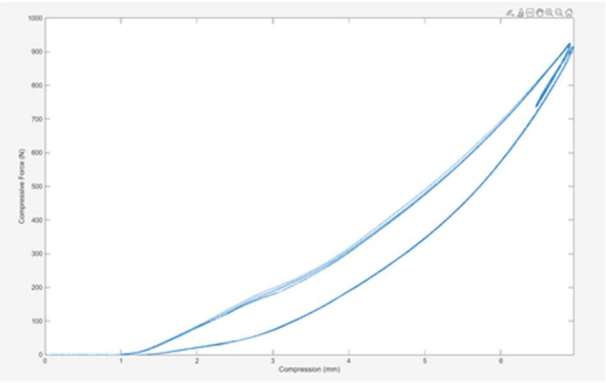

Figure A.15: M5 Test for Polyflex Insole

Table A.5: Wooden Prosthetic with Polyflex Insole

Prosthetic Foot	Polyflex Insole					
Type of Tests	CC			M5		
Trials	1	2	3	1	2	3
Loaded Energy, J	3.304	3.150	3.123	2.132	2.103	2.087
Unloaded Energy*, J	-2.553	-2.486	-2.478	-1.584	-1.581	-1.578
Absorbed Energy, J	0.751	0.664	0.645	0.549	0.522	0.509
Ratio of Absorption	0.227	0.211	0.207	0.257	0.248	0.244
Stiffness for High-Load in Loading, N/mm	240.284	240.348	281.359	-	-	-
Stiffness for High-Load in Unloading, N/mm	270.029	253.935	362.199	-	-	-
Stiffness for Low-Load in Loading, N/mm	60.600	81.891	81.689	-	-	-
Stiffness for Low-Load in Unloading, N/mm	107.047	101.114	96.425	-	-	-

* Energy is a positive quantity. The "-" signs here are simply to denote the unloaded nature of the energy.

Figure A.16: Wooden Foot with Sain Smart Insole

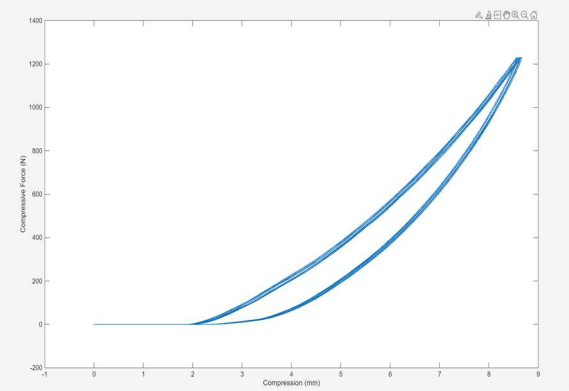

Figure A.17: CC Test for Sain Smart Insole

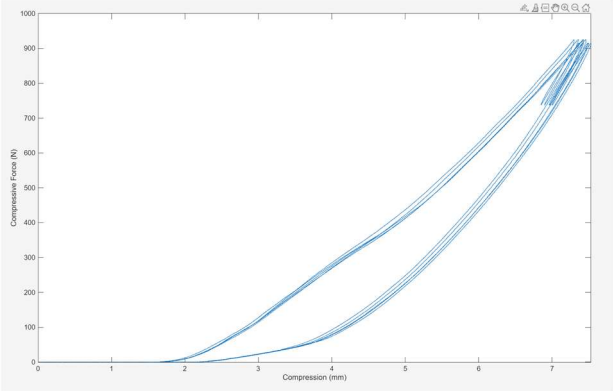

Figure A.18: M5 Test for Sain Smart Insole

Table A.6: Wooden Prosthetic with Sain Smart Insole

Prosthetic Foot	Saint Smart Insole					
Type of Tests	CC			M5		
Trials	1	2	3	1	2	3
Loaded Energy, J	3.248	3.205	3.289	2.222	2.170	2.147
Unloaded Energy*, J	-2.374	-2.383	-2.400	-1.521	-1.496	-1.490
Absorbed Energy, J	0.874	0.822	0.889	0.701	0.674	0.656
Ratio of Absorption	0.269	0.256	0.269	0.306	0.311	0.306
Stiffness for High-Load in Loading, N/mm	268.806	284.452	310.749	-	-	-
Stiffness for High-Load in Unloading, N/mm	460.609	426.922	531.689	-	-	-
Stiffness for Low-Load in Loading, N/mm	109.623	114.324	111.932	-	-	-
Stiffness for Low-Load in Unloading, N/mm	114.278	118.686	118.958	-	-	-

* Energy is a positive quantity. The “-“ signs here are simply to denote the unloaded nature of the energy.

Figure A.19: Wooden Foot with Pxmallion Insole

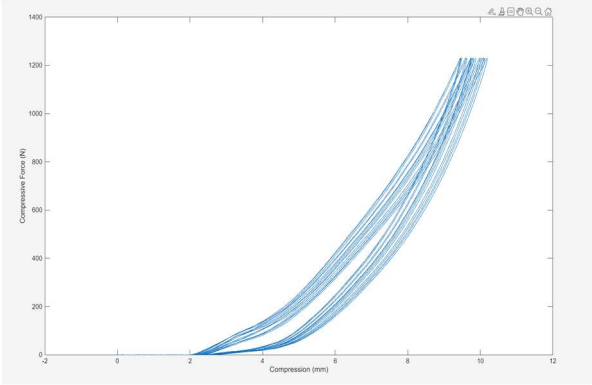

Figure A.20: CC Test for Pxmallion Insole

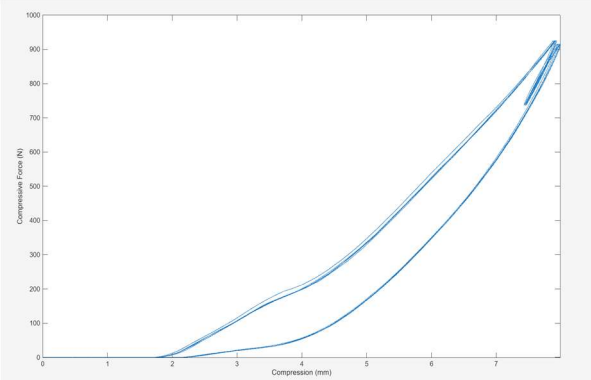

Figure A.21: M5 Test for Pxmallion Insole

Table A.7: Wooden Prosthetic with Pxmallion Insole

Prosthetic Foot	Pxmallion Insole					
Type of Tests	CC			M5		
Trials	1	2	3	1	2	3
Loaded Energy, J	3.350	3.383	3.560	2.268	2.265	2.165
Unloaded Energy*, J	-2.442	-2.488	-2.617	-1.565	-1.558	-1.503
Absorbed Energy, J	0.908	0.895	0.943	0.702	0.707	0.662
Ratio of Absorption	0.271	0.265	0.265	0.309	0.312	0.306
Stiffness for High-Load in Loading, N/mm	306.29	307.926	276.813	-	-	-
Stiffness for High-Load in Unloading, N/mm	530.229	524.389	494.695	-	-	-
Stiffness for Low-Load in Loading, N/mm	81.299	73.921	71.366	-	-	-
Stiffness for Low-Load in Unloading, N/mm	113.581	106.845	91.378	-	-	-

* Energy is a positive quantity. The "-" signs here are to denote the unloaded nature of the energy.

Table A.8: Prosthetic Feet on 15-degree Wedge for Wooden Foot

Trial	1			2			3		
Toe Position	Flat	Down	Up	Flat	Down	Up	Flat	Down	Up
Total Loaded Energy, J	3.360	2.260	4.940	3.270	2.170	4.780	3.290	2.150	4.780
Loaded Compressive Energy, J	3.350	2.050	4.140	3.260	1.980	3.990	3.280	1.950	3.990
Loaded Shear Energy, J	0.060	0.180	0.890	0.060	0.170	0.870	0.060	0.170	0.870
Total Unloaded Energy, J	-2.600	-1.770	-3.810	-2.630	-1.810	-3.910	-2.610	-1.790	-3.900
Unloaded Compressive Energy, J	-2.590	-1.610	-3.170	-2.620	-1.650	-3.250	-2.600	-1.630	-3.240
Unloaded Shear Energy, J	-0.050	-0.140	-0.710	-0.050	-0.140	-0.730	-0.050	-0.140	-0.720
Total Energy Absorption Ratio	0.230	0.220	0.230	0.200	0.170	0.180	0.210	0.170	0.180
Compressive Energy Absorption Ratio	0.230	0.210	0.230	0.200	0.170	0.190	0.210	0.170	0.190
Shear Energy Absorption Ratio	0.240	0.240	0.200	0.220	0.170	0.160	0.230	0.170	0.160

Table A.9: Prosthetic Feet on 15-degree Wedge for Otto Bock Trias Foot

Trial	1			2			3		
Toe Position	Flat	Down	Up	Flat	Down	Up	Flat	Down	Up
Total Loaded Energy, J	2.740	3.000	3.560	2.740	2.970	3.470	2.710	2.950	3.460
Loaded Compressive Energy, J	2.730	2.790	3.050	2.730	2.760	2.970	2.710	2.750	2.960
Loaded Shear Energy, J	0.020	0.200	0.540	0.020	0.200	0.530	0.020	0.200	0.530
Total Unloaded Energy, J	-2.380	-2.450	-3.090	-2.450	-2.470	-3.100	-2.420	-2.490	-3.110
Unloaded Compressive Energy, J	-2.380	-2.260	-2.640	-2.450	-2.290	-2.650	-2.420	-2.300	-2.650
Unloaded Shear Energy, J	-0.020	-0.180	-0.470	-0.010	-0.180	-0.480	-0.010	-0.180	-0.490
Total Energy Absorption Ratio	0.130	0.180	0.130	0.100	0.170	0.110	0.110	0.160	0.100
Compressive Energy Absorption Ratio	0.130	0.190	0.130	0.100	0.170	0.110	0.110	0.160	0.100
Shear Energy Absorption Ratio	0.170	0.100	0.130	0.170	0.090	0.090	0.170	0.080	0.080

Table A.10: Prosthetic Feet on 15-degree Wedge for Sierra Foot

Trial	1			2			3		
Toe Position	Flat	Down	Up	Flat	Down	Up	Flat	Down	Up
Total Loaded Energy, J	3.940	3.740	5.190	3.880	3.730	5.030	3.870	3.720	5.000
Loaded Compressive Energy, J	3.940	3.550	4.310	3.880	3.540	4.180	3.870	3.530	4.150
Loaded Shear Energy, J	0.010	0.180	1.000	0.010	0.170	0.960	0.010	0.170	0.950
Total Unloaded Energy, J	-3.480	-3.410	-4.440	-3.510	-3.410	-4.490	-3.520	-3.390	-4.490
Unloaded Compressive Energy, J	-3.480	-3.230	-3.690	-3.510	-3.240	-3.710	-3.520	-3.220	-3.710
Unloaded Shear Energy, J	-0.010	-0.160	-0.850	-0.010	-0.160	-0.880	-0.010	-0.160	-0.880
Total Energy Absorption Ratio	0.120	0.090	0.140	0.100	0.090	0.110	0.090	0.090	0.100
Compressive Energy Absorption Ratio	0.120	0.090	0.140	0.100	0.080	0.110	0.090	0.090	0.110
Shear Energy Absorption Ratio	0.030	0.100	0.150	0.020	0.090	0.080	0.030	0.100	0.070

Table A.11: Prosthetic Feet on 15-degree Wedge on Wooden Foot with Tronxy Insole

Trial	1			2			3		
Toe Position	Flat	Down	Up	Flat	Down	Up	Flat	Down	Up
Total Loaded Energy, J	4.170	3.180	6.650	3.970	3.100	6.290	4.010	3.130	6.300
Loaded Compressive Energy, J	4.160	2.850	5.470	3.960	2.780	5.140	4.000	2.800	5.140
Loaded Shear Energy, J	0.070	0.290	1.310	0.070	0.290	1.280	0.070	0.290	1.290
Total Unloaded Energy, J	-2.750	-2.030	-4.540	-2.760	-2.050	-4.610	-2.790	-2.080	-4.660
Unloaded Compressive Energy, J	-2.750	-1.820	-3.710	-2.760	-1.840	-3.730	-2.780	-1.870	-3.770
Unloaded Shear Energy, J	-0.050	-0.190	-0.930	-0.050	-0.190	-0.980	-0.050	-0.190	-0.990
Total Energy Absorption Ratio	0.340	0.360	0.320	0.300	0.340	0.270	0.300	0.330	0.260
Compressive Energy Absorption Ratio	0.340	0.360	0.320	0.300	0.340	0.270	0.300	0.330	0.270
Shear Energy Absorption Ratio	0.310	0.360	0.290	0.270	0.340	0.230	0.290	0.340	0.230

Table A.12: Prosthetic Feet on 15-degree Wedge on Wooden Foot with Polyflex Insole

Trial	1			2			3		
Toe Position	Flat	Down	Up	Flat	Down	Up	Flat	Down	Up
Total Loaded Energy, J	4.730	3.710	5.510	4.650	3.530	5.850	4.650	3.560	6.300
Loaded Compressive Energy, J	4.730	3.320	4.590	4.640	3.150	4.940	4.650	3.180	5.290
Loaded Shear Energy, J	0.090	0.350	1.010	0.080	0.340	1.000	0.080	0.340	1.110
Total Unloaded Energy, J	-3.270	-2.430	-4.020	-3.380	-2.460	-4.340	-3.370	-2.470	-4.660
Unloaded Compressive Energy, J	-3.260	-2.180	-3.320	-3.370	-2.210	-3.680	-3.370	-2.210	-3.950
Unloaded Shear Energy, J	-0.060	-0.220	-0.770	-0.060	-0.230	-0.720	-0.060	-0.230	-0.770
Total Energy Absorption Ratio	0.310	0.350	0.270	0.270	0.300	0.260	0.280	0.310	0.260
Compressive Energy Absorption Ratio	0.310	0.340	0.280	0.270	0.300	0.250	0.280	0.300	0.250
Shear Energy Absorption Ratio	0.330	0.370	0.240	0.290	0.320	0.280	0.290	0.330	0.310

Table A.13: Prosthetic Feet on 15-degree Wedge on Wooden Foot with Saint Smart Insole

Trial	1			2			3		
Toe Position	Flat	Down	Up	Flat	Down	Up	Flat	Down	Up
Total Loaded Energy, J	4.070	3.170	6.810	3.930	3.090	7.000	3.910	3.080	8.320
Loaded Compressive Energy, J	4.060	2.840	5.720	3.920	2.780	5.840	3.900	2.770	6.960
Loaded Shear Energy, J	0.070	0.290	1.200	0.070	0.280	1.280	0.070	0.280	1.500
Total Unloaded Energy, J	-2.720	-2.000	-4.640	-2.710	-2.040	-4.930	-2.740	-2.040	-5.590
Unloaded Compressive Energy, J	-2.720	-1.790	-3.900	-2.710	-1.830	-4.130	-2.730	-1.830	-4.730
Unloaded Shear Energy, J	-0.050	-0.180	-0.800	-0.050	-0.190	-0.880	-0.050	-0.190	-0.940
Total Energy Absorption Ratio	0.330	0.370	0.320	0.310	0.340	0.300	0.300	0.340	0.330
Compressive Energy Absorption Ratio	0.330	0.370	0.320	0.310	0.340	0.290	0.300	0.340	0.320
Shear Energy Absorption Ratio	0.270	0.360	0.330	0.250	0.330	0.310	0.240	0.330	0.380

Table A.14: Prosthetic Feet on 15-degree Wedge on Wooden Foot with Pxmallion Insole

Trial	1			2			3		
Toe Position	Flat	Down	Up	Flat	Down	Up	Flat	Down	Up
Total Loaded Energy, J	3.930	3.340	7.440	3.790	3.210	7.740	3.790	3.280	7.740
Loaded Compressive Energy, J	3.920	2.980	6.250	3.790	2.870	6.490	3.780	2.930	6.430
Loaded Shear Energy, J	0.070	0.310	1.300	0.060	0.300	1.370	0.060	0.310	1.440
Total Unloaded Energy, J	-2.680	-2.100	-5.020	-2.710	-2.140	-5.340	-2.730	-2.190	-5.370
Unloaded Compressive Energy, J	-2.670	-1.880	-4.250	-2.700	-1.920	-4.510	-2.720	-1.960	-4.530
Unloaded Shear Energy, J	-0.050	-0.190	-0.840	-0.040	-0.200	-0.900	-0.050	-0.200	-0.920
Total Energy Absorption Ratio	0.320	0.370	0.330	0.290	0.330	0.310	0.280	0.330	0.310
Compressive Energy Absorption Ratio	0.320	0.370	0.320	0.290	0.330	0.300	0.280	0.330	0.290
Shear Energy Absorption Ratio	0.300	0.390	0.350	0.280	0.340	0.340	0.270	0.340	0.360

Appendix B: Tables for Experimental Trials Conducted for and Included in Chapter 5

Table B.1: Created Design with Tronxy TPU

Foot Location	Heel			Forefoot		
Trial	1	2	3	1	2	3
Loaded Energy, J	4.033	3.762	3.568	1.474	1.711	2.952
Unloaded Energy*, J	-2.700	-2.563	-2.453	-1.168	-1.323	-2.039
Absorbed Energy, J	1.332	1.199	1.115	0.306	0.388	0.913
Ratio of Absorption	0.329	0.318	0.312	0.207	0.225	0.308
Stiffness for High-Load in Loading, N/mm	466.882	488.580	505.526	333.546	259.565	175.713
Stiffness for High-Load in Unloading, N/mm	987.243	997.454	1011.100	920.693	851.228	784.451
Stiffness for Low-Load in Loading, N/mm	4.634	3.917	4.659	334.307	331.479	322.444
Stiffness for Low-Load in Unloading, N/mm	5.680	6.460	7.059	364.746	356.357	326.080

* Energy is a positive quantity. The "-" signs here are to denote the unloaded nature of energy.

Table B.2: Created Design with Polyflex TPU

Foot Location	Heel			Forefoot		
Trial	1	2	3	1	2	3
Loaded Energy, J	4.036	3.942	3.733	0.891	0.887	0.885
Unloaded Energy*, J	-2.226	-2.161	-2.078	-0.724	-0.721	-0.720
Absorbed Energy, J	1.811	1.780	1.656	0.167	0.165	0.164
Ratio of Absorption	0.448	0.451	0.443	0.188	0.186	0.186
Stiffness for High-Load in Loading, N/mm	502.397	520.621	539.329	854.729	854.217	864.539
Stiffness for High-Load in Unloading, N/mm	1257.200	1291.200	1272.500	1475.600	1464.100	1484.200
Stiffness for Low-Load in Loading, N/mm	26.969	24.399	5.792	276.393	275.305	275.692
Stiffness for Low-Load in Unloading, N/mm	10.219	8.837	9.984	336.539	341.085	345.968

* Energy is a positive quantity. The "-" signs here are to denote the unloaded nature of energy.

Table B.3: Created Design, Tronxy on Tronxy Insole

Foot Location	Heel			Forefoot		
Trial	1	2	3	1	2	3
Loaded Energy, J	4.491	4.413	4.493	3.626	3.683	3.698
Unloaded Energy*, J	-3.016	-2.976	-3.009	-2.463	-2.492	-2.497
Absorbed Energy, J	1.475	1.437	1.483	1.163	1.191	1.201
Ratio of Absorption	0.328	0.326	0.330	0.321	0.323	0.325
Stiffness for High-Load in Loading, N/mm	258.859	235.708	206.906	200.078	225.802	239.799
Stiffness for High-Load in Unloading, N/mm	758.669	743.994	749.679	709.789	715.848	732.749
Stiffness for Low-Load in Loading, N/mm	3.729	4.367	4.544	206.003	201.447	199.382
Stiffness for Low-Load in Unloading, N/mm	6.544	7.009	6.980	189.753	181.567	177.324

* Energy is a positive quantity. The "-" signs here are to denote the unloaded nature of energy.

Table B.4: Created Design, Polyflex on Tronxy Insole

Foot Location	Heel			Forefoot		
Trial	1	2	3	1	2	3
Loaded Energy, J	5.583	5.619	5.762	1.126	1.119	1.125
Unloaded Energy*, J	-3.076	-3.192	-3.126	-0.889	-0.884	-0.889
Absorbed Energy, J	2.507	2.427	2.635	0.236	0.234	0.236
Ratio of Absorption	0.449	0.432	0.457	0.209	0.209	0.209
Stiffness for High-Load in Loading, N/mm	280.425	313.766	295.245	680.514	708.199	687.542
Stiffness for High-Load in Unloading, N/mm	893.948	906.721	933.159	1255.400	1289.600	1261.800
Stiffness for Low-Load in Loading, N/mm	6.082	7.054	3.907	218.506	222.559	228.690
Stiffness for Low-Load in Unloading, N/mm	34.136	31.605	20.032	269.548	273.521	273.183

* Energy is a positive quantity. The "-" signs here are to denote the unloaded nature of energy.

Table B.5: Created Design, Tronxy on Polyflex Insole

Foot Location	Heel			Forefoot		
Trial	1	2	3	1	2	3
Loaded Energy, J	5.479	5.424	5.287	4.114	4.089	4.078
Unloaded Energy*, J	-3.543	-3.495	-3.417	-2.809	-2.787	-2.778
Absorbed Energy, J	1.937	1.929	1.869	1.305	1.302	1.300
Ratio of Absorption	0.353	0.356	0.354	0.317	0.318	0.319
Stiffness for High-Load in Loading, N/mm	343.671	345.748	353.609	210.484	227.036	235.717
Stiffness for High-Load in Unloading, N/mm	774.075	783.753	794.705	638.916	660.056	663.533
Stiffness for Low-Load in Loading, N/mm	2.822	3.698	3.999	196.684	193.004	191.732
Stiffness for Low-Load in Unloading, N/mm	5.808	6.510	6.663	168.648	163.155	160.481

* Energy is a positive quantity. The "-" signs here are to denote the unloaded nature of energy.

Table B.6: Created Design, Polyflex on Polyflex Insole

Foot Location	Heel			Forefoot		
Trial	1	2	3	1	2	3
Loaded Energy, J	5.864	5.767	5.549	1.483	1.386	1.384
Unloaded Energy*, J	-3.283	-3.219	-3.185	-1.176	-1.110	-1.109
Absorbed Energy, J	2.582	2.549	2.364	0.307	0.275	0.274
Ratio of Absorption	0.440	0.442	0.426	0.207	0.199	0.198
Stiffness for High-Load in Loading, N/mm	349.141	355.201	369.696	456.659	507.784	502.916
Stiffness for High-Load in Unloading, N/mm	888.172	896.279	926.257	976.792	1024.300	997.344
Stiffness for Low-Load in Loading, N/mm	5.758	5.516	4.536	234.152	215.899	218.930
Stiffness for Low-Load in Unloading, N/mm	21.535	24.094	26.426	255.545	235.605	235.397

* Energy is a positive quantity. The "-" signs here are to denote the unloaded nature of energy.

Appendix C: Lists of Used Equipment, Instruments and Software

The tests that were conducted required the utilization of the Chatillon force tester, or the Chatillon force tester and the AMTI force plate (Figure C.1), together with custom MATLAB® scripts to compute the energy absorption and the stiffness of the corresponding prosthetic foot. The force tester applied the corresponding load to the prosthetic foot by compressing the design based on the test used, such as the CC test, the M5 test, and the AA1 test, which were covered in Chapters 4 and 5. A 15-degree angle wedge (Figure 4.16) was also fitted on the force tester to simulate the "toe up" and "toe down" positions of the foot (Figure 4.16), resulting in the force components such as the compression and shear force during both the loaded and unloaded phases, as shown in Section 4.3,

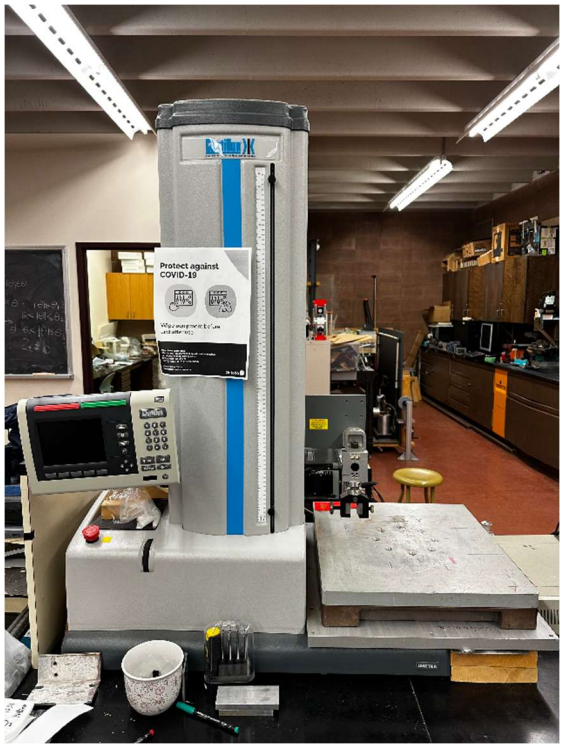

Figure C.1 – The Chatillon Force Tester and AMTI force plate

Advanced Mechanics Technologies Incorporated (AMTI) Force Plate

The AMTI force platforms (Figure 2.3) are mechanical sensing systems that measure various types of ground reaction forces (GRF) during gait analysis. They capture data along three axes: vertical GRF, anterior-posterior GRF, and mediolateral GRF (Lamkin-Kennard & Popovic, 2019). When force is applied to the platform, the sensors embedded in the plate detect the deformation and convert this information into signals that correspond to the applied force (Lamkin-Kennard & Popovic, 2019). The platform is connected to a computer running LabChart8 software, which displays the data in real-time as force versus time plots. This allows for visual analysis and interpretation of the data.

PowerLab and LabChart

In this study, a data acquisition system (a piece of hardware) known as the PowerLab connects the force plate and the LabChart (ver. 8) software such that multiple channels of data can be converted and recorded. This allowed the researcher to collect the necessary data from the force plate or force tester and analyze it to determine the effectiveness of each prosthetic foot.

Materials: TPU and Nylon

In this study, a material known as Thermoplastic polyurethane (TPU) was used with a 3D printer to create an insole that conforms to the shape of the human foot. The material was also incorporated with pads for the heel and forefoot. Additionally, another material used in this study was nylon, a polyamide, which was applied to the top and bottom plates of the prosthetic.

Commercial Designs

Three commercial prosthetic designs were used in the study: the Wooden SACH Foot, the Otto Bock Trias Foot and the Sierra Foot (Figure 4.1). Each prosthetic foot was placed on a force plate and on the 15-degree wedge to conduct a pseudo-static analysis. This setup enabled a comparison of the performance of each model, specifically in terms of energy absorption and resistance to deformation during both the loaded and unloaded phases.

3D Printers

Two different 3D printers were utilized for the creation of physical parts: the top and bottom plates of the foot were printed with nylon by Ultimaker S5; the insoles, and the pads for the heel and forefoot were printed by KingRoon KP3S with the TPUs. Both 3D printers are of the fused filament fabrication (FFF) or FDM (fused deposition modeling) type. In particular, the Ultimaker is capable of printing nylon and the KingRoon is designed to print TPUs, in addition to other materials.

SolidWorks

In this study, SolidWorks, as a 3D CAD (Computer-Aided Design) software, was used to design each component of the overall project and assemble them into a complete model. This process resulted in the final design, which includes pads for the heel and forefoot, plates, and insoles.

LISA

In this study, the design created using SolidWorks was recreated and simplified in LISA for simulations. The LISA software enabled generating a mesh consisting of a series of nodes and elements. This mesh could be analyzed to assess node displacement, allowing the researcher to evaluate the effectiveness of the model and the applied materials when deflecting the applied loads.

MATLAB

MATLAB is computing platform used by engineers and scientists to analyze data, amongst many other tasks such as creating computational/numerical models. In this study, MATLAB scripts were developed to process the experimental data including from the CC1, M5 and AA1 tests. Energy absorption ratios were computed. Stiffness for loading and unloading situations under low and high loads were evaluated.